Chemical and Spectroscopic Aspects of Polymer Ablation: Special Features and Novel Directions

Thomas Lippert*,† and J. Thomas Dickinson‡

Paul Scherrer Institut, 5232 Villigen PSI, Switzerland, and Washington State University, Pullman, Washington 99164-2814 USA

Received August 12, 2002

Contents

1 Introduction 453
1.1 History 453
1.2 Summary of Ablation Mechanisms 454
1.3 Summary of Theoretical Models 455
2 Studied Polymers 456
2.1 Doped Polymers 456
2.1.1 Photochemical Active Polyaromatic Compounds, as Fluorescence Probes 456
2.1.2 Photostable Organic Compounds and Similar Dopants 457
2.2 Neat Polymers 458
2.2.1 Designed Polymers Based on Commercial Polymers 458
2.2.2 Novel Designed Polymers for Laser Ablation at 308 nm 459
2.2.3 Detailed Analysis of a Selected Designed Polymer (Triazene-Polymer) 459
2.2.4 Commercial Polymers 464
2.3 Summary of Miscellaneous Polymer Work 467
3 Selected Experimental Tools 468
3.1 Single Pulse Ablation with Various Pulse Lengths 468
3.2 Mass Spectrometry 468
3.2.1 Review of Recent Experimental Work 468
3.2.2 Analysis of Neutral and Ionic Emissions 469
4 Structure Modification 472
4.1 Physical Surface Modification: Nano- to Microstructures 472
4.2 Chemical Surface Modification 474
5 Radiation Sources 475
5.1 Low Intensity (Lamp) Sources 475
5.2 Continuous-Wave UV Lasers 475
5.3 Ultrafast Lasers 476
5.3.1 Femtosecond Lasers 476
5.3.2 Picosecond Lasers 478
5.4 Vacuum-Ultraviolet (VUV) Lasers 478
5.5 Synchrotron Radiation (SR) 479
5.6 Mid-IR Irradiation 479
5.7 Visible Light and High Repetition Rate Ablation 480
6 Outlook 481
7 Acknowledgments 481
8 References 481

† Paul Scherrer Institut.
‡ Washington State University.

1 Introduction

1.1 History

In 1982, the first reports of laser ablation of polymers were issued almost simultaneously by Y. Kawamura et al.[1] and R. Srinivasan et al.[2] Srinivasan went on to become a leader in the field of polymer ablation. Srinivasan probably also coined the terms *laser ablation* and *ablative photodecomposition*, now in common use. The onset of material removal by laser ablation characteristically occurs at a well-defined laser fluence (energy per unit area). As the fluence is raised above this threshold, the ablation rate increases. The threshold fluence (F_0 or F_{th}) is material and laser wavelength dependent and can vary from tens of mJ cm^{-2} to more than 1 J cm^{-2}. The discovery of laser ablation of polymers sparked research in this field in many groups around the world. Many aspects of polymer ablation, and laser processing in general, are reviewed by Bäuerle.[3] Today, commercial applications of polymer laser ablation include the preparation of via-holes in polyimide for multichip modules at IBM[4] and the production of inkjet printer nozzles (also polyimide).[5]

Considerable progress has been made in understanding polymer ablation since the last series of reviews a decade ago.[6−8] New developments in polymer ablation include the application of femtosecond laser pulses, vacuum ultraviolet lasers (VUV), and free electron lasers (FEL). Some of these techniques have a great potential for the development of new applications and research tools. Much of this progress is discussed in this and other articles appearing in this special issue of *Chemical Reviews*. Current research on polymer ablation may be divided into two areas:

(i) Applications of laser ablation, novel materials, and techniques.

(ii) Studies of ablation mechanisms (databased modeling).

The first area will be discussed in detail in this article, while the mechanistic aspects, especially the theoretical part, are discussed in other articles in this special issue.

Many experimental methods and experimental polymers have been designed with a view toward improving our understanding of ablation mechanisms. It is often impossible to completely separate experiments designed to illuminate ablation mech-

10.1021/cr010460q CCC: $44.00
Published on Web 01/04/2003

Thomas Lippert was born in Germany where he studied chemistry at the University of Bayreuth. He received his Diploma in Ecological Chemistry (in 1990) and his Ph.D. in Physical Chemistry (in 1993) under Professor Alexander Wokaun. He did postdoctoral studies for Wacker Chemistry (Burghausen, Germany) and went then as a STA/Alexander von Humboldt postdoctoral fellow to Tsukuba, Japan (in 1994), where he worked at the National Institute of Materials and Chemical Research with Dr. Akira Yabe. He moved then as postdoctoral fellow (in 1995) to Los Alamos National Laboratory (Los Alamos, NM) where he later became a Director's Postdoctoral Fellow and Technical Staff Member. He then joined the Paul Scherrer Institut (Villigen, Switzerland) as Senior Scientist (in 1999), and is currently the head of a research group. He received his Habilitation at the ETH Zuerich in Physical Chemistry (in 2002), where he is also a faculty member. His work has been focused on the design of novel polymers, ultrafast spectroscopy, thin film deposition, and microstructuring/surface modification. Lippert is author or coauthor of over 90 technical articles. He has presented more than 30 invited talks on areas of laser interactions with materials.

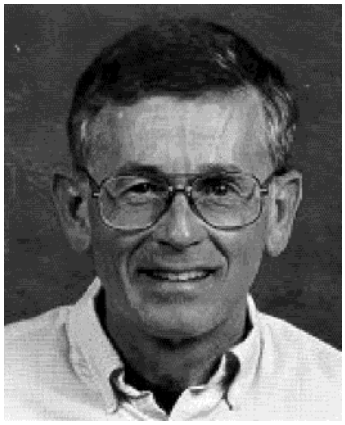

J. Thomas Dickinson received his B.A. degree in physics from Western Michigan University in 1963, and his Ph.D. degree in chemical physics from the University of Michigan in 1968. He went directly to Washington State University where he is now the Paul A. Anderson Professor of Physics. Dickinson's research has been in the general areas of materials physics, materials chemistry, and surface science. Recent research has focused on: (a) laser-ablation and laser desorption mechanisms in inorganic dielectric crystals and polymers; (b) the applications of lasers in materials and chemical analysis; and (c) use of scanning tunneling microscopy and atomic force microscopy to study laser surface modification, nano-tribology and deformation physics. Dickinson is author or coauthor of over 270 technical articles. He has presented more than 200 invited talks on areas of materials physics and chemistry over the last 15 years, including 15 Gordon Conference talks.

anisms from other experimental studies. A short summary of the various models for ablation mechanisms is given below. In many cases, experimental details and quantitative models are discussed in other articles in this issue.

1.2 Summary of Ablation Mechanisms

Polymer ablation is typically described in terms of thermal, photothermal, or photochemical models, either individually or combined.[6−8]

From an application standpoint, photochemical processes are most desirable. Photochemical decomposition is intrinsically capable of higher spatial resolution because thermal damage to the surrounding material is minimal. Polymers design for photochemical interactions could take advantage of our experience with the design of photoresists, where the photochemical properties of various chromophores dominate the interaction. Polymers designed to decompose mainly to gaseous products would reduce or eliminate the problem of redeposited material (debris). Incomplete removal of polymer debris requires additional cleaning steps and mitigates one of the big advantages of laser ablation.

Polymer ablation mechanisms have been debated for more than two decades. As a result, the original strict separation of the models (photochemical models by *chemists* and thermal/photothermal models by *physicists*) is slowly blurring. It is generally agreed that the energy of nanosecond laser pulses is initially transformed into electronic excitations. However, subsequent energy transfer can take a variety of forms. Understanding this energy transfer has been complicated by the limited range of experimental data accounted for by any given model. Comprehensive models that incorporate data acquired by several experimental techniques simply do not exist. Another problem has been the wide variety of empirical definitions for ablation phenomena, especially near the threshold fluence. Experimental facts that must be explained by such models include:

(i) Ablation depths as measured by profilometry (optical interferometry, stylus profilometry,[9] atomic force microscopy[10]) show sudden increases at the threshold fluence. This observation is supported by reflectivity[11] and acoustic measurements.[12] Experimental comparisons are complicated by the use of single laser pulses in some threshold measurements and multiple pulses in others. The resulting thresholds are not necessarily equivalent.

(ii) Ablation rates calculated from mass loss measurements using quartz crystal microbalances (QCM)[13] or mass spectrometry[14] reveal a so-called Arrhenius tail[13] (linear fluence dependence at low fluences, with much stronger fluence dependencies at still higher fluences).

(iii) Ablation can change the chemical and/or physical (morphological) properties of the remaining polymer, e.g., altered optical absorption,[15−17] modified chemical composition,[18−20] and in the case of polyimides, increased electrical conductivity.[21]

We note that at sufficiently high fluences, the ablation rates of most polymers are similar[22] being limited by screening of the radiation by the ablated products[23,24] and the associated plasma.[25] Thus, high fluence measurements of ablation rate seldom yield much information on the underlying ablation mechanisms.

1.3 Summary of Theoretical Models

The various ablation models incorporate one or more of the above-mentioned ablation mechanisms:

Photochemical models: Electronic excitation results in direct bond breaking;[7,26−29] excited-state absorption may be included (two-level model).[30−32]

Photothermal models:[23,33−36] Electronic excitations thermalize on picosecond-time scales, yielding thermally broken bonds.

Photophysical models: Both thermal and nonthermal processes are important. The models may incorporate two independent channels of bond breaking,[24,37] or employ different bond breaking energies for ground state and electronically excited chromophores.[38,39] These models are most important for short pulses (ps and fs).[40]

Photochemical and thermal models can be further categorized as *volume* and *surface* models. Surface models consider only material within several monolayers of the surface. As a result, the velocity of the interface between the gaseous and condensed phase depends explicitly on the surface temperature or laser intensity. In volume models, ablation processes in the bulk of the material are explicitly treated. In combination with the assumed ablation mechanism(s), surface and volume models typically have the following properties:

Photochemical surface models[41] typically involve longer interaction times and/or higher laser fluences.

Photochemical volume models[7,8,26−28] predict sharp ablation thresholds and ablation depths that depend logarithmically on the number of laser pulses. Linear increases in the ablation depth can result from models that account for the motion of the ablation front and neglect screening by ablation products. These models do not explain the Arrhenius tails observed in mass loss measurements.

Thermal surface models[23,24,36,42] (developed mainly for metal ablation[43]) account for smooth Arrhenius tails, due to the Arrhenius dependence of the recession velocity on temperature. These models do not account for sharp ablation thresholds, as observed in polymers.

Photothermal volume models are often oversimplified,[13,35] because it is often convenient to ignore the motion of the gas−solid interface,[34] which results in unrealistically high temperatures. These models often fail to account for Arrhenius tails.

Newer models combine various features of these models. For instance, a photochemical volume model and a thermal surface model have been combined to construct a *volume photothermal* model of Arnold et al.[44] This model treats ablation in terms of photothermal bond breaking within the bulk material (a first-order chemical reaction with Arrhenius temperature dependence). Ablation begins when the density of broken bonds at the surface reaches a critical value. These models can account for sharp ablation thresholds and Arrhenius tails, and are described in detail by Bityurin et al. in this issue. To date, this *volume photothermal* model had been applied to polyimides only, and does not account for the possibility of photochemical decomposition. This model, like other thermal models, employs many material parameters. Several of these parameters are obtained from fitting to data. One challenge has been the temperature dependence of these material parameters (e.g., thermal conductivity or specific heat). Even when data are available as a function of temperature, the temperature range is often quite limited (up to a few hundred K), and often acquired at relatively *slow* heating rates (up to several K per second). For laser ablation modeling, these data are extrapolated to temperatures of up to several thousand K and heating rates up to 10^{10} K s^{-1}.

Photothermal models typically have difficulty accounting for the way the ablation products change with laser wavelength. As emphasized by Srinivasan:[45] the products generated by ablation with CO_2-lasers are very different from the products generated by excimer laser ablation (in the UV). Thermal effects alone cannot account for this difference, suggesting that photoelectronic processes play an important role under UV laser irradiation.

Laser absorption in the UV is often dominated by photoelectronic excitations. In doped polymer systems, one can provide strongly absorbing chromophores that are responsible for the bulk of laser absorption. Subsequent thermalization of this energy can then decompose the matrix material by thermal processes. This is especially important for polymers containing polyaromatic dopants irradiated at wavelengths greater than or about 248 nm. Time-resolved absorption/emission measurements[46,47] and TOF-MS data[48] indicate the presence of *cyclic multiphoton absorption* with up to 10 photons.[49] The photon energy is transferred from the highly excited polyaromatic dopant molecules to the polymer matrix via rapid internal conversion. The associated heating results in the thermal decomposition of the polymer. Time-dependent absorption measurements suggest that excited triplet states in the dopants play a key role in the process, due to their long lifetimes.

The multiphoton absorption cycle was confirmed by comparing the temporal profile of the fluorescence of anthracene-doped polystyrene films with computational results based on the cyclic process.[50] In the computational studies, the ground state, first excited singlet state, and lowest triplet state were included. The calculated temperature rise during the laser pulse depends nonlinearly on the laser intensity. Rapid internal conversion within the triplet manifold is the most effective mechanism for depositing heat at the irradiated surface.

Progress in computational hardware and software has allowed the development of entirely different kinds of models for laser ablation, including molecular dynamics (MD) calculations.[51−53] To gain a microscopic view of laser ablation, the breathing sphere model was developed. Each molecule (or appropriate group of atoms) is typically represented by a single particle with no true translational degrees of freedom, but an approximate internal degree of freedom.[54,55] This internal (breathing) mode allows one to describe a realistic conversion of internal electronic energy (due to laser absorption) to translational motion. Using molecules (are larger groups of atoms) rather than the atoms themselves, the

system size can be large enough to describe the collective dynamics leading to laser ablation and damage. Similarly, neglecting the high-frequency atomic vibrations allows one to use longer time-steps in the numerical integration and model the effect of realistic laser pulses.[56] Molecular dynamics models yield a microscopic view of ablation,[54−57] including properties of the ejected material: the velocity distribution of matrix and analyte molecules in MALDI,[58,59] the ejection of clusters,[56−61] and their dependence on the irradiation conditions (laser fluence,[54,55,57,60] pulse duration,[56] and initial sample temperature[61]). One effect that cannot be directly simulated in polymers (possible for metals and ultrashort pulses[62]) within the breathing sphere model is the propagation of laser induced pressure waves from the absorption region deeper into the bulk of the irradiated sample. This can be remedied by combining molecular dynamics models of molecule-scale processes with the continuum finite element models[63] of the long-range propagation of waves and their interaction with other regions of a large system. Long-range wave propagation can spall material from the free surface at the back of such samples,[64] for instance, as the wave of compression produced by laser absorption reflects from the back free surface. Spallation results when the dynamic tensile strength of the material is exceeded by the (tensile) pressure of the reflected wave, which may also result in material removal from the front surface of samples.[65]

The plume development in molecular dynamics simulations of the bulk is usually only followed for a few nanoseconds after the laser pulse, which is not enough to compare the data with various experimental techniques (such as MALDI, TOF-MS, shadowgraphy, interferometry or for PLD). Long-term plume expansion can be simulated by extending the bulk models with direct simulation Monte Carlo techniques, which have been recently applied to systems relevant to MALDI.[66] Details of molecular dynamics models are discussed by Zhigilei et al. in this issue.

2 Studied Polymers

Two major kinds of polymers have been studied: doped polymers and neat polymers.

2.1 Doped Polymers

The ablation of doped polymers was reviewed in 1997 by Lippert et al.[67] and the ablation process was classified according to the absorption properties of the polymer−dopant system. These systems range from polymer blends, to systems where only the dopant or only the polymer are absorbing. The authors suggested a qualitative scheme where ablation results from a complex mixture of processes originating from the dopants or the matrix. Depending on the properties of the dopant, different ablation pathways are dominant.

The ablation behavior of doped polymer systems with absorbing dopants depends strongly on whether absorption actually decomposes the dopant molecule. Photolabile dopants that decompose to gaseous products typically produce pronounced surface swelling

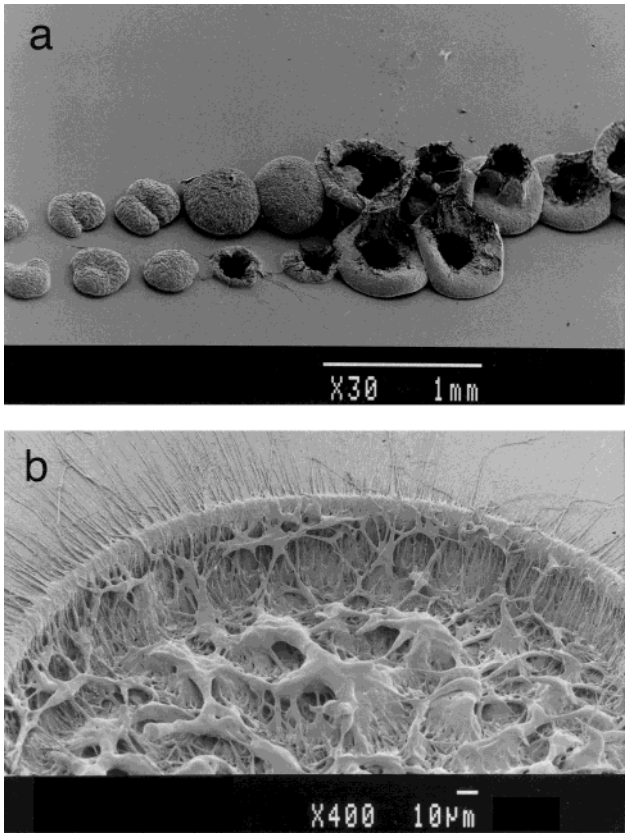

Figure 1. (a) Surface swelling and bubble formation during ablation of PMMA doped with low dopant concentration (0.25 wt% of a dialkyl−aryl triazene-compound). Irradiation at 308 nm with single pulses and increasing fluence (from left to right). (b) PMMA doped with 2 wt% of the dopant and irradiated with 2 pulses with 5.8 J cm^{-2}.

at low fluences (shown in Figure 1 a). Very high ablation rates (up to 80 μm per pulse) can be achieved at high fluences,[68] but always with pronounced signs of surface melting (shown in Figure 1b). In contrast, photostable dopants (e.g., polyaromatic compounds) produce much less surface swelling and lower ablation rates. As discussed above, the behavior of photostable dopants can be understood in terms of *cyclic-multiphoton absorption*.

Recent studies of photochemically active, photolabile, or photostable dopants include the following.

2.1.1 Photochemical Active Polyaromatic Compounds, as Fluorescence Probes

These compounds are typically substituted naphthalenes (i.e., Br and I substituted), which do not exhibit pronounced fluorescence. In contrast, the photoproduct naphthalene exhibits a very pronounced emission ($^1B_{3u} \rightarrow {}^1A_{1g}$). This difference allows one to probe the photochemical modification of the dopant by time-dependent fluorescence measurements. Georgiou et al. performed such measurements using polymethyl-methacrylate (PMMA) and van der Waals films as matrices[69−72] (discussed in detail in this issue) at two wavelengths (193 and 248 nm)[73] and pulse lengths (30 ns and 500 fs).[74−76] As shown in Figure 2, the onset of increased photoproduct yield at 248 nm (i.e., naphthalene and naphthalene dimers) coincides with the onset of significant surface swell-

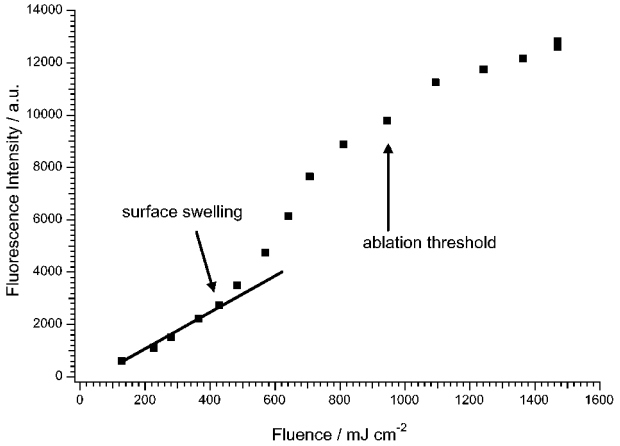

Figure 2. Fluorescence intensity of the NapH-like photoproduct (λ = 337 nm) remaining in the substrate, following irradiation at 248 nm with various fluences and a probe wavelength of 248 nm. The dopant was 0.4 wt% of iodo-naphthalene in PMMA. The threshold of swelling and ablation are marked in the figure. [Figure by S. Georgiou].

ing (Figure 2). In contrast, the photoproduct yield at 193 nm increased with laser fluence, even below the threshold of ablation, and no surface swelling was observed (Figure 3). The photoproduct yield above the

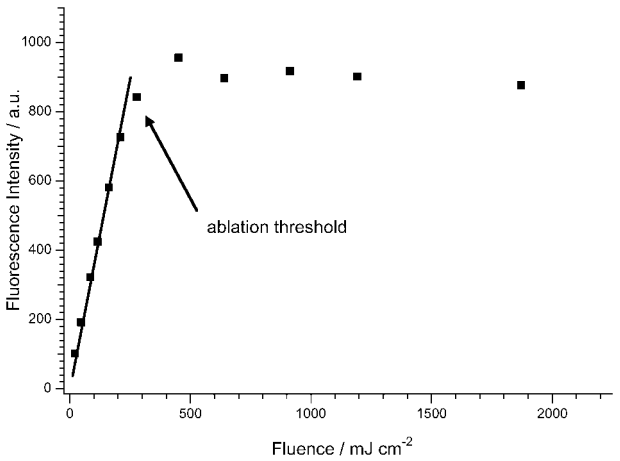

Figure 3. Fluorescence intensity of the NapH-like photoproduct (λ = 337 nm) remaining in the substrate, following irradiation at 193 nm with various fluences and a probe wavelength of 248 nm. The dopant was 0.4 wt% of iodo-naphthalene in PMMA. The ablation threshold is marked in the figure. [Figure by. S. Georgiou].

ablation threshold is more or less constant. The authors suggest that the efficient material removal at 193 nm is due to the stronger laser absorption at 193 nm, both in the polymer and in the resulting photoproduct.

Significantly, femtosecond (fs) irradiation of these polymers produces a sharp increase of the photoproduct yield at fluences below the ablation threshold. Crossing the ablation threshold yields only very small changes in product intensity (Figure 4). In addition, no dimers are observed under femtosecond irradiation. This suggests that the resulting photoproducts are removed by ablation and that extremely inefficient thermal dissipation among the products inhibit the dimer formation.

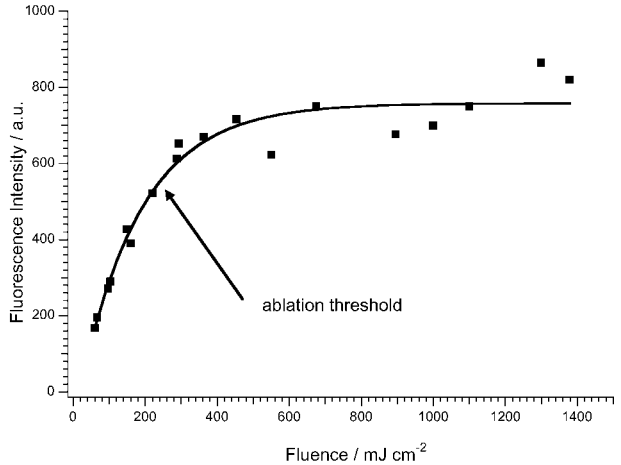

Figure 4. Fluorescence intensity of the NapH-like photoproduct (λ = 337 nm) remaining in the substrate, following irradiation at 248 nm with 500 fs long pulses and various fluences. The dopant was 0.4 wt% of iodo-naphthalene in PMMA. The ablation threshold is marked in the figure. [Figure by. S. Georgiou]

As noted above, the definition of ablation threshold as a quantitative characteristic of the ablation process requires careful attention. Previous studies have employed profilometry (measurable removal of material from the surface) or beam defection parallel to the polymers surface to determine the onset of material removal. More recently (see above), profilometry,[9] atomic force microscopy[10] (both surface material removal), surface reflectivity,[11] quartz microbalance (mass loss),[13,77] beam deflection,[78,79] and acoustic detection[12,80] (either in the material[81] or in air above[82]) has been employed. It is also of utmost importance to consider whether single- or multipulse experiments are employed for threshold determination. Material modification in multipulse experiments may alter the results, while for single pulse experiments surface contamination may be important.

2.1.2 Photostable Organic Compounds and Similar Dopants

Many photostable organic compounds are typically polyaromatic, such as pyrene and anthracene. The ablation mechanisms are mainly photothermal and can be described in terms of *cyclic multiphoton absorption*. The laser intensity dependence of the absorption coefficient of PMMA doped with polyaromatic compounds has been measured by Yabe et al.[83]

Other dopant−polymer systems include a system incorporating gold-loaded, polystyrene-based inverse micelles, used to form metallic gold nanodots on mica.[84] Composite materials, where one of the components is a polymer, can also be usefully described in terms of a doped polymeric material. Such composites range from elastomer−carbon composites, which yield elastic conical structures when ablated,[85,86] and ceramic-[87] or metal-[88]polymer composites.

Dopants can also be employed as probes of the ablation process for polymers in general. However, one must account for dopant-induced changes in the polymer properties (e.g., depression of the glass transition temperature). One must also distinguish

the role of dopant as a molecular probe from potential active involvement in the ablation mechanism. As noted above, *dopant-induced ablation* is a real possibility, with behavior often sharply contrasting with the neat polymer (e.g., wavelength dependence). When these influences are properly accounted for, then doped polymers are an important tool to elucidate the role of polymer chemistry in polymer ablation. The wide range of behaviors that have been demonstrated with various dopants offer many possibilities for practical applications. For instance, carefully chosen dopants allow for the structuring of "unprocessable" polymers (PTFE)[89] or structuring at longer more economic wavelengths.[67]

2.2 Neat Polymers

The ablation of pure polymers may be usefully treated in terms of the ablation of existing commercial polymers and the ablation of polymers especially designed to yield desirable ablation behavior. The design of polymers to maximize ablation rates and quality was recently reviewed by Lippert et al.[90]

2.2.1 Designed Polymers Based on Commercial Polymers

The polyestercarbonates (PEC, structural scheme shown in Figure 5), for instance, are standard

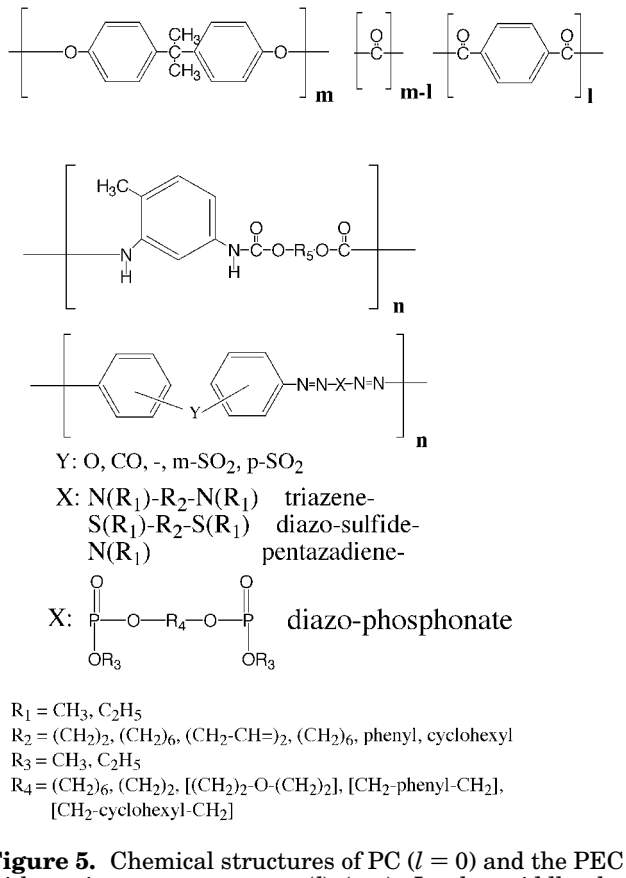

Figure 5. Chemical structures of PC ($l = 0$) and the PEC with various ester content (l) (top). In the middle the general structure of the PU is shown, while the designed azo-polymers with variable "X" and different substituents R_x are shown in the bottom.

polymers whose ablation properties are readily altered by introducing chemical modifications.[91] The absorption edge in these materials can be shifted to longer wavelengths by incorporating additional ester groups. At 308 nm, fluences above 2 J cm^{-2} are required to structure pure polycarbonates (Figure 6

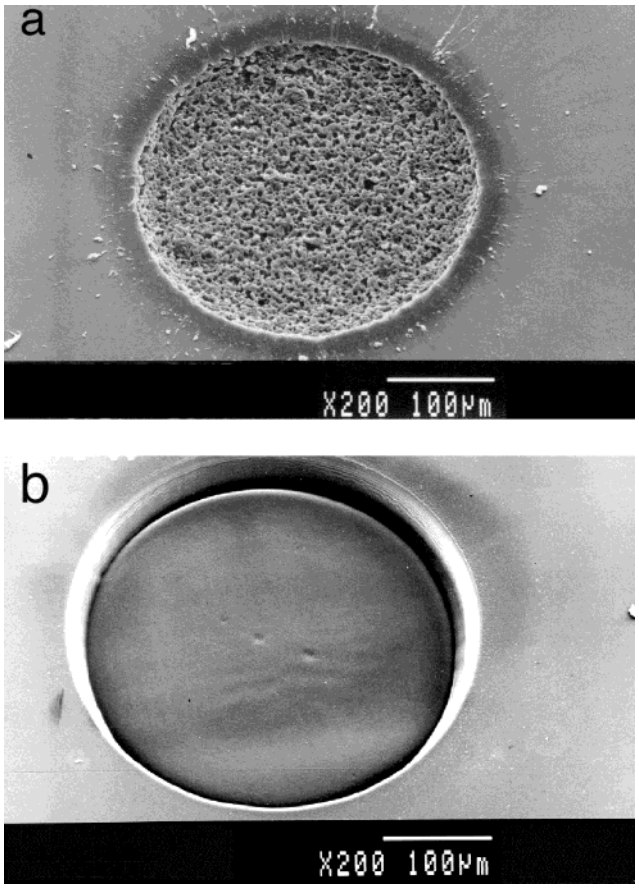

Figure 6. SEM picture of an ablation crater in (a) polycarbonate film PEC with $l = 0$ in Figure 5 (top). Irradiation at 308 nm with 15 pulses and a fluence of 7.66 J cm^{-2}. (b) Polyester-carbonate film PEC with a 30% molar fraction of the ester l in the structure (see Figure 5). Irradiation at 308 nm with 15 pulses at a fluence of 18.45 J cm^{-2}.

a), and the quality of the ablated surfaces are relatively poor. Increasing the ester increases the absorbance, lowers the threshold fluence, and increases the ablation rate. The structures formed in the modified PEC in Figure 6b exhibit sharp edges, very smooth bottoms, and no surrounding debris. One possible explanation for this improvement is the increased release of gaseous decomposition products, e.g., CO/CO$_2$ from the ester group. [Similar effects are observed in azopolymers (see below), which release N$_2$.] Larger ablation fragments are entrained in the high velocity gas and transported away from the surface. In PEC systems, one can also study the influence of covalent bonding of the absorbing ester group. Polymer blends consisting of pure PC with PEC with 100% ester content have been prepared. Although the ablation rates for the blends are always slightly lower than for the PECs, increasing the concentration of the ester-containing component has the same effect as increasing the ester content in the pure PECs.[91]

Hitachi developed a variety of polyurethanes (more than 50, general structural scheme shown in Figure

5), which display an absorption maximum near 248 nm. Their goal was to identify polymers that exhibit high ablation rates at low fluences (<200 mJ cm^{-2}). The threshold fluence of the most promising polyurethane was around 50 mJ cm^{-2}; the corresponding ablation rates were 50 nm per pulse at 100 mJ cm^{-2} and around 150 nm per pulse at 200 mJ cm^{-2} over a 1×2 mm^2 illuminated area. (At these fluences, the ablation rate depends on laser spot size. Similar effects have been described for other polymers[24]). At these relatively low fluences, the polymer could not be totally removed from the substrate.[92−94]

2.2.2 Novel Designed Polymers for Laser Ablation at 308 nm

Irradiation at 308 nm is convenient from a commercial point of view due to the lifetime of optical components and laser gas (XeCl excimer) laser. Applications which do not require submicron resolution are often well-served with 308 nm lasers. At 308 nm, it is possible to selectively irradiate into the absorption band of a photochemically active chromophore, with little absorption by other parts of the polymer, such as aromatic or aliphatic groups. Experiments with such materials can clarify the role of photochemically active chromophores during the ablation of more resistant polymer material.

The first step for the development of polymers sensitive to 308 nm irradiation was to design photolabile compounds for physical doping (solvent mixing).[67,68] The best results were achieved with triazene- (−N=N−N−) or pentazadiene compounds (−N=N−N(R)-N=N−). The $\pi-\pi^*$ transition of the −N=N−X− chromophore is near 300 nm.[95] The chromophores decompose into N_2 and other gaseous products, which can promote ablation. Early work indicated that the photochemical properties of the dopants influenced the resulting ablation characteristics.[68] Subsequently, polymers containing the −N=N−X− chromophore in the polymer main chain were developed. Early attempts yielded a relatively low molecular weight material with a low glass transition temperature (below room temperature), and consequently displayed poor ablation characteristics (e.g., quality of ablation structure).[96] Subsequent polymers synthesized by interfacial polycondensation yielded polymers with higher molecular weights and glass transition temperatures,[97] and better ablation characteristics.

This synthetic route was used to synthesize various classes of polymers, with a variety of chromophores ("X"-groups in Figure 5). The reactive groups included nitrogen (described later as triazene-polymers), sulfur, or −N−N=N−. The latter two classes of polymers were too sensitive. A more stable class of polymers (poly-arylazophosphonates) was subsequently developed which revealed satisfactory ablation characteristics,[98,99] but decomposed under the scanning electron beam of a microscope.[100]

Other synthesized polymers included polymers with the triazene-group (−N=N−N<) in conjunction with an ester group. Using a series of these polymers (diazo-copolyesters), the optimum triazene content of these polymers was determined to lie between 35 and 90% of the copolymer.[101,102] Another series of polymers was synthesized by replacing the ester group with a sulfide group, yielding polysulfides with triazene groups in the main chain. Under 193-nm irradiation, these polymers displayed better ablation structures than PMMA.[103]

2.2.3 Detailed Analysis of a Selected Designed Polymer (Triazene Polymer)

The triazene polymers (structure unit shown in Figure 5, and marked as TP) in particular have been studied in detail. The studied polymers have two triazene units per repetition unit, display absorption maxima between 290 and 380 nm, and show glass transition temperatures between 33 and 110 °C. Their decomposition temperatures (220−300 °C) can be controlled within certain limits by changing the substituent units, labeled R_x in Figure 5.

The ablation rates (ablation depth per pulse) at 308 nm were calculated from linear plots of the ablation depths vs pulse number at a given fluence. All plots were linear, showing no incubation behavior as expected for highly absorbing polymers. At low fluences, one expects the etch rate to vary as the natural logarithm of the fluence according to the relation,[104,105]

$$d(F) = \frac{1}{\alpha_{\mathrm{eff}}} \ln\left(\frac{F}{F\mathrm{th}}\right) \qquad (1)$$

where $d(F)$ is the etch rate, α_{eff} is an effective absorption coefficient, and F_{th} is a threshold fluence. Figure 7 compares images of ablation-formed structures in a designed polymer (TP, Figure 7a) and a standard polyimide (PI, Figure 7b). The polyimide (Kapton) was chosen because its absorption coefficient at 308 nm is very similar to that of the triazene polymers (with $R_1 = O$, $R_2 = CH_3$, and $R_3 = C_6H_{12}$ -TP). The structures in TP (Figure 7a) are well defined with no debris, while the PI displays a pronounced ring of contamination surrounding the structure. Close inspection of the PI structures reveals lower effective resolution, as well as substantial contamination inside the structured area. The PI debris consists mainly of amorphous carbon with some crystalline components. The carbon inside the structured area reveals a higher degree of crystallinity, suggesting that prolonged irradiation modifies the deposited material.[106,107]

The triazene polymer displays a sharp ablation threshold of 25 mJ cm^{-2} (±5 mJ cm^{-2}) for 308 nm irradiation, while F_{th} is not as well defined (F_{th} = 16−28 mJ cm^{-2}) for irradiation at 248 nm.[17,108] These thresholds were determined by several different methods, including UV-spectroscopy and profilometry for multiple pulses.[22]

Figure 8 shows the etch rates for the TP polymer at low fluences as a function of the logarithm of the fluences for laser wavelengths of 193, 266, 308, and 351 nm. For comparison purposes, the inset shows the same data on a linear scale.[109] Data at somewhat higher fluences are shown for 248 nm.[96] The etch rates at each wavelength can be interpreted in terms of the UV−Vis absorption spectrum of this material, shown in Figure 9. The strong band near 196 nm

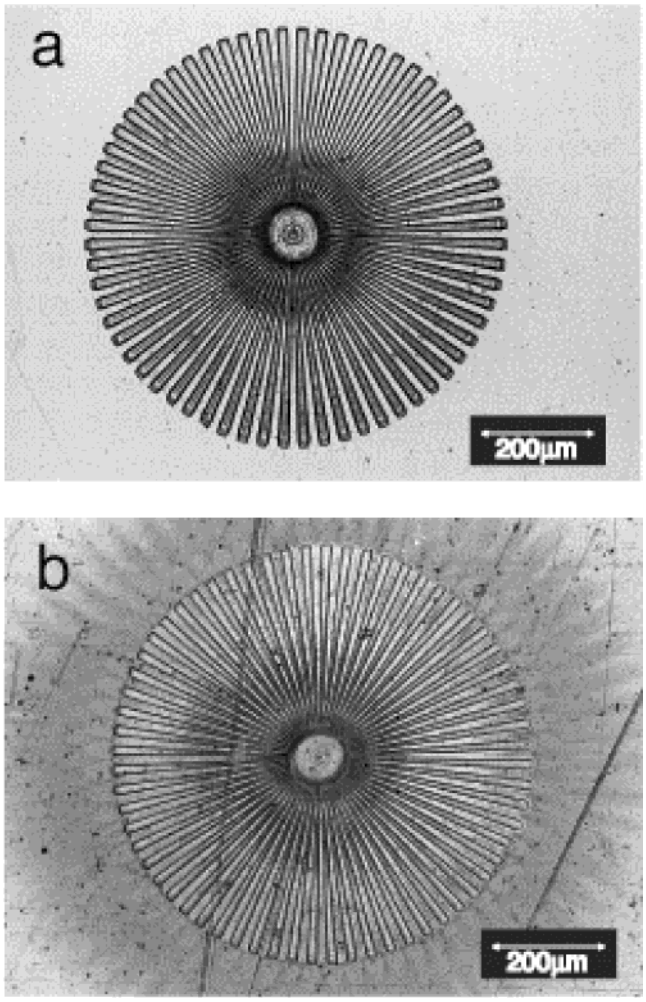

Figure 7. SEM images of Siemens stars fabricated by laser ablation. Siemens stars in the triazene polymer (a) and in polyimide (b) using five pulses. The deposited carbon material is clearly visible in the surrounding of the structure in PI. [From ref 119, copyright 2002, with permission from Elsevier Science].

correspond principally with aromatic parts of the polymer, while the band at 332 nm corresponds mainly to the triazene chromophore.[17] The laser wavelength in resonance with the aromatic system displays the lowest etch rates. These etch rates are below the etch rates predicted by eq 1 on the basis of the linear, Beer's Law absorption coefficient α_{lin} (shown in Figure 8). In contrast, all the wavelengths that access the triazene system (266, 308, and to a lesser extent, 351 nm) display much higher etch rates. These etch rates exceed the predictions on the basis of eq 1, and the linear, Beer's Law absorption coefficient α_{lin}. The ablation rates at 308 are typically several times that at 193 nm, despite the similar absorption coefficients. Low threshold fluences are observed at all four fluences: 12 ± 2 mJ cm^{-2} at 193 nm, 8 ± 2 mJ cm^{-2} at 266 nm, 27 ± 3 mJ cm^{-2} at 308 nm, and 25 ± 3 mJ cm^{-2} at 351 nm.

Excimer lamps were employed to study the effect of low fluences at 222 and 308 nm, where linear (no ablation) photochemistry is expected.[14] Excimer lamps emit incoherent, quasi-continuous radiation at the same wavelength as the excimer laser. At the low photon fluxes provided by the lamps, multiphoton processes can be neglected. Decomposition of the triazene chromophore was detected by UV spectroscopy at both laser wavelengths, while decomposition of the aromatic chromophore was detected only at 222 nm. Thus the triazene chromophore decomposes at fluences well below the ablation threshold. Further, it is clearly the most sensitive unit in the triazene polymer.

Surface analysis after irradiation at fluences above and below the ablation threshold (e.g., 10 mJ cm^{-2} and 30 mJ cm^{-2} at 308 nm) reveal pronounced differences. Surface modification at fluences below the ablation threshold is solely chemical at all laser wavelengths, principally oxidizing the surface. Oxidation is confirmed by a decrease of the nitrogen signals and an increase in the oxygen signals in X-ray photoelectron spectroscopy (XPS) measurements. Oxidation also decreases the contact angle of water droplets in the irradiated area. SEM inspection revealed no physical change of the surface at fluences below the ablation threshold.

In contrast, surface modification at fluences above the ablation threshold is a strong function of irradiation wavelength. At 308 nm, the chemical composition remains unchanged after several pulses, consistent with a photochemical mechanism where polymer is removed completely layer by layer without redeposition of ablation products. At 248 nm, SEM observations show truncated cone-like structures, possibly due to cross-linked polymer structures; cross-linking is consistent with the presence of insoluble residues after irradiation. The surface appears black and carbonized; a carbon excess is confirmed by XPS spectra.

An attempt to account for the different ablation behavior at 308 and 248 nm was made using a photochemical model with two absorption levels (see above[30−32]). This model incorporates a first and second excited state with corresponding absorption cross-sections σ_1 and σ_2. The transmission of the laser radiation (T_{pulse}) was compared with the transmission measurements with a UV−Vis spectrometer (very low photon fluxes) of thin film samples (T_{film}). The two level model was used to describe the etch rate and transmission ratio T_{pulse}/T_{film} data measured at each wavelength.[17] Although it was not possible to find a consistent set of fitting parameters that would apply to both sets of data, each data set could be fitted individually with high correlation with its own set of parameters. The chromophore densities inferred at each wavelength were similar to values previously calculated by semiempirical methods (AM1/PM3 and ZINDO). (The curve fit procedure constrained this parameter to values less than the number of chromophores per repetition unit.) An increase in transmission with increasing fluence was observed, suggesting the presence of a bleaching process at higher fluence. In principle, this bleaching could be transient or permanent (= decomposition). Our inability to fit both sets of data with the same set of parameters could be due to the lifetimes of the excited states, the presence of stimulated emission, or an additional thermal component of ablation.

To address the issue of a possible photothermal contribution, a nanosecond imaging technique[47,110−112]

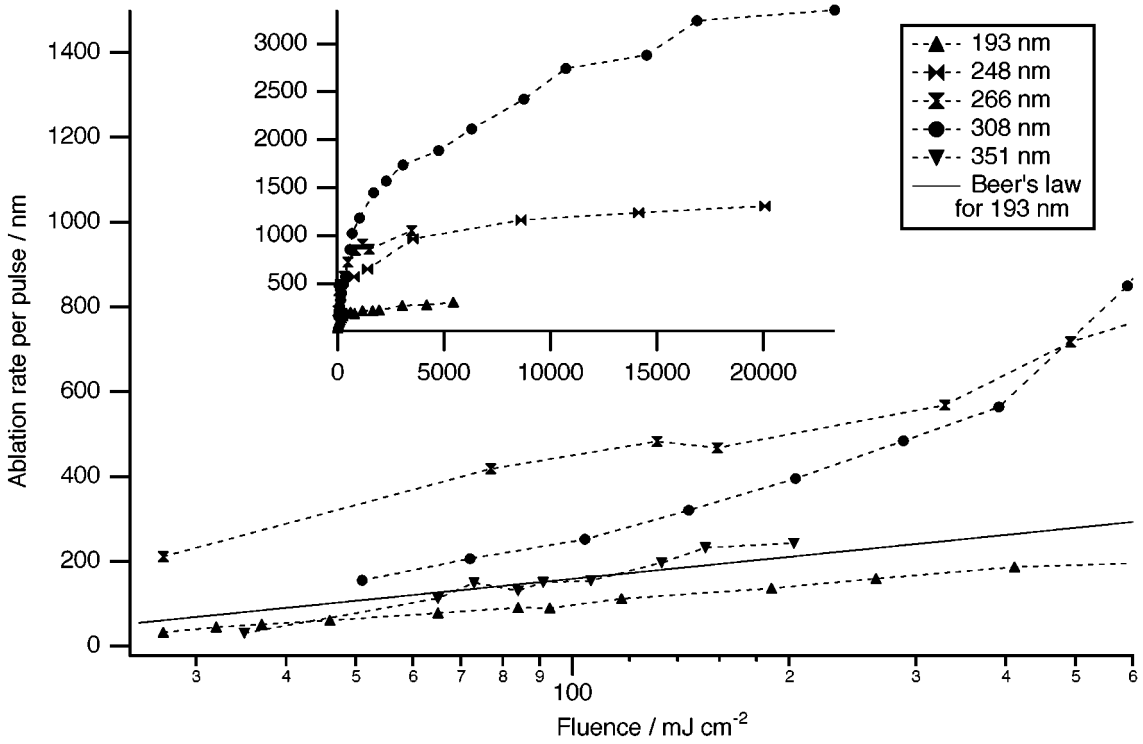

Figure 8. Measured etch rates of TP vs the logarithm of the fluence (up to 600 mJ cm-2) for different irradiation wavelengths. The inset shows the same plot for the complete linear fluence range. [From ref 109, copyright 2002, with permission from Elsevier Science].

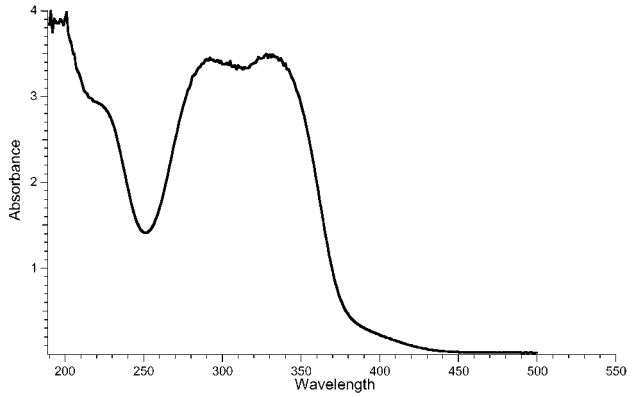

Figure 9. UV−Vis spectrum of a thin film of the triazene-polymer on quartz (cast from chlorobenzene). The chemical structure is shown in Figure 12.

was employed that produces a series of shadowgraphs of the air−polymer interface. Pictures taken shortly after the laser pulse show high velocity plume material which drives a blast wave in the surrounding air. At times less than 100 ns after the peak laser intensity, only one front can be observed, but two fronts are observed at later times. Figure 10 shows plume and blast wave fronts imaged at a fluence of 250 mJ cm^{-2}. The photos also confirm the absence of solid products, as suggested from the lack of redeposited material. The advance of these supersonic shock waves can be modeled by a model of the blast wave that incorporated the mass of the ablated polymer and the decomposition enthalpy of the polymer.[113] Irradiation at 193 nm yields higher shock wave speeds than irradiation at 308 nm, despite the similar absorption coefficient, presumably due to more efficient polymer fragmentation by the high-

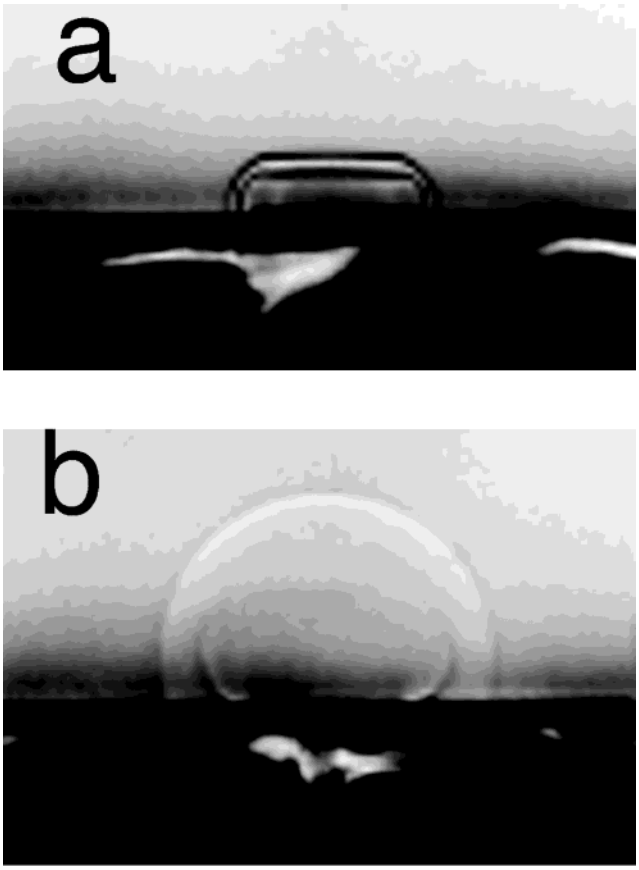

Figure 10. Nanosecond shadowgraphs showing the shock fronts formed for 351 nm irradiation with 250 mJ cm^{-2} of a triazene-polymer at 204 ns (a) and 1000 ns (b) delay. [From ref 116, copyright 1996, with permission from Springer Verlag.]

energy, 193-nm photons. The large number of small molecules at 193 nm results in higher pressures and therefore faster shock waves.[114]

Shadowgraph imaging was supplemented by nanosecond-surface interferometry.[111,115,116] Interferometric images can reveal changes in surface morphology on nanosecond-time scales, both during and after the laser pulse. Some of these changes are potentially related to photochemical and photothermal ablation mechanisms: photothermal ablation is often associated with a pronounced surface swelling and delayed material ejection, while photochemical ablation is expected to yield instantaneous etching. Interferometric images of TP at 193, 308,[114,117] and 351 nm[116] show that etching of the film begins and ends with the laser pulse (shown in Figure 11 for 308 nm

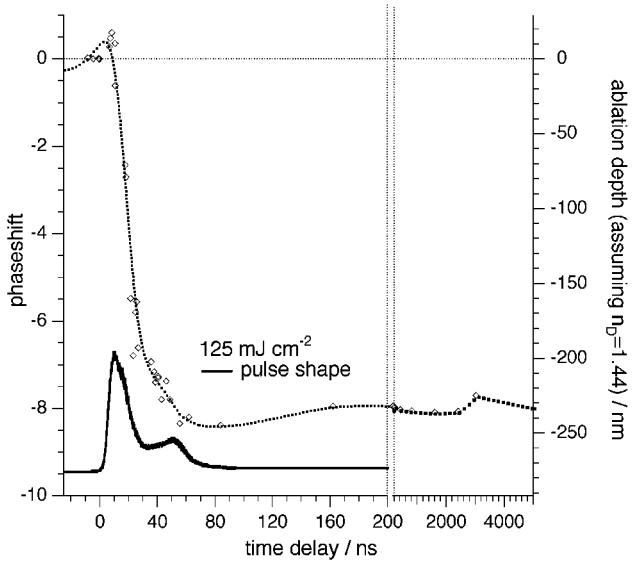

Figure 11. Ablation of the triazene polymers (with X = O, $R_1 = CH_3$, and $R_2 = (CH_2)_6$) after irradiation at 308 nm with 125 mJ cm^{-2}. The time-resolved ablation has been measured by nanosecond-interferometry.[115] A smoothed spline curve is added to guide the eyes along the data points. The relative intensity of the laser pulse is included in the figure. The ablation depths were obtained by measuring the final ablation depths with a profilometer and calibrating the observed fringe shift with this value.[117]

irradiation). In contrast, corresponding images of polyimide at 351 nm reveal pronounced swelling, followed by material removal that persists for microseconds after the laser pulse.[118,119]

Significantly, surface reflectivity measurements (probed at 532 nm) during ablation at 308 nm show a decrease in reflectivity (darkening) during the laser pulse which recovers completely after the laser pulse.[116] During ablation at 351 nm, a similar decrease in reflectivity is observed in conjunction with simultaneous increase of transmission (at 580 nm); this suggests that the decrease in reflectivity is not due to bubble formation but to photodecomposition itself.

Insight into ablation mechanisms is also provided by study of the ablation products, e.g., by mass-spectrometry. This technique is described in more detail below. Here we note that time-resolved mass spectrometry at 248 and 308 nm identified all the expected fragments of polymer decomposition (shown in Figure 12).[14,120,121] Thermal decomposition yields

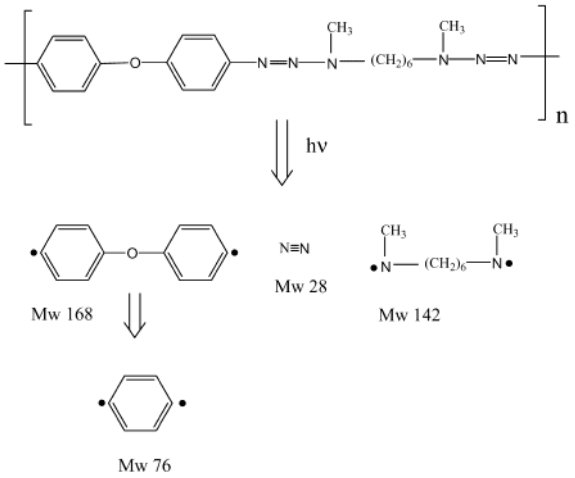

Figure 12. Decomposition pathway of the triazene polymer with all fragments that were observed in TOF-MS measurements.

similar products.[122] Importantly, three different species of nitrogen were detected in the signals, including a very fast ground state neutral (up to 6 eV of kinetic energy), a slower neutral ground state species with a broad energy distribution (probably thermal product), and a metastable (excited) neutral N_2 species.[123] The latter can only be created by an electronic excitation.

The high sensitivity and ablation quality of the triazene polymer allow one to form high quality, complex, 3-dimensional structures. Figure 13 shows

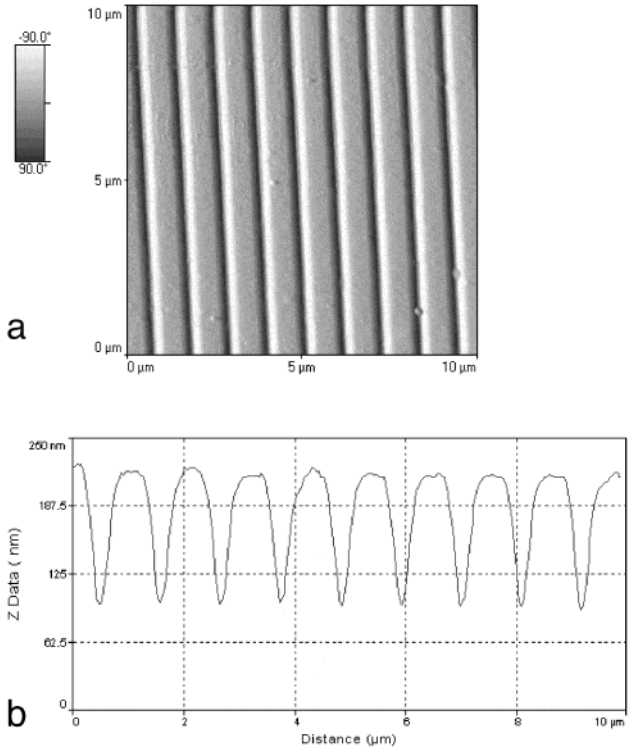

Figure 13. Holographic (interference) grating fabricated into the triazenepolymer with a single pulse of 80 mJ cm^{-2} and a 3 ns pulse at 355 nm. The grating has a spacing of 1090 nm, corresponding to the value expected from the experimental setup [Michelson interferometer, where the spacing of the grating (S) can be varied by changing the intersection angle (θ) according to $S = \lambda/2 \sin^{-1}(\theta/2)$].

an interference grating created with a Michelson interferometer.[124] Figure 14 shows a more compli-

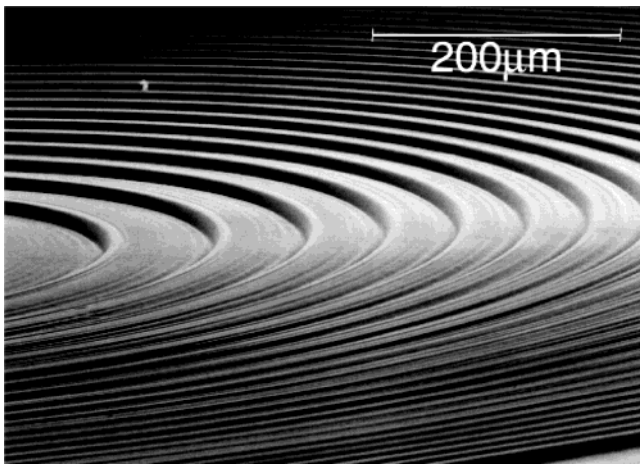

Figure 14. Fresnel lens fabricated by laser ablation, using five pulses at 308 nm and a diffractive gray-tone phase mask. [From Lippert, T.; David, C.; Hauer, M.; Wokaun, A.; Robert, J.; Nuyken, O.; Phipps, C. *J. Photochem. Photobiol. A: Chem.* 2001, *145*, 87. Copyright 2001, with permission from Elsevier Science].

cated structure (Fresnel lens) created with a gray tone phase mask using less than five laser pulses.[125] The absence of debris and undesired surface modifications allows the fabrication of high quality micro-optical elements.

The designed triazene polymers are very sensitive to laser irradiation, but are also sensitive to chemical treatments that may be applied later in an industrial process cycle, i.e., oxidation during thin film transistor production.[126] In such applications, polymers that are chemically more stabile are desired. Higher chemical stability was achieved with malonyl-ester-groups (shown in Figure 15). The synthetic procedure

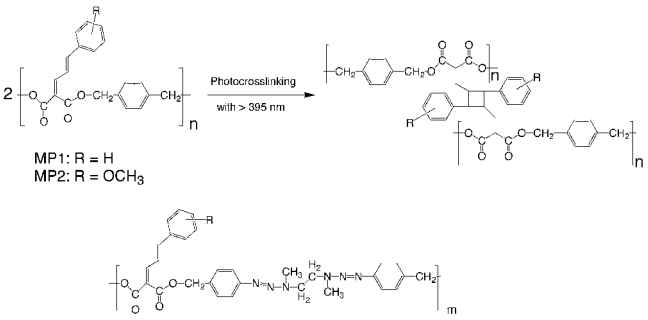

Figure 15. Chemical structure of the cinnamylidene-malonic ester polymer (MP) with different substituents R and the product of the photochemical 2+2 cycloaddition, which results in an insoluble (negative) polymer film. Cross-linking was carried out with irradiation at $\lambda > 395$ nm for 20 min and 100 mW cm^{-2}. The chemical structure of the mixed designed polymer (TM) with different substituents R is also shown.

allows for polymers with "mixed" malonyl- and triazene-functionality (structure shown in Figure 15). The malonyl polymers fulfill all the requirements for good ablation behavior, i.e., high absorptivity and gaseous ablation products (CO and CO_2). The ablation properties of the malonyl polymers are superior to commercial polymers with similar absorption coefficients (e.g., Kapton), but are somewhat inferior to triazene polymers. The threshold fluences for several malonyl and triazene polymers are plotted against absorption coefficient in Figure 16.[22] This

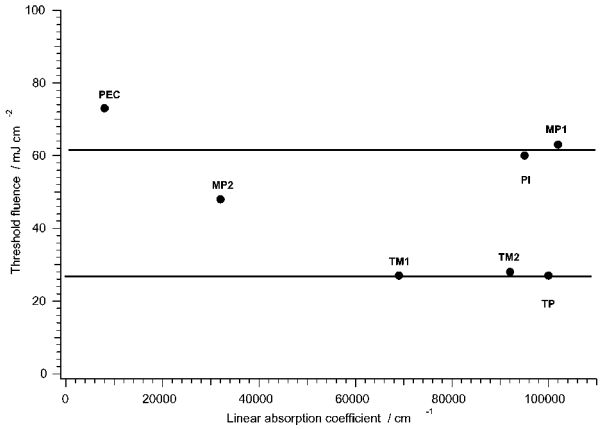

Figure 16. Comparison of the threshold fluences for various polymers as a function of the linear absorption coefficient (Lambert−Beer). PI = polyimide, PEC = polyestercarbonate, MP = cinnamylidene-malonic ester polymer (for MP1 and MP2 different substituents R are used, see Figure 15), TP = triazene polymer, and TM = the mixed polymer with a triazene and cinnamylidene-malonic ester functionality (see Figure 15). The plot shows, that the polymers with a triazene functional group (TP and TM) reveal much lower threshold fluence values, and that the absorption coefficient has no obvious influence.

comparison also shows that the absorption coefficient has little effect on the threshold fluence. All polymers containing the triazene functional group display similar low threshold fluences at 308 nm of about 30 mJ cm^{-2}. The most important factor in determining the threshold fluence is the chemical structure.

The cinnamylidene group in the side chain of the malonyl polymers can be exploited for photo-cross-linking processes (shown in Figure 15) at wavelengths longer than 395 nm. Thus, these polymers can be employed as negative resists (the cross-linked regions become insoluble and remain upon wet development) that can be subsequently ablated (positive resist, the irradiated material is removed) under conditions similar to those described above (slightly higher ablation threshold and slightly lower ablation rate). With this processing order, negative−positive resists (with ablation as positive step) are obtained. The order of processing can also be reversed with no significant change in the quality of the resulting structures.[127]

The design of polymers for ablation was a logical development, building on the design of photoresists for photolithography. Many ablation properties, including threshold fluence, ablation rate, and ablation quality, can be improved by incorporating appropriate chemical structures into a polymer. Special functionalities can be built into a polymer to tailor optical and mechanical properties. Further improvements are expected. This may create new applications for laser ablation in microfabrication. The incorporation of special chromophores, e.g., photochemically active groups, can be used to study ablation mechanisms from a fundamental point of

view. In the case of the designed triazene polymers, several experimental techniques indicate that photochemistry plays an important role. For example, TOF-MS evidence for a metastable product suggests that dissociative electronic excitations play an important role, while other emission components indicate a possible role for thermal processes (details see below). Other data, e.g., etching rates during the laser pulse, low ablation thresholds, the lack of surface modification, and the relative etch rates of different polymers, support the importance of photochemical processes.

2.2.4 Commercial Polymers

The ablation of commercially available polymers have been studied extensively. Of these, polyimide (PI), poly-methyl methacrylate (PMMA), polyethylenterephthalate (PET), and various fluoropolymers, such as Teflon (PTFE), are most well studied. (The structural schemes are shown in Figure 17.) Due to

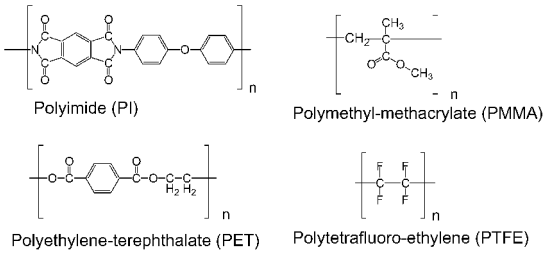

Figure 17. Chemical structures of the most studied commercial polymers.

the large number of publications, only a limited number of works can be discussed and cited here.

Polyimide (Kapton). Polyimide (PI) is probably the most studied polymer, as it can be ablated with all common excimer lasers and pulse lengths,[44] and because its material properties are well characterized. Therefore, many ablation models are based on data taken on PI (see above). PI is also technically very relevant, serving as a dielectric in microelectronics for multichip modules[128,129] and printed circuit boards,[130] as a substrate for inkjet printer nozzles,[5] and as a precursor for graphite materials.[131] PI characteristically carbonizes during laser ablation, a fact that can be exploited to produce conducting surface layers (discussed in more detail below). The decomposition mechanism had been probed by several time-resolved techniques, including shadowgraphy,[45] interferometry,[118] transmission,[15,29,30] and reflectivity.[15] Surface analysis[106,132−138] after irradiation has also been exploited.

Nanosecond shadowgraphy[45] shows that all the excimer wavelengths yield similar blast waves. Nevertheless, the nature of the ejected material depends strongly on laser wavelength. At 248 nm, only a faint trace of opaque material is visible in shadowgraphs. As the wavelength is increased (308 nm and 9.17 μm), increasing amounts of solid material are observed. Interferometry measurements[118] confirm this observation. At 248 nm, material removal from PI was confined to the duration of the laser pulse and yielded no solid debris; at 351 nm, pronounced surface swelling was observed, followed by the ejection of solid particles and prolonged material removal. This was interpreted as a shift of the ablation mechanism from photochemical (248 nm) to photothermal at 351 nm.

The ablation products have been analyzed using emission spectroscopy,[137,139] gas-phase FTIR,[18] gas chromatography−mass spectrometry (GC-MS)[140] and quadrupole MS.[141] Mainly low mass species are detected by emission spectroscopy, i.e., C_2 and CN. In addition, mass spectroscopy identified molecules with masses corresponding to C_2H_2, HCN, CO, CO_2, C_4H_2, C_6H_2 (phenyl radical), C_6H_5-CN, C_6H_5-CNO, and a species at mass 153 amu assigned to a cyanonaphathalene species.[141]

Transient optical properties were measured by time-resolved transmission, reflectivity, and scattering measurements. At 193 nm, a sharp increase in transmission and decrease in scattering and reflectivity during the laser pulse is observed,[15] consistent with a significant change in refractive index at fluences above a certain threshold. Possible mechanisms for this behavior include: rapid thermal decomposition, ground-state depletion (photochemical model; see above and refs 30−32), and a thermal phase transition.

Significantly, quartz crystal microbalance (QCM) measurements of mass loss at 193 nm show no evidence for an Arrhenius tail, consistent with a more photochemical ablation mechanism.[13] As noted above, the pronounced Arrhenius tails at the longer wavelengths are consistent with mainly thermal mechanisms.

Surface analysis by XPS[106,132−136] and Raman-microscopy[106,107] show carbonization in the irradiated area, with more extensive carbonization in the surrounding area. Raman microscopy indicates that this carbon is principally amorphous, with some crystalline features. TEM observations indicate that the thickness of the carbon deposits surrounding the crater increases with the number of pulses, while the area increases with the fluence.

Further identification of the decomposition products was probed by diffuse reflectance infrared Fourier transform spectroscopy (DRIFT) after irradiation at 308 nm.[137] These products show important differences to those observed for thermal decomposition.[138] Suggested decomposition schemes for laser-induced decomposition at 308 nm and for thermal decomposition are indicated in Figures 18 and 19, respectively. Under 308 nm irradiation, initial decomposition appears to occur at two sites: the phenyl-O and the N−C bond (Figure 18). Initial decomposition during heating appears to be confined to the C−N bond (Figure 19). In both cases, further decomposition produces small carbon containing fragments, which form the bulk of the observed carbon deposits. The similarity of these decomposition mechanisms and the resulting fragments help account for much of the controversy concerning the ablation mechanism.

Laser-induced carbonization can increase the electrical conductivity of polyimide surfaces by up to 17 orders of magnitude[142,143] with submicron spatial resolution.[144] Practically, this treatment requires fluences just above the ablation threshold,[145] where a thin polymer layer (0.5 to 2 μm thick) is trans-

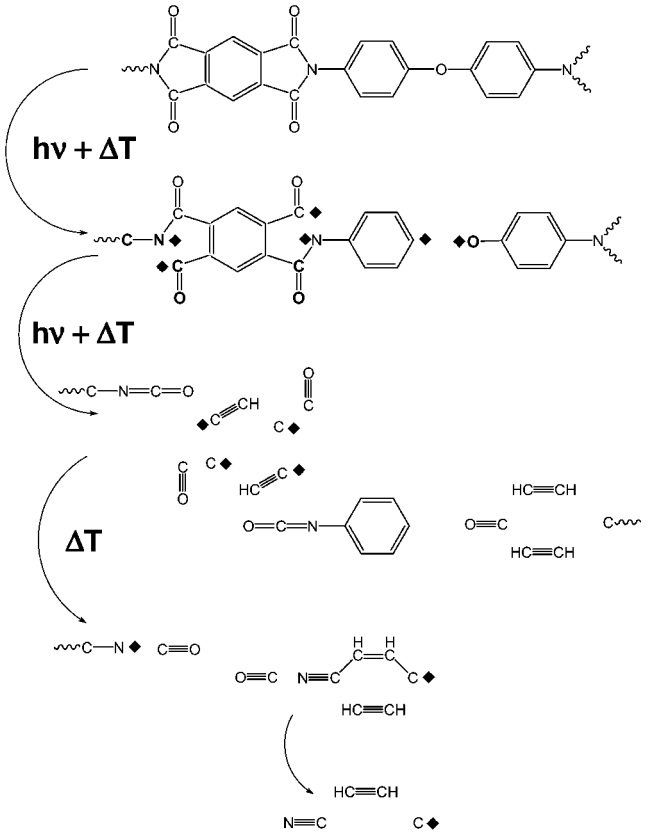

Figure 18. Suggested decomposition scheme of the laser-induced decomposition of PI with 308 nm irradiation. The different functional groups, gaseous products, and decomposition steps were assigned from DRIFT, mass spectrometry, and emission spectroscopy. ♦ indicates a broken bond; information on the character (radicalic, ionic, terminated) is not available from the experiments.

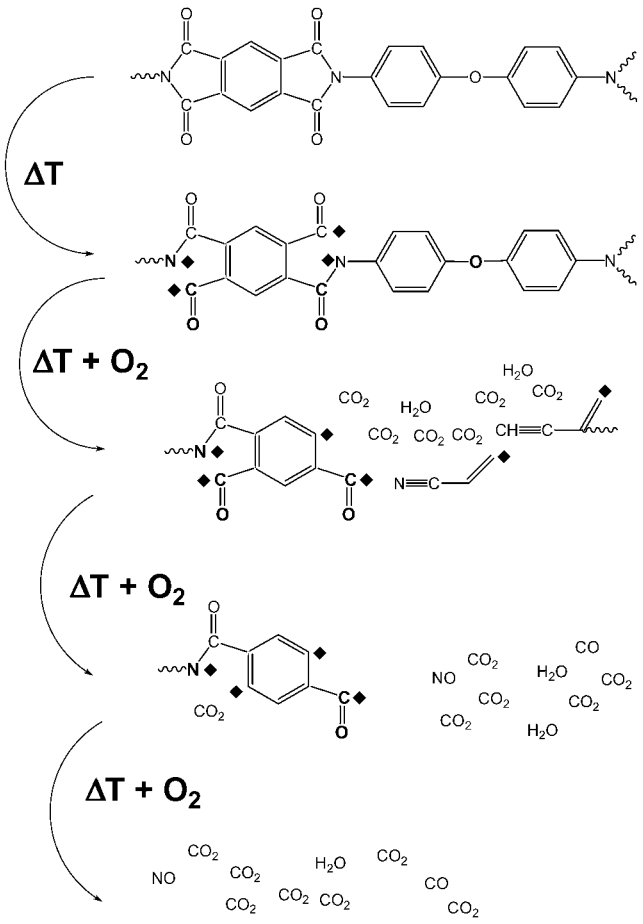

Figure 19. Suggested decomposition scheme of the thermal decomposition of PI. The different functional groups, gaseous products, and decomposition steps were assigned from DRIFT and mass spectrometry, assuming a total oxidation. ♦ indicates a broken bond; information on the character (radicalic, ionic, terminated) is not available from the experiments.

formed into carbon clusters of 50−100 nm in diameter. The cluster density increases from pulse to pulse until a conducting path is formed. The formation of the carbon layer most probably involves thermal mechanisms. The conductivity is also influenced by the laser repetition rate (1−40 Hz at 248 nm) and the ambient temperature.[146] At higher ambient temperatures and laser repetition rates, more polycrystalline graphite-like clusters are formed, resulting in higher conductivities.

In some cases, carbonization can significantly affect the ablation rate. At lower fluences, it can be impossible to ablate holes through the thickness of sheet-like samples due to the accumulation of carbon inside the ablation crater; carbon has a higher ablation threshold than pure polyimide, and therefore acts as an lithographic mask.[147]

Irradiation of PI at 248 nm (KrF excimer, repetition rate of 250 Hz) using a mask projection system[148] can produce microhumps 17−150 nm high and 1−3 μm wide surrounding the ablation crater. Hump formation has been attributed to a diffraction effect which exposes the region surrounding the ablation crater to subthreshold laser fluences. The resulting heat and thermal deformation produces the microhumps. These microhumps are not comparable to the structures described below (due to swelling), but are formed by cumulative heating of the polymer by the high repetition rate laser. Although some have suggested that repetition rate effects in PI may become important at a few Hz,[149] others suggest that tens of kilohertz may be required.[150]

PMMA. PMMA has also been extensively studied. In contrast to PI, the ablation of PMMA requires wavelengths less than 308 nm. Ablation at 308 nm yields poor quality structures,[151] due to the very low absorption coefficient; but ablation at 248, 222,[152] 216,[153] and 193 nm yields high quality structures.[154,155] At 193 nm direct structuring is possible, while at most other wavelengths significant incubation is observed.

Incubation is often observed in weakly absorbing polymers (e.g., with film absorption coefficients < 8000 cm^{-1}). Stuke[156] and Srinivasan[157] showed that chemical structures produced during incubation gradually raise the absorption coefficient until ablation starts. The number of pulses required to initiate ablation at a given wavelength and fluence is defined to be the incubation pulses. Stuke et al.[156] showed that a broad UV absorption band appears simultaneously with the FTIR signature of unsaturated species. Even CW UV light from Hg lamps can be used to incubate the material; after incubation, ablation is readily induced at longer wavelengths (e.g., 308 nm).

Srinivasan et al.[157] showed that material is removed as vapor during incubation, although no surface etching is observed. Incubated material is soluble in many solvents and can be removed without dissolving the PMMA. Material incubated at 248 nm consists of PMMA with a lower molecular weight and C=C chain ends.[158] Incubation proceeds by photochemical reactions that create defects which serve as absorption sites, while the resulting ablation is more thermal in nature.

The ablation products identified by TOF-MS are also consistent with an initial photochemical reactions (incubation) followed by a more thermal ablation.[159] A possible decomposition scheme for PMMA with incubation and ablation steps is shown in Figure 20. Steps 1−3 are principally associated with incubation, while Step 4 is an unzipping reaction (= depolymerization) which may be either thermal or photochemical. The photochemical incubation reactions are readily observed under low fluence irradiation of PMMA at 248 nm; these reactions induce small changes in the refractive index.[160] Similar photochemical reactions are presumably responsible for surface reflectivity decreases during ablation at 193 nm; the drop in reflectivity is followed by material ejection and shock wave formation.[161] Nanosecond shadowgraphy shows pronounced differences between ablation at 193, 248, and 9.17 μm.[162] The main product of IR ablation is a volatile refractive vapor, most likely MMA (methyl-methacrylate), while irradiation with the UV wavelengths yields mostly gaseous products with a small amount of MMA.[162] Monomer creation is expected to involve an unzippling reaction similar to that shown in Figure 20, Step 4. Unzipping is a depolymerization reaction, where the polymer chain fragments into its constituent monomer units. In PMMA, unzipping is catalyzed by chain end radicals, formed when the PMMA chain is broken. At 443 K, up to 200 MMA units may be formed for each chain end radical.

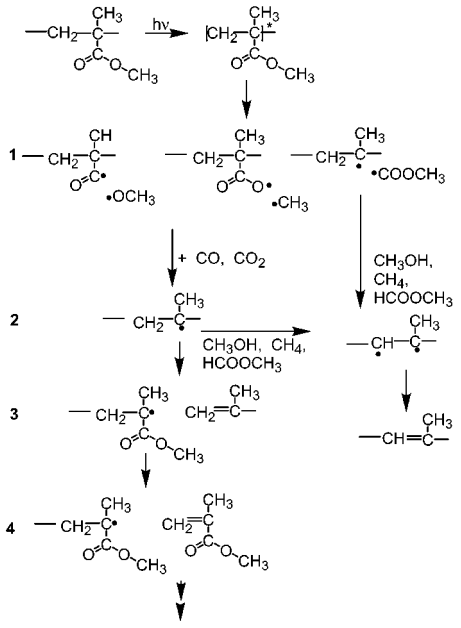

Figure 20. Suggested decomposition scheme for the laser-induced (308 nm) decomposition of PMMA. Steps 1 and 2 show the photolysis of the ester side chain, the typical small products detected in mass spectrometry measurements, and the double bonds that are created during incubation (chain end and chain). Step 4 shows the photochemical and thermal activated reaction to release MMA (= decomposition).

MMA has also been identified as product of PMMA ablation using CARS (coherent anti-stokes Raman spectroscopy) during picosecond, near-IR irradiation (1064 nm).[163] Raman band shifts were used to infer a temperature jump to 550 K, certainly high enough to decompose PMMA thermally.[164] The ceiling temperature of PMMA (the temperature at which the equilibrium concentration of the polymer goes to zero and the equilibrium concentration of monomer reaches 100%) is only 550 K. Although many of the small fragments detected during PMMA ablation[159] may be formed by photochemical process, in the case of the monomer, thermal effects must be important as well. Additionally, it is noteworthy to mention that the higher temperature jumps associated with UV lasers relative to the IR lasers may induce additional decomposition of the main thermal product MMA. The resulting small fragments are then quite similar to the fragments obtained by photochemical reactions.

Other Polymers. Other polymers that have been studied in detail are poly(ethylene terephthalate) (PET) and the fluoropolymers. The ablation of PET has been studied at 157,[165] 193,[166−168] 248, 266,[169] and 308 nm.[170] At 157 nm, ablation yields mainly gaseous products. The low ablation threshold at 157 nm suggests that photochemical processes contribute significantly.[165] Most recent studies have been directed at the analysis of chemical and physical changes of the surface. Chemical changes were probed by XPS,[171−176] surface-enhanced Raman scattering (SERS)[172] and by color tests.[177] The XPS and SERS data suggest a decrease of the surface oxygen content, while the color test indicated the formation of OH and CHO groups. At 248 and 308 nm, the surface crystallinity of the surface is also reduced during ablation;[172] in contrast, a high degree of surface crystallinity is reported for ablation at 193 nm.[178] Changes of the physical topography are discussed in more detail below.

Fluoropolymers (poly(tetrafluoroethylene)-PTFE-Teflon;[179−185] ethylen-tetra-fluoroethylene copolymers,[186] poly-vinylidene fluoride-PVdF[187]) are all important commercial polymers with technical applications. PTFE in particular absorbs only weakly at wavelengths longer than 193 nm, and is thus a prime candidate for ablation with femtosecond laser pulses (discussed below). Recent studies, e.g., by shadowgraphy,[179,185] have been undertaken to distinguish among the proposed ablation mechanisms, which include multiphoton effects (PVdF and the copolymer)[186,187] and photothermal degradation (PVdF).[187] Thermal unzipping reactions are especially important in the case of PTFE.[180−182]

One of the most valuable characteristics of PTFE, its chemical inertness, is a liability in applications that require metallization or coating. Laser treatment (e.g., at 193 nm), either in reactive atmospheres

(e.g., hydrazine)[188,189] or under various liquids [e.g., $B(CH_3)_3$],[190,191] can break F−C bonds and promote additional reactions to produce more suitable surfaces for coating. These surface modifications take place without detectable ablation. Alternatively, surface modification can be generated by low fluence VUV sources (e.g., excimer lamps[192,193] or helium microwave plasmas[194]). Irradiation with excimer lamp (Xe_2* at 172 nm) in reactive atmospheres, for instance, effectively modifies PTFE and poly-tetrafluoroethylene-*co*-hexafluoropropylene (FEP) surfaces.

2.3 Summary of Miscellaneous Polymer Work

To illustrate the wide variety of polymers whose ablation properties have been studied in less detail, a partial list of studies follows:

(i) Polyethylene-glycol (PEG):[195,196] Ablation at 193 nm has been studied with shadowgraphy for liquid and solid samples. (PEG melts at 35 °C.) Plasma and shock wave development are independent of state, although differences in material ejection are detected. Dense material clouds are observed from solid samples, while liquid samples yield vapor and droplets.

(ii) Polyethylene (PE):[197] PE ablation at 193 nm has been studied using HeNe probe beam deflection, laser transmission, and scanning electron microscopy (SEM). PE is a weakly absorbing polymer (500 cm^{-1} at 193 nm), and, as expected, displays pronounced incubation behavior due to photoinduced chemical modifications.

(iii) Polypropylene (PP):[198] Studies at 248 nm suggest that both photochemical and thermal effects operate during ablation.

(iv) Polycarbonates (PC):[91,199,200] At 308 nm, PC displays poor ablation quality. Ablation quality can be improved by modifying its chemical structure (see above, designed polymers). Incorporation of TiO_2 does not improve the ablation quality significantly at 248 nm. At 193 nm, sharp ablation contours are obtained, but at fluences below 600 mJ cm^{-2} cone-like structure are formed. The formation of these structures is attributed to impurities in the polymer (discussed in more detail below).

(v) Cycloolefin (COC):[201] At 193 nm, high quality structures can be formed in COC with no debris. These structures are suitable for microfluidic applications.

(vi) Polyether-etherketone (PEEK):[202] At 193 nm, irradiation produces polar groups along the surface that are absent under 248-nm irradiation. The absence of surface polarity at 248 nm is attributed to enhanced thermal effects.

(vii) Chlorinated rubber (CR):[203] The removal of CR from concrete by laser ablation at 10.6 μm (CO_2 laser), 810 nm (diode laser), and 193 nm (ArF laser) has been studied. CO_2 lasers yield the highest ablation rates, but complete removal is not obtained. ArF lasers exhibit fine control of removal, but yield low ablation rates. Diode lasers yield intermediate results and present an alternative to the other two more costly and bulky laser systems.

(viii) Nylon-6,6 [= Polyamide-6,6 (PA)]: Irradiation with XeCl (308 nm), Nd:YAG, and CO_2 lasers yields pronounced thermal damage, suggesting that a thermal ablation mechanism dominates from 308 nm to 10.6. μm.[204] Ablation craters formed at 248 nm have been analyzed by SEM and described phenomenologically. [205]

(ix) Proteins: Studies have ranged from the laser-ablation deposition of silk films,[206,207] to the wavelength-selective transformation of the secondary structure of silk,[208] to the structuring of insect exoskeletons.[209]

(x) Polyurethane (PU):[210] Ablation rates at 248 nm for commercially available PU (as opposed to the special designed PU's described above) have been studied by QCM and stylus profilometry. The data from these two techniques are in good agreement, although lower threshold fluences are obtained by QCM. The lower QCM results are attributed to outgassing, surface chemistry, or some low quantum-yield process.

(xi) Silicone Rubber (SR):[211,212] At 193 nm, $(Si-O)_n$ species are ejected from SR films.[211] Pronounced incubation behavior is observed at 266 nm; OH and Si−O groups are formed during incubation.[212]

(xii) Conducting polymers: Conducting polymers have promising applications in microelectronics as semiconductors or metal-like conductors. The ability to pattern these materials on micron or submicron scales would facilitate applications in all-organic devices (light emitting diodes, thin film field effect transistors or Schottky-barrier devices). Patterning can be achieved by patterned polymerization or doping,[213] by laser ablation,[214] and plasma etching.[215] Three classes of conducting polymers have been studied to date: poly-thiophenes (PTP), polypyrroles (PPY), and poly-aniline (PAN). PPY and PAN have been ablated and patterned with a resolution of around 50 μm at 308 nm.[214] PAN has also been structured in doped and undoped (nonconducting) form at 308 nm; comparable ablation rates are obtained for both forms.[216] This suggests two possible processing strategies: structuring the nonconducting material followed by doping, and structuring of the doped, conducting material. No ablation debris is detected adjacent to the structures, but XPS reveals carbonization inside the ablation crater (with the imine group as preferred decomposition site). PTP can be structured with He−Cd lasers at 442[217] and 325 nm[218] with line widths of 1−6 μm. Direct structuring of PTP derivatives can also be achieved at 193 and 248 nm,[219] with ablation thresholds as low as 30 mJ cm^{-2}. Emission spectroscopy indicates a higher degree of fragmentation at 193 than 248 nm. Observation of a thermochromic PTP derivative indicates that the polymer films are heated above their melting point (136 °C) at 193 nm.[220]

Despite the large number of studies of the ablation of commercial polymers, many open questions remain. This is true even for PI and PMMA, which have been studied for more than 20 years. New techniques and methods yield data that sometimes do not fit into the current understanding of ablation. A large body of data strongly supports photothermal

ablation mechanisms, especially in the case of PI and PMMA; but other studies provide evidence for photochemical processes. This is especially true at low fluences for PMMA, where incubation involves photochemical reactions. At higher fluences, photothermal processes may be more important, but to exclude photochemistry completely is too extreme. The same is true for PI, which is THE classical polymer for thermal ablation studies. Even for PI, the products of ablation by excimer lasers and thermal decomposition are not identical. Pronounced differences in nanosecond interferometry measurements at 351 and 248 nm suggest the operation of nonthermal processes, at the shorter ablation wavelength. These results are supported by QCM measurements at 193 nm.

The ablation behavior of designed polymers and commercial polymers taken together suggests that photothermal vs photochemical mechanisms are occurring simultaneously. In the case of PI and PMMA, thermal processes are dominant. Nevertheless, pure thermal models cannot explain all the data. In the case of the highly absorbing, designed polymers, photochemical processes dominate. Yet even here thermal processes contribute. This is especially true in view of the exothermic nature of decomposition (both photochemical and thermal) and strong UV absorption in these materials. Thus, high temperatures are expected for any decomposition of the designed polymers.

3 Selected Experimental Tools

3.1 Single Pulse Ablation with Various Pulse Lengths

Bäuerle[3] has emphasized the value of single-pulse ablation studies as a function of pulse length, with tightly focused beams, in revealing ablation mechanisms. Under these conditions:

(i) Photochemical processes should depend on the product of intensity (I) and pulse length (τ_l), while photothermal and photophysical processes should depend more strongly on τ_l.

(ii) Changes in physical and chemical properties due to successive laser pulses are avoided, including the changes in material parameters responsible for incubation.

(iii) Shielding of the incident laser beam by the ablation plume, a problem with nanosecond pulses and larger spot sizes, can be ignored. For tightly focused beams, the expansion of the vapor plume is essentially three-dimensional. Then plasma shielding can be igorned even at relatively long pulse lengths.

Single pulse laser experiments of PI at 302 nm (Ar ion laser) and pulse lengths between 140 ns and 50 ms have been performed using an acousto-optic modulator to control pulse length.[10,221,222] Changes in surface topology and the crater depths have been studied by atomic force microscopy (AFM). As the pulse length is increased, the threshold fluence increases in a power law fashion (slope of 0.36 on a log−log plot), consistent with a thermal model.[223] Quantitative agreement was especially good for pulse lengths $\tau_l > 100$ ns, where the heat penetration depth exceeds the optical penetration depth. Surface swelling (about 20 nm) is observed at fluences below the ablation threshold, possibly due to amorphization, but more likely due to trapped decomposition fragments.

These data strongly support a thermal decomposition mechanism for PI, at least for pulses longer than 100 ns. (These pulses are longer than typical 10−30 ns excimer laser pulses.) AFM and single-pulse ablation are powerful tools for the analysis of polymer ablation, but careful sample selection (preparation) is of utmost importance, as surface contamination and skin layers (e.g., detected on PMMA[159]) may alter ablation properties. It would be interesting to see whether this model applies to other materials, e.g., the designed polymers.

3.2 Mass Spectrometry

3.2.1 Review of Recent Experimental Work

Mass spectrometry plays an important role in ablation studies. Simply identifying the ablation products can provide valuable clues to the underlying ablation mechanisms. Mass spectrometry (MS) is readily extended to yield time-of-flight (or more accurately, time-of-arrival) information on selected products. Time-of-arrival experiments have also been performed by measuring the rapid change in reflectivity of a substrate that was used to collect the ablated material.[224] With care, time-of-flight mass spectrometry (TOF-MS) can often be analyzed to yield detailed information about product energy distributions—another important clue to ablation mechanisms.

Mass spectrometric studies have been performed on a variety of polymers, often as a function of laser wavelength and fluence.[225] Analysis of the ejected material has revealed ionic and neutral species with masses ranging from small degradation fragments,[226,227] to monomers from unzipping reactions,[228,229] to large carbon clusters,[230,231] and finally to polymer fragments with molecular weights of up to 2500.[139,232] In a time-resolved study, Shibagaki et al. have observed the growth of ion clusters in the ablation plume.[233] For polystyrene, poly(tetrafluoroethylene) (PTFE), and poly(methyl methacrylate) (PMMA), many of the neutral fragments have Maxwell−Boltzmann energy distributions corresponding to surface temperatures appropriate to photothermal decomposition.[234−236] In the case of polystyrene at 193 nm, an adiabatic expansion model yielded temperatures of about 2350 K.[237] When absorbing chromophores are deliberately added to PMMA, a combined photochemical/photothermal mechanism is evident.[159]

Most TOF-MS studies show strong indications for photothermal ablation mechanisms. This is especially true of polymers that are relatively transparent at the laser wavelength. The energy densities require for thermal decomposition are much lower that those required for wholesale photochemical decomposition. As one might expect, photochemical processes are more apparent at deep UV wavelengths.[238,239] Specially designed polymers, with chromorphores that absorb strongly at the laser wavelength, can show significant photochemical effects. Typical mass-selected time-of-flight signals from a designed tria-

zeno-polymer detected at a charge-to-mass ratio of 28 (N_2) under 308 and 248 nm irradiation appear in Figure 21. The peak in chromophore absorption is close to 308 nm; although absorption is much weaker at 248 nm, the absorption can still be characterized as strong.

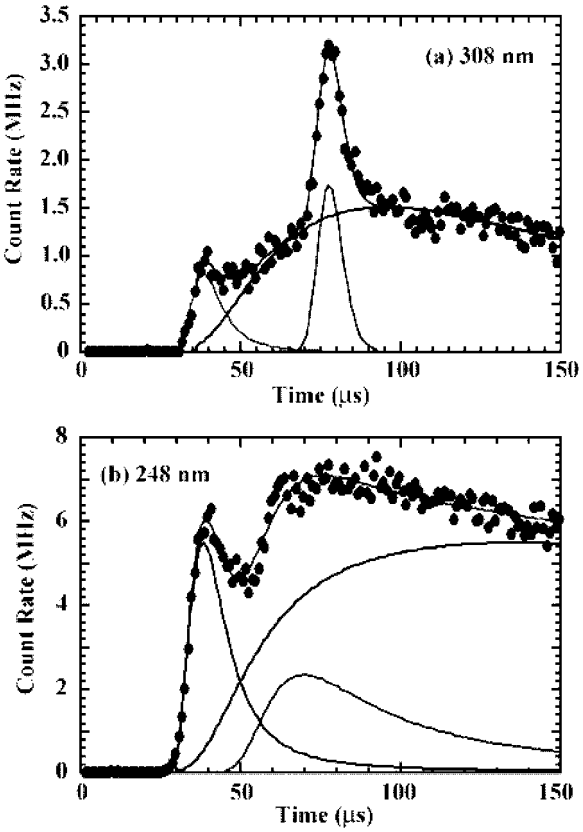

Figure 21. Mass-selected neutral signals acquired at a charge-to-mass ratio of 28 (N_2) from a designed triazene polymer under excimer laser irradiation at (a) 308 nm and (b) 248 nm. The fluence in each case was about 200 mJ/cm2. The fast emission component on the leading edge is attributed to hyperthermal neutral N_2. The broad, slow emission component continues for hundreds of microseconds after the laser pulse and is consistent with thermal emission. Near the center of each plot is a moderately fast peak that does not mass select, is not affected by electric fields, and requires a line-of-sight path to the detector; this peak is attributed to metastable N_2. The high kinetic and internal energies of the fast and metastable emissions indicate a photochemical origin.

Nitrogen emission from the designed polymer shows two distinct populations: a fast component with kinetic energies of 3−6 eV, and a broad slower component consistent with thermal or thermalized products. A third peak appears at all mass settings and is not affected by applied electric fields (including the sign of the bias voltage on the quadrupole detector). In the absence of a line of sight path, this peak is not observed (as in ref 240). This third peak is attributed to metastable N_2 ($A^3\Sigma_u^+$). Both the fast and the metastable N_2 molecules must have photochemical, rather than photothermal origins.

The fate of energy deposited in electronic excitations is poorly understood in many polymer systems. In the designed polymer described above, some products are clearly produced by dissociative electronic transitions. A significant fraction of the energy required to excite these transitions typically appears as kinetic energy of the products. Nevertheless, rapid thermal relaxation of electronic excitations into thermal modes can yield thermal decomposition as well.[241] The cyclic multiphoton absorption process described above is an important example.

In the case of the photosensitive triazeno-polymer, the energy distribution corresponding to the slow N_2 component in Figure 21 is consistent with photothermal decomposition if one allows for very high, transient thermal spikes (> 3000 K).[120] As a function of fluence, the peak intensity of the principal product, N_2, can be fitted with an Arrhenius type -function that includes the measured activation energy of thermal decomposition.[121] The intensity of this quasi-thermal slow peak is much higher at laser wavelengths well above the center of the chromophore adsorption (248 nm in Figure 21), suggesting that excess photon energy appears in vibrational modes. Similarly, the more photochemical fast and metastable peaks are broader at 248 nm than at 308 nm, consistent with thermal broadening. The excited states produced at 248 nm may be highly excited vibrationally, as well as electronically.

A definitive determination of the role of thermal processes in this and similar materials will require a more thorough understanding of the role of collisions in the bulk and gas phase (after emission). Measurements at higher fluences (which would saturate the detectors in Figure 21) may be necessary to probe conditions more relevant to etching applications. Even if thermal decomposition plays a significant role in decomposition, the high energy densities near the surface may mitigate many of the negative consequences of thermal decomposition at lower excitation densities, including droplet formation, redeposition, and extensive heat-affected zones.

In addition to providing information on ablation mechanisms, mass spectrometry provides important inputs for laser ablation of polymer films. In general, one desires a high fraction of monomers and dimers in the ablation products, but a small fraction of lighter, energetic species are also required. Laser ablation mass spectroscopy can also be useful in special cases to identify unknown polymeric materials. Matrix-assisted laser desorption/ionization in conjunction with mass spectroscopy is a similar technique for determining the composition of large molecules.

3.2.2 Analysis of Neutral and Ionic Emissions

Much of the value of TOF mass spectroscopy is its ability to discriminate between various models of the emission process. In practice, discrimination is limited to relatively simple systems that can be described in terms of a few variables. More complex systems are often ambiguous and not unique. With enough free parameters, one can metaphorically "fit an elephant"—that is, fit the data even if the model is physically inappropriate. In complex systems, one must often be content with demonstrating consistency between a certain model and the data, although it helps if the model parameters can be compared

with independent measurements. Such comparisons are complicated by our lack of knowledge of polymer properties at the high (and rapidly changing) temperatures associated with laser ablation.

The most direct information about emission processes is obtained when the observed products experience no collisions as they travel from the polymer to the quadrupole detector. Assuming monatomic products only, this requires etch rates (during the laser pulse) less than about 0.1 nm/ns.[242] Because polymer ablation typically yields large numbers of heavier fragments, higher etch rates are required to violate this condition. Collisions after emission change the TOF distribution. This deviation is relatively easy to detect for simple models, where they create poor model fits or unphysical model parameters. Grivas et al.,[243] for instance, analyzed the TOF distribution for a variety of species produced when PP and PE are exposed to 248-nm radiation. The failure of a Maxwell−Boltzmann distribution to describe their data was attributed to collisions. Applying a model appropriate to collision-shifted TOF distributions, they concluded that ablation was largely photothermal, with important multiphoton absorption effects.

An especially straightforward emission mechanism to model is the case of neutral particles when emission is confined to the laser pulse (a delta function in time) in thermal equilibrium with a surface at a constant temperature. Although the surface temperature is definitely not constant, this approximation works when product formation is rate-limited by a thermally activated step at high temperatures. In this case, almost all the product is formed as the surface reaches its peak temperature, toward the end of the laser pulse. For nanosecond pulses, the product is often in thermal equilibrium with the surface at this temperature, and is emitted with a velocity distribution consistent with the Maxwell Boltzmann velocity distribution for effusing particles.

Experimentally, one must also account for the time required for the detected particles to pass through the quadrupole mass filter. Although particles may travel from the surface to the quadrupole ionizer with a constant velocity, detected particles must be ionized before passing through the mass filter. These ions are created at a positive potential energy, typically about 15 eV, and pass through the mass filter with this kinetic energy. For thermal emissions, the ion energy is much greater than the initial thermal velocity, so that the time through the mass filter is a simple function of ion energy, filter length, and particle mass. For travel times through the mass filter t', the signal intensity at time t after the laser pulse due to particles of mass m and effective surface temperature T is given by:

$$I(t) = \frac{ANd_I}{2\pi(t-t')^4}\left(\frac{m}{kT}\right)^2 \exp\left(\frac{-md_I^2}{2kT(t-t')^2}\right) \quad (2)$$

where A is the quadruple sensitivity (amps per molecule per m^3 measured at the ionizer), N is the total number of emitted particles of mass m, d_I is the distance from the sample to the ionizer, and k is the Boltzmann constant. Equation 2 strictly applies only to particles emitted normal to the emitting surface, and when the particle density in the ionizer is uniform. If the distance d_I is not much greater than the physical dimensions of the ionizer, the particle density at the ionizer will not be uniform. Equation 2 is readily generalized to nonuniform particle densities and off-normal emission.

The thermal model incorporates only two parameters (a parameter equal to the product of A and N, and the effective surface temperature T) and is rather inflexible. Deviations from the model assumptions, including those due to collisions, are typically clear when present. In addition, eq 2 is normalized: if the quadruple sensitivity A is known, the total number of emitted particles N can be estimated from the resulting curve fit. (The quadrupole sensitivity can be estimated from the signal due to a known partial pressure of a gas with an appropriate mass.) Equation 2 can be used to estimate effective surface temperatures without performing an actual curve fit, because it predicts a definite relation between the temperature and the location (in time) of the intensity peak.[244] Nevertheless, curve fitting provides a valuable check on the assumptions of thermal emission, delta function source, and collisionless flight.

When applied to the PTFE monomer produced during 248-nm laser irradiation (30-ns laser pulses), curve fits of eq 2 yield physically plausible surface temperatures that increase linearly with fluence.[228] PTFE undergoes thermal unzipping at elevated temperatures, consistent with a thermal decomposition mechanism (shown in Figure 22 a for the C_2F_4

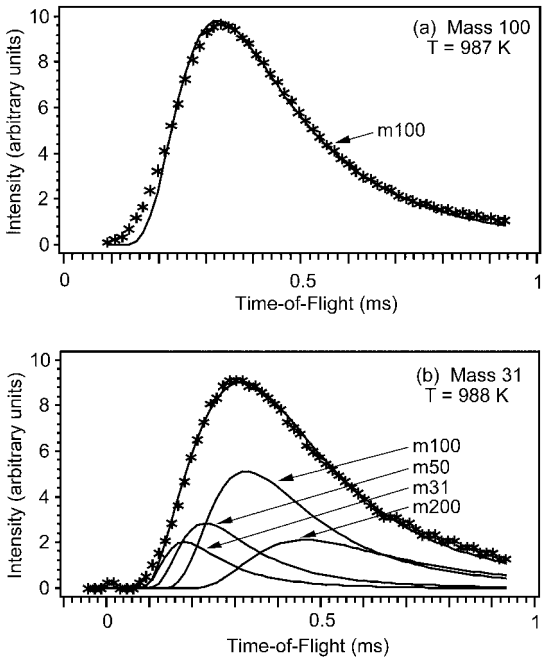

Figure 22. Time-of-flight curves for neutral emission from PTFE detected with a quadrupole mass filter tuned to (a) 100 amu/e (the PTFE monomer) and (b) 31 amu/e (CF). The sample was treated with 30-ns pulses of 248-nm radiation at 2 J/cm2. The dark lines show curve fits to Maxwell Boltzmann distributions [from eq 2] at the indicated temperatures. Four parent species were employed to describe the signal at 31 amu/e. [Reprinted from ref 28, copyright 1993, with permission from American Institute of Physics].

monomer). At lower masses, the TOF mass spectra are complicated by fragmentation in the quadrupole ionizer. For instance, most of the signal at a charge-to-mass ratio of 31 amu/e (CF) from PTFE is actually due to CF fragments generated in the ionizer from the dimer, the monomer, and CF_2. These heavier, parent species travel more slowly than CF, and substantially broaden the TOF signal observed at 31 amu/e. To derive surface temperatures from the CF signal, one must account for the CF generated as heavier parent species move through the ionizer. When this is done, good curve fits are obtained with surface temperatures that agree well with temperatures based on the TOF of the monomer, where contributions due to fragmentation are not significant (shown in Figure 22b). If possible, surface temperatures and model testing should be based on TOF signals at masses that can unambiguously be attributed to a single species. As noted above, complex models are often not unique and easily misinterpreted.

For low numbers of collisions (less than four or five per particle), collisions tend to sharpen the velocity distribution, move the peak to shorter time-of-flights, and make the distribution more forward directed (normal to the polymer surface).[245] When a variety of particles are emitted simultaneously, collisions tend to slow the lighter particles and accelerate the heavy ones—both light and heavy particles tend to display similar peak time-of-flights. With somewhat larger numbers of collisions, the velocity distribution can be modeled in terms of an unsteady, adiabatic expansion into vacuum.

Neutral molecules produced by photochemical processes can be ejected from the surface with hyperthermal energies. As the physical TOF distribution of these particles is not known, an empirical TOF distribution based on a Gaussian energy distribution in one dimension is useful. This distribution often fits the data adequately, and has the advantage of being easily interpreted. Since the observed signal is proportional to a density, we form a one-dimensional density by transforming the Gaussian energy distribution, $dN/dx = (dN/dE)(dE/dx)$, or

$$\frac{dN}{dx} = \frac{N_0 m d_I}{\sqrt{2\pi}\sigma(t-t')^2} \exp\left[\frac{-\left(E_0 - \frac{m d_I^2}{2(t-t')^2}\right)}{2\sigma^2}\right] \quad (3)$$

where E_0 is the most probable kinetic energy, and σ is the standard deviation. For low energy particles, t' is well approximated by the time required for a particle to pass through the mass filter with a kinetic energy equal to the potential energy at which the ion was created in the ionizer (as above). Hyperthermal energies can be a significant fraction of this energy, in which case t' can calculated by equating the particle kinetic energy through the mass filter with the sum of its initial kinetic energy and the ion energy setting.

Ions are detected without an ionization step by a fundamentally different process. Whereas the signal intensity due to neutral particles is proportional to the particle density in the quadrupole ionizer (particles per unit volume), the signal intensity due to ions is proportional to the flux of ions striking the detector (particles per unit time). This difference affects the expected time behavior of the signal. Another difference between ion and neutral detection is that ion detection usually requires a clear line-of-sight path from the laser spot, through any apertures in the quadrupole optics, to the quadrupole detector. This requires careful alignment of the quadrupole mass filter. It is often reasonable to expect ion intensities and velocities to vary strongly with the angle at which they are emitted relative to the surface normal. In most work, emission normal to the surface is reported.

Analysis of ion velocity distributions is greatly simplified if the sample is kept at ground potential, and electric fields between the sample and the detector minimized. This generally requires that the electron optics associated with the ionizer be removed and/or grounded. If the axis of the mass filter is well aligned with the laser spot, the electric fields in the mass filter are predominately perpendicular to the ion flight path and have little effect on the ion velocities. In this case, ions should move from the sample to the quadrupole detector a constant velocity, and the ion velocity can be determined from the TOF.

As with high-energy neutral particles, a one-dimensional Gaussian energy distribution often provides a good, albeit empirical, description of the TOF signal. Because the detector output is proportional to the particle flux, the signal as a function of time is proportional to $dN/dt = (dN/dE)(dE/dt)$.

$$\frac{dN}{dx} = \frac{N_0 m d_D^2}{\sqrt{2\pi}\sigma t^3} \exp\left[\frac{-\left(E_0 - \frac{m d_D^2}{2t^2}\right)}{2\sigma^2}\right] \quad (4)$$

where d_D is the distance between the sample all the way to the quadrupole detector.

Campbell et al.[246,247] has analyzed the ionic products (both + and −) generated during ablation of PI and PS during exposure to 14 ns 308 nm excimer radiation using a reflectron TOF unit. Large masses (up to 900 amu) were observed and very high plume velocities (between 1400 and 10 000 m/s), attributed to electrostatic effects.

Although less common, metastable particles with sufficient internal energy (> 5 eV) can be detected without an ionization step by many charged particle detectors. In this case, the detector output reflects the particle flux, as in the case of ions, and eq 4 can be used to describe the results. In principle, the velocity distribution of metastables is not affected by the electric fields of the ionizer optics. However, strong electric fields can de-excite metastables. Slower particles spend more time in the strong-field region and can be preferentially de-excited, which effectively shifts the apparent TOF distribution to shorter times. This effect can be probed by changing the mass setting of the mass filter, which changes the internal fields.

Fitting eqs 2−4 to experimental data can often provide important information about the observed

emissions, such as average kinetic energies. In most cases, the precision of these estimates is rather good. However, we emphasize that these equations are quite nonlinear, and that uncertainty estimates provided by nonlinear curve fitting packages seldom reflect actual experimental and numerical uncertainties.[248] The best procedure is to take several sets of experimental data under identical conditions, fit each one, and use the standard deviations of the fit parameters as the uncertainty. Due to the large amount of effort involved, error estimates are often made under a few laser conditions and used as representative values.

Traditionally, sensitive TOF measurements have required nuclear physics instrumentation for identifying and counting individual output pulses in a time-resolved fashion (binning). This procedure does not produce a record of the arrival time of each ion. With the advent of mass data storage, this information can now be recorded for later analysis. One relatively simple procedure involves digitizing and recording the TOF signal for each laser pulse individually. Later, the arrival time of each particle can be determined later using software, instead of hardware. The velocity and energy of each individual ion can be computed and binned in appropriate velocity or energy levels. Curve fitting techniques are still valuable for comparing the results with the predictions of various models, but the experimental velocity or energy distributions can often be calculated directly from the data.

4 Structure Modification

4.1 Physical Surface Modification: Nano- to Microstructures

As noted above, UV radiation can be employed to produce chemical and physical changes in polymer surfaces produced on polymer surface. In some cases, unique structures are produced.

Dyer et al.[249,250] have produced conical structures on a variety of polymers, including PI, PET, PC, polyethylene(naphthylate), and nylon, at irradiation wavelengths ranging from 157 to 308 nm. The apex angle of the cones (Θ) varies with the applied fluence (F) and the ablation threshold (F_0) according to the relation:

$$\Theta = 2 + \sin^{-1}\left[\frac{F_0(1 - R_0)}{F(1 - R(\Theta))}\right] \qquad (5)$$

where R_0 and $R(\Theta)$ are the surface reflectivities for incidence angles of 90° (normal to the surface) and Θ degrees, respectively. The threshold fluence for laser light incident at the angle Θ can be calculated from eq 5. Dyer[249,250] suggested cones development initiates when impurity-rich regions shield the underlying polymer from the incident light. Near-field diffraction from these impurity-rich regions yields a gradual rise in fluence as one moves away from the impurity center and promotes the production of sloping walls rather than a sharp, well-defined edge. This will lead to sloping walls as etching proceeds. As irradiation continues, the walls steepen until the effective laser fluence drops below the ablation threshold, at which time ablation stops. Depending on the fluence,[199,251] the resulting features can be almost perfectly conical (Figure 23 a) or more "volcano like" (Figure 23b). Conical structures are often observed within a rather narrow range of fluences. Higher fluences presumably exceed the ablation threshold for the impurity-rich region and yield clean, uniform ablation.[252]

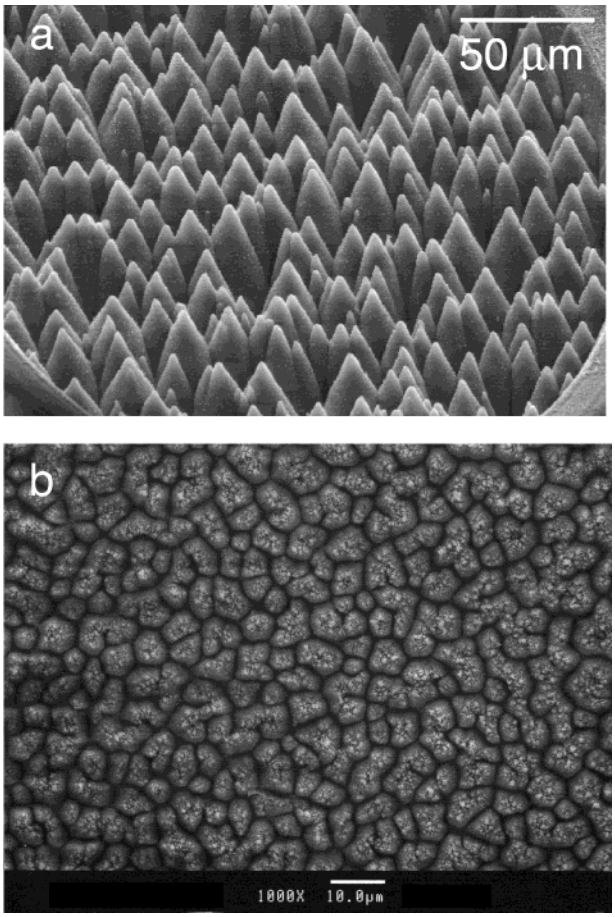

Figure 23. Cone structures in polyimide, created by 200 pulses with 250 mJ cm^{-2} and 308 nm irradiation (a) [Reprinted from ref 107, copyright 2000 American Institute of Physics]. Volcano structures created in the triazene-polymer with 250 pulses, a fluence of 36 mJ cm^{-2} and 248 nm irradiation (b). [Reprinted from ref 20, copyright 1996, with permission from American Chemical Society].

Volcano-like and/or ripple-like (wall-like) structures have also been obtained in other work with PEEK, PET, PEN, and PI. Several different mechanisms for these noncoherent structures have been discussed,[172] including:

(i) Contrasting etch rates in crystalline and amorphous domains of stretched polymers such as PET.[253] Simplistically, this would suggest that microstructure formation is different in more homogeneous polymers. However, very similar structures are observed in nonstretched polymers.

(ii) A synergism between Marangoni convection in the molten surface layer and frozen in-stress fields in the solid phase.[254] However, structure formation is also observed in nonmelting polymers such as PI.[255]

(iii) Microcracking of stressed surface material. Crack coallescence would produce a textured surface

which evolves in to the observed structures (for PI).[256] However, the similarity of structures observed in a variety of materials with contrasting mechanical and thermal properties suggests that a more general mechanism is responsible.

(iv) Scattered surface waves.[257]

(v) Thermal processes in the heated surface layer during and after laser irradiation.[258]

(vi) A nonlinear relation between etch rates and the incident laser fluence. [169]

As suggested Bäuerle et al.,[255] a combination of several mechanisms is probably required to account for structure production in a wide variety of polymers under a wide range of irradiation conditions. A multimechanism model incorporating several parameters agrees well with data for PET and PI, for instance.[259]

Dendritic structures have been observed on PET at fluences near the ablation threshold, as shown in Figure 24.[260,261] Structure formation was analyzed as

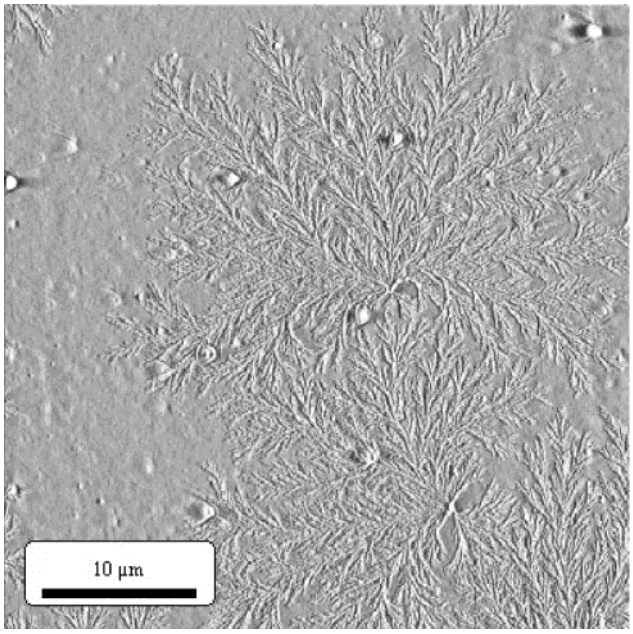

Figure 24. Dendritic structure formed in PET after irradiation with 248 nm and a fluence of 30 mJ cm^{-2}. The PET film was annealed after irradiation. [Figure by J. Heitz]

a function of laser wavelength (193, 248, and 308 nm) and ambient atmosphere. The size and density of the dendrites can be related to the amount and the composition of the redeposited material, which is affected by both laser wavelength and ambient pressure and gas composition. At low ambient pressures, the distance between neighboring dendrites is large, and individual dendrites grow unhindered. The effect of laser fluence and wavelength on dendrite size can be related to the total quantity of ablated material and the degree of fragmentation. Dendritic structures are only observed inside the irradiation area, despite the fact that material is redeposited upon surrounding material. Thus, it appears that the physical and chemical characteristics of the freshly ablated surface play a significant role in dendrite formation.[170]

Similar features produced on PI and PTFE after irradiation at 308 nm have been analyzed in detail.[262] The ablated surfaces show irregularly shaped edges and fractal-like formations, which have been analyzed by fractal techniques. Pronounced differences between structures on PI and PTFE have been interpreted in terms of a combination of photochemical and thermal processes. The higher roughness for PI surfaces was attributed to a smaller amount of thermally induced smoothing.

Branching, ripple-like microstructures, denoted "scanning structures," have been observed in PET during scanning excimer laser ablation for microfluidic channels in air at 193 nm.[168] These structures are typically observed along sloping ramps toward the end of fluid channels. These structures appear only when the angle between the ramp and the nonirradiated sample surface is greater than 10.55 (±0.15) degrees.[166] Three different kinds of structures are observed, which are described in terms of three different stages of suppression of "normal" wall structures associated with frozen-in stresses perpendicular to the irradiated surface. Depending on the orientation of the ramp with respect to these frozen-in stresses, certain components of the frozen-in stresses become inactive and structure formation is to some degree suppressed.[167]

Submicron-sized, laser-induced periodic surface structures (LIPSS) were first reported by Lazare et al. in poly(butylene terephthalate) (PET) and polystyrene (PS) at 193 and 248 nm.[263] These structures require some degree of polarization. For instance, excimer laser light incident on a fused silica plate with an oblique incidence of 60° develops a linear polarization of approximately 80%. The range of fluences yielding structures is typically narrow, e.g., 3−5 mJ cm^{-2} at 193 nm for PET, and below the ablation threshold (17 mJ cm^{-2} for PET). The structure spacing is proporational to the laser wavelength, e.g., 150 nm for 193 nm irradiation and 190 nm for 248 nm irradiation. A typical example of the ripple structure is shown in Figure 25. These initial results

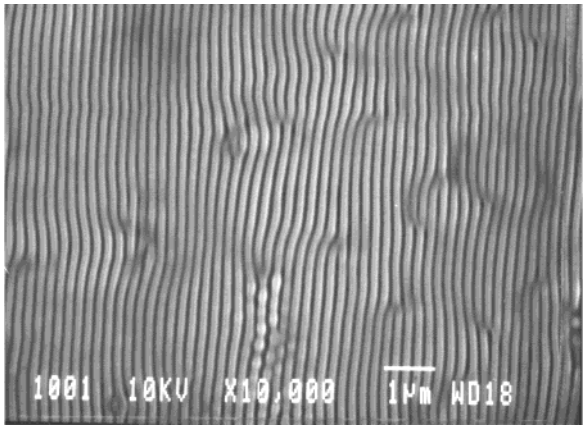

Figure 25. LIPSS structure in PC. Irradiation at normal incidence with 1000 pulses at 248 nm with a fluence of 10 mJ cm^{-2}. [Figure by S. Lazare].

have been extended to other polymers and other laser wavelengths. The structure period (Π) depends on the laser wavelength and the angle of incidence (Θ) according to eq 6.

$$\Pi = \frac{\lambda}{n \pm \sin \Theta} \quad (6)$$

where n is the refractive index of one of the two media (solid or ambient). It has been suggested[264] that the applied fluences allow local surface melting, but not ablation. Significantly, the presence of oxygen plays a major role, at least for the formation of ripples in PS. Thus photooxidation may play a key role.[264] The growth mechanism involves a surface wave, which interferes with the main beam to produce a spatially modulated electromagnetic field on the surface. The simple experimental geometry for LIPPS formation allows large areas of polymer surface to be structured. These structures may be used to improve surface properties such as adhesion and friction,[265,266] or for liquid crystal alignment.[267]

Some materials, such as poly-α-methylstyrene (PαMS), yield somewhat different structures. Here the structures did not consist of complete lines, but bead like droplets about 200 nm diameter. These droplets are readily removed mechanically. This different response is attributed to the different chemical and physical properties of PαMS.[268] Similar, more durable dot arrays structures can be created in other polymers by exposing the sample to create ridges (say, with 10 laser pulses) and then rotating the sample by 90°.[269] Figure 26 shows a mixed ripple-

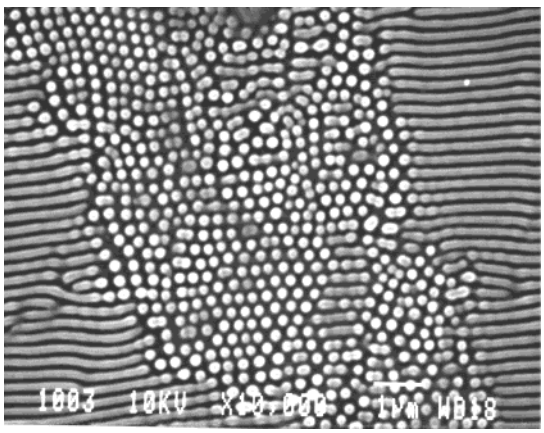

Figure 26. LIPSS structure in PC. Irradiation in air at normal incidence with 3000 pulses at 248 nm with a fluence of 10 mJ cm^{-2}. The sample was rotated by 90° every 10 pulses. [Figure by S. Lazare].

dot structure in PC. Time-resolved measurements of LIPSS formation in PET at 193 nm showed that the structures form 5−10 μs after the laser pulse.[270] Film structure and thickness strongly influence structure formation in PC at 193 nm.[271] Thick spin-coated films display line-shaped structures, while films thinner than a critical value display droplets. Droplet formation is attributed to melting across the whole film thickness, followed by substrate de-wetting. The critical thickness can often be predicted by heat-conduction models. Film preparation, surface roughness, and refractive index all can affect structure formation. Structure periods are typically largest for oriented thick films, somewhat smaller for amorphous thick films, and slightly smaller for thin spin-coated films.

Hiraoka et al.[272] developed a somewhat simpler geometry for structure formation using the forth harmonic of an Nd:YAG laser (266 nm), which does not require external polarization. LIPSS structures were obtained in Kapton (PI), PET, and in a special polyimide designed for spin-coating. AFM measurements of the structure periodicity followed the predications of eq 6. Well-defined, regular patterns were obtained only for angles of incidence <70°. In a single experiment, the ripple spacing can vary within a range of 30 nm. Dot patterns were fabricated with two orthogonally polarized laser beams. No changes in the chemical composition of PET were obtained after LIPSS formation.[273] A phenomenological model for ripple formation in terms of waveguide modes on the polymer surface was suggested.[274] The resulting LIPSS patterns were exploited in an image transfer process to fabricate 100-nm structures in Si with vertical walls.[275,276]

4.2 Chemical Surface Modification

Chemical surface modification during laser ablation depends strongly on whether the fluence is above or below the ablation threshold. Most experiments have focused on fluences above the threshold of ablation. Recent reviews of polymer surface modification appear in refs 277 and 278 Some general trends are summarized below:

(i) Polymers containing aromatic groups (e.g., polyimide) are often carbonized at fluences above the ablation threshold of ablation. One notable exception is the designed triazene-polymers, where ablation at 308 nm does not alter the chemical composition.

(ii) Absorbing species (incubation) are often produced (e.g., −C═C− bonds in PMMA, described above), either due to reactions between active groups within the polymer or between active groups and the ambient. The ambient could be air, supplied gases, or supplied liquids (see the fluoropolymers above).

(iii) Particle removal from polymer surfaces (laser cleaning), a special case of surface modification, can often be achieved.[279]

Irradiation of polymer surfaces at fluences below the ablation threshold can be exploited to alter surface properties (e.g., hydrophilicity, wettability, and adhesion). Polymer metallization[280] is employed in microelectronics packaging and MCM technology, as well as in the production of decorative overlayers, diffusion barriers, and electromagnetic shielding. State-of-the-art, two-step, wet chemical metallization involves pretreatment (cleaning, activation, and prenucleation) followed by metal deposition (laser-assisted deposition, liquid-phase deposition, or vacuum deposition[281]).[282] Plasma discharge and ion etching[283] and photochemical surface modification[284] (both dry processes) work well as pretreatment steps, where photochemical modification may be performed with UV lasers.

PBT: At 248 nm, both poly(butylene terephthalate) (PBT)[285,286] and PI display a loss of oxygen functionality (PI also loses nitrogen functionality) in FTIR and XPS measurements. This treatment improves the adhesion of subsequently deposited metal films.

PI: Laser treatment was also employed to selectively deposit copper on PI by electroless plating.[287] Irradiation at 193 nm changes the surface potential in the irradiated region. Selective metallization in the irradiated region is then achieved by treating the surface with a negatively charged Pd-solution, followed by copper deposition.

PET: Excimer laser treatment of PET can improve metallization by thermally evaporated Al.[288] Some of this improvement was attributed to an increase in surface wettability and acidity. However, surface amorphization and microroughening seem to be responsible for most of the improvement. Surface amorphization of PET at 193 and 248 nm has been previously detected by Lazare et al. using ellipsometry.[289]

PEEK: The adhesive bonding properties of polyether-etherketone were significantly improved by surface cleaning, surface amorphization, and chemical modification.[290] The latter depends on the oxidizing properties of the surrounding environment. Irradiation reduces the aromaticity of the polymer and breaks ether bonds. In oxidizing atmospheres, an increase of carboxylic functionality on the surface is detected. These changes all tend to improve the surface adhesion.

Fibers: Synthetic fibers can be treated to improve surface adhesion, especially if the fibers are treated with UV sensitive compounds. For instance, UV treatments have been employed to improve rubber-fiber adhesion.[291]

Polymers doped with IR chromophores can be modified by IR lasers. Volatile species have been produced in this way, as well as microcavities.[292]

An interesting variation of polymer surface modification has been demonstrated by Yabe et al.[293,294] The polymer (PET) was not irradiated directly, but modified by reactive species created by irradiation of a frozen azide (pentafluorophenyl azide) at 248 nm in a vacuum. After treatment, the PET surface displayed a pronounced increase in nitrogen and fluorine content.

5 Radiation Sources

5.1 Low Intensity (Lamp) Sources

Modifications of polymers surfaces are of course possible with lasers, but commercial applications are hindered by the high cost of laser photons. Laser are nevertheless cost-effective if they are the only way to achieve a required modification, if high spatial resolution (over small areas) is required, or if modification speed is an issue. In many cases, low intensity UV and VUV lamps can modify large areas at much lower photon costs. Low intensity lamps included mercury lamps at 185 nm, Xe resonance lamps at 147 nm, helium discharge lamps with $\lambda <$ 160 nm, and excimer lamps at 146 (Kr_2), 172 (Xe_2), 222 (KrCl), and 308 (XeCl) nm. Under well-controlled conditions, even polymer etching has been achieved with mercury lamps, excimer lamps, and discharge lamps.

Surface modification of PMMA, PI, and PET has been studied at 185 nm, and diverging results (depending on the conditions) have been published by the same group. In earlier publications[176,295] an increase of the O/C ratio (surface oxidation) was determined by XPS measurements for irradiation in air, while more recent work reports a decrease in the O/C ratio for irradiation in a vacuum.[171] The decrease of oxygen in the surface of the film was attributed to the loss of small gaseous molecules, such as CO and CO_2. Surface oxidation was attributed to the reaction of surface carbon radicals with atmospheric oxygen.

Xe resonance lamps (147 nm) have been used to increase the surface polarity of a variety of very unpolar polymers, including siloxanes and FEP. An increase of CO and OH functionalities is observed.[296−298]

As noted above, excimer lamps have been used to modify fluoropolymer surfaces. Surface roughening is also often observed.[299] In the presence of appropriate oxygen concentrations, etch rates with excimer lamps can be much higher (factor 40 to 100)[300] than etch rates with Hg lamps (etch rates around 50 Å min^{-1}).[301,302] For PI and PMMA irradiated at 172 and 222 nm, the optimum oxygen pressure is about 1 mbar. The etching mechanism has been described as *photooxidative etching*, where irradiation produces reactive oxygen species (free radicals $O(^1D)$, $O(^3P)$, and excited molecular oxygen). Etching is obtained when these reactive species oxidize the surface to form gaseous products, e.g., CO and CO_2. Excimer lamps have also been used to etch various acrylates in high vacuum (<0.03 Torr). The degradation efficiency depends on the structure of the ester side chain. Polymers with low glass transition temperatures were easily decomposed; etching was observed during irradiation at elevated temperatures (50−130 °C).[303]

Different etching processes are active for irradiation with Kr_2 excimer lamps at 146 nm[304] and He discharge lamps (<160 nm)[305] in N_2, He, or H_2 atmospheres. Different behaviors are observed in different polymers: 146 nm irradiation etches PMMA and other polyacrylates, but not PS. (The radiation resistance of PS under VUV irradiation has been attributed to the ability of the aromatic side groups to sustain nondissociative excitations.) Poly-phenylquinoxaline (PPQ) is etched with He discharge radiation, with the C−H bond as a possible initial decomposition site.

Although etching under oxidative conditions is reasonably well understood, etching in non-oxidizing atmospheres (at even shorter irradiation wavelength) is not. Research on these effects will most probably increase in coming years, in parallel with the use of shorter wavelengths in the microelectronics industry to produce ever-smaller structures. 157 nm radiation sources are already under development, and it will be necessary to characterize and control polymer chemistry under VUV irradiation.

5.2 Continuous-Wave UV Lasers

Continuous wave (CW) UV lasers can also be used to structure polymers (PMMA, PET, and PI). Ar-ion lasers at 351, 363, 300−330, or 350−380 nm have been used to structure polymers by either scanning

the beam across the surface to be processed (transit time over beam diameter 1−1000 μs) or by mechanically chopping the beam (10−400 μs pulses). In the case of PI, the fluences required for etching are similar to the fluences employed with excimer lasers, but typical etch depths per joule are about 100 fold less.[306] Etching is observed only when the laser beam is translated across the sample. Irradiation at a single position merely blackens and swells the surface. No acoustic report (audible snap) is heard, in contrast to ablation with pulsed lasers. Nevertheless, only a very small fraction of the material is removed as debris. By chopping the laser beam (350 μs pulses) holes can be drilled in PI. Although the walls of the hole are heavily carbonized, no signs of debris are observed.[307] Under irradiation with very long (millisecond) pulses, a chemical transformation yields carbon, similar to glassy carbon.[18]

PET behaves differently.[308] PET is five times more sensitive than PI and PMMA to etching, with etch rates that increase with pulse width. Pulse widths longer than 200 μs damage the surrounding material. A significant fraction of removed material (about 20%) is ejected as molten droplets and deposited along the edge of the structure. Etching is attributed to largely thermal processes.

PMMA has been studied in its pure form or doped with a UV chromophore (Tinuvin) to increase absorption at the laser wavelength. Doped PMMA could be etched by scanning the laser beam, with an optimum scan rate (transit time over the beam diameter) of about 50 μs.[309] As in the case of PI, no acoustic report or ablative material ejection was observed. This process operates at power densities about 50 times lower than those in "normal" laser ablation, and was denoted *photokinetic etching*.

At the 351 and 363 nm emission lines of the Ar-ion laser, CW irradiation of neat PMMA (transparent at both wavelengths)[310] produces an effect similar to incubation. The incubation time decreases with increasing laser intensity or sample temperature. At sufficiently high intensities, the incubation time depends only on the sample temperature. This behavior can be described in terms of an incubation process followed by a volume explosion.[311]

Structuring with these long pulses, or better, by scanning the cw-laser beam, apparently involves different processes than structuring with excimer lasers. As suggested by Bäuerle (see above), these processes are probably thermal for the most part.

5.3 Ultrafast Lasers

With the development of chirped pulse amplification (CPA), IR solid state (Ti:sapphire) lasers have become compact, extremely high-brightness sources.[312] Material processing with femtosecond lasers is already an established technique. Ablation with femtosecond pulses has unique advantages, including a negligible heat-affected zone, lower ablation threshold, absence of plasma shielding, and the ability to structure "transparent" materials. In addition to polymers (discussed here), these lasers are used to process metals, glasses, ionic crystals, ceramics, and semiconductors. Laser-induced breakdown in dielectrics has been described in terms of producing a critical electron density in the conduction band,[313] either by avalanche ionization or multiphoton ionization.[314] The rapid transfer of laser technology from experimental systems to industrial environments (as in mask repair[315,316]) has been astonishing. We have come a long way since the first reports of femtosecond laser ablation of polymers in 1987 by Srinivasan et al.[317] and Stuke et al.[318]

5.3.1 Femtosecond Lasers

Srinivasan showed,[317] that it is possible to produce high quality structures in PMMA with 160 fs pulses at 308 nm, whereas nanosecond pulses at the same wavelength only "damage" the surface. Stuke's[318] work on PMMA with 300 fs, 248-nm laser pulses showed that femtosecond pulses have a lower threshold for structuring by a factor of 5 relative to nanosecond pulses, and produce much better structures. Femtosecond pulses also produce high quality structures in Teflon,[319] with no signs of the thermal degradation associated with nanosecond pulses.[320] Removal rates up to 1 μm per pulse can be achieved. Time-resolved studies[321] with a pair of time-delayed (−200 to 200 ps) 500 fs pulses at 248 m showed that the ablation rate is very sensitive to the time delay. When the combined fluence is close to the ablation threshold, significant changes in the ablation rate of PMMA and Teflon are observed for delays < 3ps. For the absorbed energy density to exceed the threshold fluence, the two pulses must overlap sufficiently in time. Thus, multiphoton absorption dominates the ablation process in PMMA and Teflon. In the case of PI,[322] excited state absorption actually decreases the ablation rate for delay times below 30 ps.

The first ablation experiments for medical applications using femtosecond pulses were published in 1994 using a femtosecond dye laser at 615 nm.[323] Femtosecond lasers produced heat-affected zones (HAZ) less than 0.5 μm thick, while comparable nanosecond lasers (at 600 nm) produced severe thermal damage.

Chirped-pulse Ti:sapphire systems were first applied to polymers in 1994.[324] The ablation rates for Teflon, PI, and FEP were adequately described by a two-level absorption model with the chromophore density as a free parameter.[32] In the case of FEP, raising the pulse length from 170 fs to 12 ps shows a pronounced degradation of ablation quality at about 500 fs.[325] The ablation threshold in this fluence range is inversely proportional to the square root of the pulse duration. Femtosecond laser ablation can be used for high aspect ratio micro-machining of polymers (PMMA, PC, and PTFE). The aspect ratio is normally limited to about 10; deeper structures are often tapered and sometimes even bend.[326]

Studies of Nylon 6−6 and PMMA indicate that the ablation rates for 0.8-ps pulses at 595 nm (dye laser) are lower than the rates for 100-ps pulses at 532 nm.[327] Subsequent work with nanosecond pulses showed that the highest ablation rates are achieved with picosecond pulses.[328]

Kautek et al.[329−332] have studied the ablation of PI, PC, PET, and PMMA due to 150-fs pulses at 800 nm.

The single pulse threshold increases from 1 J cm^{-2} for PI to 2.6 J cm^{-2} for PMMA. The ablation thresholds correlate with the optical band gaps of these materials, consistent with multiphoton absorption. All polymers show pronounced incubation effects, with stronger incubation in PC, PET, and PMMA relative to the more "stable" polymers PI and Teflon. The ablation crater of all polymers, except PI, show clear signs of melting and redeposition of molten material (splashing), in contrast with the clean ablation contours obtained by UV-femtosecond laser ablation.[317] The absence of splashing for PI is not really surprising, as typically PI decomposes rather than melts. Interestingly, the etch rates for PI depend on laser polarization.[329] Circular polarization yields slightly higher ablation rates than linear polarization (shown in Figure 27). After more than 50 laser

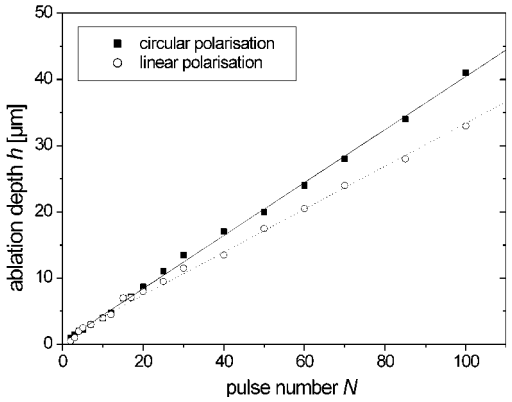

Figure 27. Ablation depths as a function of laser pulses and polarization in PI. Irradiation at 800 nm with 150 fs pulses and a fluence of 1.3 J cm^{-2}. [Figure by S. Baudach].

pulses, the ablated surfaces show surprising structural differences. Linearly polarized light produces a ripple structure with a period of ≈ 0.8 μm (Figure 28 a), while circularly polarized light produces a pattern of conical structures (Figure 28b). The ripples in the ripple structure are always parallel to the electric field of the incident light. Unlike the cones formed with nanosecond pulses, each of the cones formed with femtosecond pulses has a small hole near the top. Cone formation in PI and the incubation process in all the above polymers have not yet been analyzed.

Surface structures in PET and PI are also obtained using 500-fs pulses of linearly polarized light at 248 nm.[333] Coherent ripple structures are produced at fluences above the ablation threshold, typically superimposed on surface structures similar to those produced by nanosecond pulses. The ripple structures have a period of 100 to 250 nm and are oriented either parallel or perpendicular to the electric field of the incident light.

The structure formation of an elastomer composite (acrylate-polymer with carbon black) has been studied at various pulse lengths, i.e., 30 ns (248 nm), 8 ps (263 nm), and 500 fs (248 nm).[334] Nanosecond and picosecond pulses produced conical structures, while femtosecond pulses merely roughened the surface.

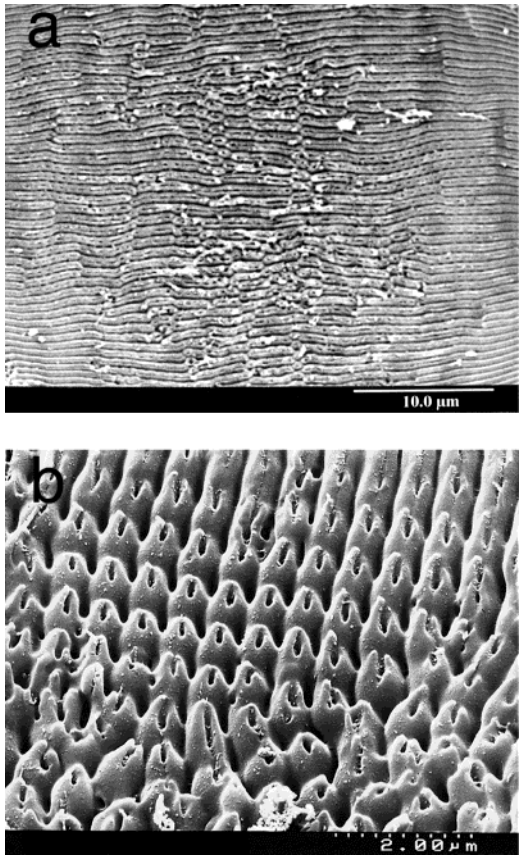

Figure 28. SEM picture of the center part of ablation crates in PI obtained with 50 laser pulses (150 fs at 800 nm with 1.3 J cm^{-2}) for (a) linear and (b) circular polarization. [Reprinted from ref 329 copyright 1999, with permission from Springer Verlag].

Ablation of PTFE and FEP with the third harmonic (268 nm) of a Ti:sapphire laser produced clean ablation contours without debris for both materials.[335]

Reversible microstructuring *inside* (10 μm below the surface) of *cis*-1,4-polybutadiene (PB) films has been observed with femtosecond pulses.[336] The structures produced inside the film by single laser pulses were probed by optical transmission. Two different threshold fluences are observed: the "normal" threshold at the onset of ablation, and a second threshold, marking the onset of permanent structuring. Between these two thresholds, transmission changes recover on time scales of 10−100 s. Fluences above the second threshold permanently change the optical transmission. Doping PB with a photolabile compound (pentazadiene) lowers the (first) ablation threshold by 20%.

Time-resolved reflectivity measurements on PMMA and PS show reflectivity increases of factors of 1−5 after exposure to 500 fs laser pulses.[337,338] Even higher reflectivities are observed for naphthalene doped PMMA, where photoproduct formation has been studied.[76] (See above, Figure 4.) The reflectivity increase was attributed to competing processes involving the formation of a high-density free electron gas and the expansion of the ablation plume.

The ablation of thin microcrystalline films of Cu-phthalocyanine by femtosecond pulses (780 nm, 120 fs) displays an unusual fluence dependence,[339] which

the authors described as multistep etching.[340] The ablation depth increases in a stepwise fashion with increasing laser fluence—not a continuous fashion, as in all other ablation studies.

5.3.2 Picosecond Lasers

Picosecond pulses have not found many applications, as they lack the advantages of femtosecond pulses, and perform not much better than nanosecond pulses, at least in the UV. The effect of picosecond and nanosecond pulses on PMMA has been studied in the UV (266 nm) and the near-IR (1064 nm).[341] Both sets of work employed dopants: IR-165 at 1064 nm and diazomeldrum's acid (DMA) at 266 nm. Both dopants are associated with photothermal ablation. With IR-165, the polymer matrix is heated by vibrational relaxation and multi-phonon uppumping.[342] In the IR, 100-ps pulses produced clean etch features, while 6-ns pulses yielded rough surface features. This is consistent with the fast vibrational relaxation in IR-165, which allows for higher temperature jumps with picosecond pulses. In the UV, heating of DMA-doped PMMA is attributed to cyclic multiphoton absorption[46] (see above). In the UV, ablation was obtained only with the nanosecond pulses, and even then only low quality features were obtained. Picosecond pulses merely swell the surface. With cyclic photon absorption, longer pulses produce more highly excited chromophores and thus higher ablation temperatures and cleaner ablation features.

Dlott et al. have performed several studies of picosecond ablation, with an emphasis on spectroscopy (CARS, absorption, and ultrafast imaging) to elucidate the ablation mechanisms. This complex field can be discussed only briefly here.

When exposed to 93-ps pulses at 532 nm,[343,344] PMMA is rapidly heated by coherent two-photon absorption and induces explosive thermal decomposition. Ultrafast imaging (2-ps resolution) shows that surface damage is accompanied by the production of transient optical filaments. The intensity dependence of these features suggests that they are produced by cumulative changes in the transient refractive index that yield self-focusing. At all laser intensities, the onset of ablation was delayed by 20 ps.

The absorption spectra of some IR dopants (e.g., IR-165, or rhodamine 6G) shift in a characteristic way with temperature, allowing them to be used as "molecular thermometers." Picosecond studies of doped PMMA show heating rates between 5×10^9 and 10^{12} deg s^{-1}, with peak surface temperatures as high as 600 °C.[345,346] By calibrating the pressure and temperature dependence of a PMMA transition at 808 cm^{-1} in static experiments, CARS was employed to determine both the pressure and temperature during 150-ps laser pulses in PMMA doped with IR-165 at 1064 nm.[164,347] It was shown that picosecond pulses produce solid-state shock waves, which are not produced by longer pulses. This pressure jump, often several kbar, is produced when the film is heated faster than the characteristic hydrodynamic volume relaxation time. Pressure release occurs by the propagation of a rarefaction wave. The tensile forces generated when this rarefaction wave reaches the substrate can easily fracture the substrate-thin film bond. The pressure in the thin film at ablation threshold, $P_{abl} \approx 0.5$ GPa, is generated by roughly equal contributions from the shock and thermochemical decomposition. Ablation under these conditions can be described in terms of *shock-assisted photothermal ablation*. Pressure and temperature jumps as high as 2.5 GPa and 600 °C have been calculated from CARS measurements. The CARS measurements also showed an absorption feature which was assigned to the monomer MMA—an ablation product.[163]

Picosecond laser pulses have found an interesting technical application in the transfer of polymer films to substrates (e.g., for printing).[348] This process has been termed laser-ablation transfer.

Polymer ablation by ultrafast laser pulses is a relatively new field, with many open questions. In the case of femtosecond pulses, the pronounced difference in the quality of features formed in PMMA by UV and near-IR lasers has not been explained. The nature of incubation and the mechanisms for microstructure formation (for polarized beams) are fertile fields for further study. Femtosecond ablation in particular has the potential for structuring even transparent materials, such as Teflon, with high precision and minimal heat affected zones. A significant gap in our understanding of femtosecond pulses is the small amount of work on associated shock effects (see picosecond-ablation above). Shock formation by femtosecond pulses should be even more pronounced than shock formation by picosecond pulses. Shock effects have been confirmed, for instance, in the femtosecond ablation of glass.[349]

Ultraviolet femtosecond ablation may be an important future alternative to the more common near-IR femtosecond ablation.[350] UV femtosecond pulses produce no sign of incubation or melting in PMMA,[317] for instance, in contrast to femtosecond pulses at 780−800 nm.[332]

Picosecond pulses often display very different ablation mechanisms, including shock-assisted photothermal ablation. The boundary between "real" ultrafast ablation (e.g., with less than 500-fs pulses) and picosecond ablation (e.g., with 0.8-ps pulses) is not clear and needs to be refined.

5.4 Vacuum-Ultraviolet (VUV) Lasers

In the case of polymers, VUV structuring provides and important alternative to femtosecond laser ablation. The necessary laser wavelengths, e.g., at 157 nm (F_2 excimer) are already available. Even shorter wavelengths are expected as pressure from the microelectronic industry pushes lithography to smaller and smaller features. Most materials are opaque in the VUV and the high photon energies (e.g., 7.9 eV at 157 nm) can break chemical bonds; this bond breaking ability should minimize thermal loading at the target surface. The sub-quarter-micron-features that can be produced with VUV lasers are not accessible at the fundamental of the Ti:sapphire laser. The disadvantages of VUV radiation include the necessity to perform irradiation in a vacuum, or at least in inert gases. At 157 nm, fluoride-based

optics (e.g., CaF_2 or MgF_2) are required. Even shorter wavelengths will likely require reflection optics.

The first reports of polymer ablation at 157-nm appeared in the mid-80s with a self-developing (direct ablation) nitrocellulose resist.[351] Dyer's subsequent work was the first to characterize ablation thresholds for a variety of polymers,[352] including PET (29 mJ cm^{-2}), PI (36 mJ cm^{-2}), and PE (67 mJ cm^{-2}). The resulting high qualitiy structures showed no visible thermal damage. A more detailed study of PET, including analysis of the volatile ablation products, indicates that photochemical processes contribute significantly to ablation.[165]

The potential of VUV ablation was explored in several studies of PTFE using 6-ns anti-Stokes Raman pulses at 160 nm[353] and 20-ns pulses at 157 nm from an F_2 laser. Threshold fluences of 57 mJ cm^{-2} were obtained.[354−356] The observed ablation structures were of high quality, similar to thoses observed in PMMA, PI, polyhydroxybutyrate, and poly-2-hydroxyethl methacrylate.[357] A photochemical model was suggested for etching at 157 nm, based on considerations of polymer structure, Lambert−Beer absorption, and a kinetic model of the moving interface.[7,77]

In the case of PMMA, ablation rates of up to 200 nm per pulse at a fluence of 200 mJ cm^{-2} were obtained.[358] Atomic force microscope images of the ablated areas yielded surface roughnesses $R_a < 10$ nm for single and multiple pulses. Stuke et al. has used 157 nm radiation to form a variety of microstructures (e.g., fluidic microchannel systems for genomic analysis) in PMMA, PC, and PS using a silicone membrane contact mask.[359] More complicated structures, including 6-μm high micro-mesas, were constructed by applying a water-based, microdroplet masking fluid into which air bubbles were injected.[360] The bubble in conjunction with the droplet served as a gray tone mask, allowing for the fabrication of 3-dimensional structures without diffracting optics.

A low-fluence VUV source at 125 nm was developed by Castex et al.[361] using four wave sum frequency mixing in Hg vapor at room temperature. The resulting pulses were 6 ns long (fwhm) with an intensity of 2 μJ $pulse^{-1}$ at a repetition rate of 20 Hz. The pulse was typically focused to a diameter of 10 micron, corresponding to a fluence of 1 J cm^{-2}.[362] Threshold fluences for PMMA and PTFE under these conditions are about 1 mJ cm^{-2}, with corresponding ablation rates of 9.7 Å $pulse^{-1}$ for PMMA and 6.7 Å $pulse^{-1}$ for PTFE. The extremely low threshold fluences and the ablation rates (much lower than the thermal diffusion lengths of 56 nm for PMMA and 76 nm for PTFE) argue strongly for predominantly photochemical ablation.[363] Existing models for VUV photochemical ablation have not yet been applied to these data.[364]

The experimental data on VUV polymer ablation strongly support the operation of photochemical ablation processes. Systematic studies of the ablation products and their temporal evolution and energies are required to determine the role of photothermal processes, if any. VUV ablation is an attractive alternative to ultrafast structuring, as the laser system is quite simple. In contrast to the relatively small, Gaussian beams produced by Ti:sapphire lasers, VUV excimer laser beams are relative large, with flat-topped intensity profiles. This simplifies the optical design of patterning systems and facilitates the patterning of large areas. The short wavelengths of VUV radiation simplify the production of small features. Advantages of the ultrafast, Ti:sapphire lasers include high repetition rates for fast machining, and the absence of laser absorption by ablation products.

5.5 Synchrotron Radiation (SR)

Even shorter wavelengths and higher photon energies can be obtained with synchrotron radiation. PTFE, PMMA,[365] and cross-linked PTFE[366] have been structured using 170-ps pulses of 0.4−5 keV X-rays produced by a compact, 575 MeV, superconducting electron storage ring (AURORA).[367] Synchrotron micro-machining (SMM) has little in common with laser ablation. No threshold for structuring is observed. In the case of PTFE, the principal products of SMM is CF_2^+,[368] whereas the principal thermal (laser) decomposition product is C_2F_2. In SMM, the etch rates increase with increasing temperature, consistent with an Arrhenius activation energy of 0.1 eV. The corresponding activation energy for vacuum pyrolysis of PTFE is much higher—3.6 eV. Etch rates up to 100 μm min^{-1} (typically 50 to 60 μm min^{-1}) are obtained for PTFE, with aspect ratios of up to 25. Complex 3-dimensional objects can be fabricated.[369] Synchrotron radiation can also be used to deposit polymer films, including highly oriented Teflon.[370,371] Deposition of polymers films is discussed in detail by Chrisey in this issue.

Although SR structuring is not a likely alternative to "standard" polymer structuring, it may be a possible alternative to deep X-ray lithography (e.g., in the LIGA process).

5.6 Mid-IR Irradiation

The majority studies have concentrated on the application of UV lasers, which provide excellent spatial resolution. Nevertheless, several studies of pulsed IR CO_2 lasers have appeared.[372−376] These studies provide important data for comparisons with UV studies. In the IR, photothermal mechanisms typically dominate and thus provide a baseline for determining ablation mechanisms at shorter wavelengths. In addition, CO_2 lasers are widely accepted in industry and are relatively inexpensive to operate. Where high resolution is less critical, IR lasers may play a valuable role in polymer micromachining.

The TEM_{00} mode of a TEA CO_2 laser at 1091 cm^{-1} (9.17 μm) excites the C−O stretching vibration in PET.[377] The relationship between etch depth and fluence is similar to that observed in the UV, but with a less well-defined ablation threshold. Etch rates in excess of 10 μm $pulse^{-1}$ are acheived at a fluence of 10 J cm^{-2}. Time-resolved photoacoustic measurements suggest that ablation at 1.8 J cm^{-2} starts 100−200 ns after the pulse. At fluences just above the ablation threshold, the products are mainly invola-

tile, high molecular weight fragments. At higher fluences, the products are mainly gaseous (CO, CO_2, CH_2, C_2H_2, C_2H_4, C_6H_6, and CH_3CHO). Complex microstructures are observed in the ablation crater, similar to structures obtained with excimer lasers.

The morphology of thin films ablated with TEA CO_2 laser radiation is better on PEEK films (poly ether-ether ketone at 10.77 μm) than with PES films (poly-ethersulfone at 9.32 μm).[378] Ablation rates up to 50 μm pulse^{-1} are obtained in PEEK. Interestingly, higher ablation rates are obtained in air than in pure gas ambients (N_2 and O_2) and vacuum.

The influence of the absorption coefficient on ablation was probed with line-tunable CO_2 lasers and polyimide (Upilex) films.[379] High quality through-holes are obtained when the laser is tuned to a strongly absorbing wavelength. The ablation mechanism appears to be thermal decomposition. At weakly absorbing wavelengths, incubation was observed. This incubation is apparently related to particulate impurities. Ablation rates up to 25 μm are obtained at high fluences (10 J cm^{-2}). Holes with diameters as small as 10 μm can be obtained,[380] suggesting that optical resolution rather than thermal effects limit feature size. XPS analysis of surfaces ablated at 9.3 μm show reduced oxygen and nitrogen signals, indicating carbonization. Initial decomposition presumably produces volatile CO.[136]

To minimize problems with redeposited material, a second tunable CO_2 laser can be used to remove debris.[381] Through-holes can be drilled in polyimide films at 9.3 μm and 13.5 J cm^{-2}. Debris removal can be performed at lower fluences (0.2 to 2 J cm^{-2}) without pronounced charring. Best cleaning results are obtained when the laser for debris removal is tuned to a strong polyimide absorption band (9.22 μm).

Spectral analysis of emission plumes from polyimide films ablated at 10.6 μm in a vacuum or low-pressure He or Ar reveals the presence of neutral CN and C_2 and ionic C_{II}, C_{III}, C_{IV}, O_{II}, O_{III}, and N_{II} species (the subscripts denote the ionization state of the elements with II = singly ionized and III = doubly ionized etc.). With the exception of nitrogen-containing species, similar products are observed from PET and PMMA.[382]

Continuous wave (CW) CO_2 lasers with up to 100 W power decompose PTFE at low pressures, despite the high transparency of PTFE at 10.6 μm. Thermal decomposition produces large quantities of the volatile monomer, C_2F_4. Solid PTFE fibrils, 5−20 μm in diameter, are also produced.[383]

Less common mid-IR sources include CO lasers, emitting between 4.9 and 6.5 μm, and free-electron lasers (FEL) emitting in the 2−10 μm range (e.g., for the FEL at Vanderbilt University).

PET and Nylon fibers have been treated with frequency-selected, Q-switched CO lasers. The Q-switched laser delivers pulse lengths in the range of 1−10 μs. PET irradiated at 5.81 μm (1721 cm^{-1}) shows regular ("diffraction like") microstructures, while Nylon fibers irradiated at 6.1 μm (1639 cm^{-1}) showed an irregular pattern of holes or bubble-like structures.[384]

The wide range of available wavelengths produced by FEL lasers provides for great flexibility in experimental design.[385] These lasers produce a stream of picosecond micropulses delivered in microsecond bursts. Using the FEL at Thomas Jefferson National Accelerator Facility, PI was exposed to a 18.75 MHz stream of 1 ps micropulses, delivered in 10 μs bursts (macropulses) at 2 Hz. At a wavelength of 5.8 μm (1724 cm^{-1}), corresponding to a carbonyl stretching mode, SEM observations showed relatively high structure qualities were obtained with a minimum of carbonization. TOF−SIMS measurements of the irradiated surface (by sputtering wit Ga ions) showed no signs of thermal transformation under these conditions.[386] Substantial improvements in IR etching can be achieved under optimum conditions of laser absorption. The use of FEL lasers for polymer film deposition[387] are discussed in detail by Chrisey in this issue.

Mid-IR studies of polymer ablation have considerable potential for clarifying ablation mechanisms, especially with tunable sources. Mid-IR radiation typically induces thermal decomposition. The presence of similar or contrasting features (surface structures, ablation products, temporal evolution of ablation processes) under UV irradiation then provides strong evidence for or against thermal decomposition mechanisms at the shorter wavelength. The tunability of some mid-IR sources allows us to determine the role of excitations in specific functional groups (e.g., C=O versus C−H, C−N, etc.) in thermal decomposition. FEL-PLD data show that ablation behavior depends strongly on which functional group is excited.[388]

5.7 Visible Light and High Repetition Rate Ablation

Laser ablation of polymers in the visible is difficult because of the transparency of most polymers in the visible. Exceptions include doped polymers and ablation by ultrafast lasers (see above). The need for special polymers, and the relatively low resolution of VIS ablation relative to UV ablation, is probably responsible for the limited number of studies in the visible range.

A frequency doubled Nd:YAG laser (532 nm) has been employed to produce periodic structures on a special plasma polymerized polymer film (PPP).[389] The polymer was prepared from ethylene and an additional gas to produce thin, dense films with good substrate adhesion. An intermediate fluence (2 J cm^{-2}) focused 0.25 μm beneath the polymer surface produces clean structures (2 μm features) with no visible debris.

Ar-ion lasers at 488 nm have been applied to generate grating structures into on a special, highly absorbing urethane-urea copolymer with an azo-group in the side chain.[390] QCM mass loss measurements for nanometer scale etch rates (per pulse) show a linear relation between mass loss and fluence at low fluences (2 J cm^{-2}).

High repetition rate lasers (usually in the kHz range, but up to 20 kHz) have been used for drilling and wire stripping in the electronic industry for

several years. Commercial UV laser systems specifically designed for PCB drilling became available around 1995.[391,392] Currently available systems employ 266 and 355 nm radiation. The laser beam is generally highly focused, yielding fluences up to 50 J cm^{-2} at 266 nm[393] or up to 200 J cm^{-2} at 355 nm.[394] These high fluences, combined with high repetition rates, allow structuring (drilling, wire removal and micromachining) of Teflon, PI, resins, copper, glass, ceramics, metals, and other materials. Ablation rates are much higher at these high repetition rates. Ablation depends on pulse length, which is typically in the nanosecond range (e.g., from 24 to 36 ns).

The influence of pulse repetition rate on the ablation of PI and a glycol-modified PET (PETG) has been studied in more detail at 255 nm (frequency doubled copper vapor laser).[395,396] At repetition rates between 0.7 and 17 kHz, the etch rate increases gradually with increasing repetition rate at a fluence of 0.59 J cm^{-2}. No attenuation of the ablation laser beam by ejected material is observed. After a large number of pulses interact with the sample, the etch rates increase substantially with pulse repetition rate. The increase in etch rate is attributed to cumulative heating of the sample and subsequent pyrolytic decomposition.

The ablation rate and surface composition of PI (Upilex) has been studied as a function of the repetition rate (5 to 20 kHz) using a Nd:YAG laser at 355 nm. Blind holes were obtained at 5 kHz, while through holes were produced at 20 kHz. XPS analysis after irradiation revealed an increase of the carbon content with increasing repetition rate, while the relative oxygen and nitrogen content were reduced.[397]

High repetition rate lasers are now commonly employed in material processing, largely because the ablation products do not interfere with laser absorption even for nanosecond pulses. The increase in ablation rate due to cumulative heating can be useful, especially if the structure quality remains high. A detailed understanding of the onset of these cumulative effects and their exact nature is still lacking. (Compare, for instance, refs 149 and 150).

6 Outlook

The laser ablation of polymers is an established technique in the electronic industry. The large number of studies published annually indicate that this is still an attractive area of research. Discussions of ablation mechanism are ongoing and will continue. The development of polymers designed specifically for laser ablation is a unique tool for probing ablation mechanisms as well as for improving ablation properties. New commercial applications will require improved ablation rates and control of undesirable surface effects, such as debris.

The complexity of interactions between polymers and laser photons are illustrated by the various processes associated with different irradiation conditions:

(i) Photothermal−photochemical laser ablation under excimer laser irradiation.

(ii) Dopant-induced laser ablation.

(iii) Photooxidative etching with lamps in an oxidizing atmosphere.

(iv) VUV etching in the absence of oxidizing conditions.

(v) Photokinetic etching with CW UV lasers.

(vi) Ultrafast laser ablation, affected by pulse length, wavelength, and possibly shock waves.

(vii) Shock assisted photothermal ablation on picosecond time scales.

(viii) VUV laser ablation: purely photochemical?

(ix) Synchrotron structuring.

(x) Mid-IR ablation, the influence of exciting various functional groups.

The ongoing maturation of laser techniques will increase the number of applications of laser ablation. In the past decade, we have seen the development of several exciting laser ablation tools, including femtosecond lasers, VUV lasers, free electron lasers, and high repetition-rate lasers. All these new techniques are applied in ongoing research in conjunction with a variety of analytical techniques. Femtosecond lasers and VUV lasers in particular are expected to lead to important industrial applications.

7 Acknowledgments

This work was supported by the Swiss National Science Foundation and by the US Department of Energy under Grant DE-FG03-98ER14864. We thank Steven Langford, WSU, for helpful comments on this manuscript and Macarena Montenegro, PSI, for the help with the literature database.

8 References

(1) Kawamura, Y.; Toyoda, K.; Namba, S. *Appl. Phys. Lett.* **1982**, *40*, 374.
(2) Srinivasan, R.; Mayne-Banton, S. *Appl. Phys. Lett.* **1982**, *41*, 576.
(3) Bäuerle, D. *Laser Processing and Chemistry*; 3rd ed.; Springer-Verlag: Berlin, 2000.
(4) Patel, R. S.; Wassick, T. A. *Proc. SPIE-Int. Soc. Opt. Eng.* **1997**, *2991*, 217.
(5) Aoki, H. U.S. Patent 5736999, 1998.
(6) Dyer, P. E. *Photochemical Processing of Materials*; Academic Press: London, 1992; p 359.
(7) Lazare, S.; Granier, V. *Laser Chem.* **1989**, *10*, 25.
(8) Srinivasan, R.; Braren, B. *Chem. Rev.* **1989**, *89*, 1303.
(9) Babu, S. V.; D'Couto, G. C.; Egitto, F. D. *J. Appl. Phys.* **1992**, 692.
(10) Himmelbauer, M.; Arenholz, E.; Bäuerle, D. *Appl. Phys. A* **1996**, *63*, 87.
(11) Paraskevopoulos, G.; Singleton, D. L.; Irwin, R. S.; Taylor, R. S. *J. Appl. Phys.* **1987**, *70*, 1938.
(12) Taylor, R. S.; Singleton, D. L.; Paraskevopoulos, G. *Appl. Phys. Lett.* **1987**, *50*, 1779.
(13) Küper, S.; Brannon, J.; Brannon, K. *Appl. Phys. A* **1993**, *56*, 43.
(14) Lippert, T.; David, C.; Dickinson, J. T.; Hauer, M.; Kogelschatz, U.; Langford, S. C.; Nuyken, O.; Phipps, C.; Robert, J.; Wokaun, A. *J. Photochem. Photobiol. A Chem.* **2001**, *145*, 145.
(15) Ball, Z.; Hopp, B.; Csete, M.; Ignacz, F.; Racz, B.; Sauerbrey, R.; Szabo, G. *Appl. Phys. A* **1995**, *61*, 547.
(16) Ball, Z.; Hopp, B.; Csete, M.; Ignacz, F.; Racz, B.; Szabo, G.; Sauerbrey, R. *Appl. Phys. A* **1995**, *61*, 575.
(17) Lippert, T.; Bennett, L. S.; Nakamura, T.; Niino, H.; Ouchi, A.; Yabe, A. *Appl. Phys. A* **1996**, *63*, 257.
(18) Srinivasan, R.; Hall, R. R.; Loehle, W. D.; Wilson, W. D.; Allbee, D. C. *J. Appl. Phys.* **1995**, *78*, 4881.
(19) Lippert, T.; Nakamura, T.; Niino, H.; Yabe, A. *Macromolecules* **1996**, *29*, 6301.
(20) Lu, J.; Deshpande, S. V.; Gulari, E.; Kanicki, J.; Warren, W. L. *J. Appl. Phys.* **1996**, *80*, 5028.
(21) Schumann, M.; Sauerbrey, R.; Smayling, M. *Appl. Phys. Lett.* **1991**, *58*, 428.
(22) Wei, J.; Hoogen, N.; Lippert, T.; Nuyken, O.; Wokaun, A. *J. Phys. Chem. B* **2001**, *105*, 1267.

(23) Arnold, N.; Luk'yanchuk, B.; Bityurin, N. *Appl. Surf. Sci.* **1998**, *127*, 184.
(24) Schmidt, H.; Ihlemann, J.; Wolff-Rottke, B.; Luther, K.; Troe, J. *J. Appl. Phys.* **1998**, *83*, 5458.
(25) Lazare, S.; Granier, V. *Chem. Phys. Lett.* **1990**, *168*, 593.
(26) Deutsch, T. F.; Geis, M. W. *J. Appl. Phys.* **1983**, *54*, 7201.
(27) Andrew, J. E.; Dyer, P. E.; Foster, D.; Key, P. H. *Appl. Phys. Lett.* **1983**, *43*, 717.
(28) Sutcliffe, E.; Srinivasan, R. *J. Appl. Phys.* **1986**, *60*, 3315.
(29) Mahan, G. D.; Cole, H. S.; Liu, Y. S.; Philipp, H. R. *Appl. Phys. Lett.* **1988**, *53*, 2377.
(30) Pettit, G. H.; Sauerbrey, R. *Appl. Phys. Lett.* **1991**, *58*, 793.
(31) Pettit, G. H.; Ediger, M. N.; Hahn, D. W.; Brinson, B. E.; Sauerbrey, R. *Appl. Phys. A* **1994**, *58*, 573.
(32) Pettit, G. H.; Sauerbrey, R. *Appl. Phys. A* **1993**, *56*, 51.
(33) Cain, S. R.; Burns, F. C.; Otis, C. E. *J. Appl. Phys.* **1992**, *71*, 4107.
(34) Cain, S. *J. Phys. Chem.* **1993**, *97*, 7572.
(35) D'Couto, G. C.; Babu, S. V. *J. Appl. Phys.* **1994**, *75*, 3052.
(36) Luk'yanchuk, B.; Bityurin, N.; Himmelbauer, M.; Arnold, N. *Nucl. Instrum. Methods Phys. Res. B* **1997**, *122*, 347.
(37) Srinivasan, V.; Smrtic, M. A.; Babu, S. V. *J. Appl. Phys.* **1986**, *59*, 3861.
(38) Luk'yanchuk, B.; Bityurin, N.; Anisimov, S.; Bäuerle, D. *Appl. Phys. A* **1993**, *57*, 367.
(39) Luk'yanchuk, B.; Bityurin, N.; Anisimov, S.; Arnold, N.; Bäuerle, D. *Appl. Phys. A* **1996**, *62*, 397.
(40) Bityurin, N.; Malyshev, A.; Luk'yanchuk, B.; Anisimov, S.; Bäuerle, D. *Proc. SPIE*, 1996; p 103.
(41) Bityurin, N. *Appl. Surf. Sci.* **1999**, *138*−*139*, 354.
(42) Treyz, G. V.; Scarmozzoni, R.; Osgood Jr., R. M. *Appl. Phys. Lett.* **1989**, *55*, 346.
(43) Anisimov, S. I.; Khokhlov, V. A. *Instabilities in Laser-Matter Interaction*; CRC−Press: Boca Raton, 1995.
(44) Arnold, N.; Bityurin, N. *Appl. Phys. A* **1999**, *68*, 615.
(45) Srinivasan, R. *Appl. Phys. A* **1993**, *56*, 417.
(46) Fujiwara, H.; Fukumura, H.; Masuhara, H. *J. Phys. Chem.* **1995**, *99*, 11844.
(47) Fukumura, H.; Takahashi, E.-i.; Masuhara, H. *J. Phys. Chem.* **1995**, *99*, 750.
(48) Fukumura, H.; Mibuka, N.; Eura, S.; Masuhara, H.; Nishi, N. *J. Phys. Chem.* **1993**, *97*, 13761.
(49) Fujiwara, H.; Hayashi, T.; Fukumura, H.; Masuhara, H. *Appl. Phys. Lett.* **1994**, *64*, 2451.
(50) Fukumura, H.; Masuhara, H. *Chem. Phys. Lett.* **1994**, *221*, 373.
(51) Wu, X.; Sadeghi, M.; Vertes, A. *J. Phys. Chem. B* **1998**, *102*, 4770.
(52) Dutkiewicz, L.; Johnson, R. E.; Vertes, A.; Pedrys, R. *J. Phys. Chem. A* **1999**, *103*, 2925.
(53) Chang, T.-C.; Dlott, D. *J. Phys. Chem.* **1989**, *90*, 3590.
(54) Zhigilei, L. V.; Kodali, P. B. S.; Garrison, B. J. *J. Phys. Chem. B* **1997**, *101*, 2028.
(55) Zhigilei, L. V.; Kodali, P. B. S.; Garrison, B. J. *J. Phys. Chem. B* **1998**, *102*, 2845.
(56) Zhigilei, L. V.; Garrison, B. J. *J. Appl. Phys.* **2000**, *88*, 1281.
(57) Zhigilei, L. V.; Kodali, P. B. S.; Garrison, B. J. *Chem. Phys. Lett.* **1997**, *276*, 269.
(58) Zhigilei, L. V.; Garrison, B. J. *Appl. Phys. Lett.* **1997**, *71*, 551.
(59) Zhigilei, L. V.; Garrison, B. J. *Rapid Commun. Mass Spectrom.* **1998**, *12*, 1273.
(60) Zhigilei, L. V.; Garrison, B. J. *Appl. Phys. Lett.* **1999**, *74*, 1341.
(61) Zhigilei, L. V.; Garrison, B. J. *Appl. Phys. A* **1999**, *69*, S75.
(62) Afanasov, P. A.; Nedialkov, N. N.; Imamova, S. E.; Ruf, A.; Hugel, H.; Dausinger, F.; Berger, P. *Appl. Surf. Sci.* **2002**, *186*, 369.
(63) Smirnova, J. A.; Zhigilei, L. V.; Garrison, B. J. *Comput. Phys. Commun.* **1999**, *118*, 11.
(64) Dekel, E.; Eliezer, S.; Henis, Z.; Moshe, E.; Ludmirsky, A.; Goldberg, I. B. *J. Appl. Phys.* **1998**, *84*, 4851.
(65) Lippert, T.; Wokaun, A.; Stebani, J.; Nuyken, O.; Ihlemann, J. *J. Phys. Chem.* **1993**, *97*, 12297.
(66) Zeifman, M.; Garrison, B. J.; Zhigilei, L. V. *J. Appl. Phys.* **2002**, *92*, 2181.
(67) Lippert, T.; Yabe, A.; Wokaun, A. *Adv. Mater.* **1997**, *9*, 105.
(68) Lippert, T.; Stebani, J.; Ihlemann, J.; Nuyken, O.; Wokaun, A. *Angew. Makromol. Chem.* **1993**, *213*, 127.
(69) Koubenakis, A.; Labrakis, J.; Georgiou, S. *Chem. Phys. Lett.* **2001**, *346*, 54.
(70) Koubenakis, A.; Elmioti, T.; Georgiou, S. *Appl. Phys. A* **1999**, *69*, S637.
(71) Georgiou, S.; Koubenakis, A.; Labrakis, J.; Lassithotaki, M. *J. Chem. Phys.* **1998**, *109*, 8591.
(72) Koubenakis, A.; Labrakis, J.; Georgiou, S. *J. Chem. Soc., Faraday Trans.* **1998**, *94*, 3427.
(73) Atanassiou, A.; Andreou, E.; Fragouli, D.; Anglos, D.; Georgiou, S.; Fotakis, C. *J. Photochem. Photobiol. A: Chem.* **2001**, *145*, 229.
(74) Atanassiou, A.; Lassithotaki, M.; Anglos, D.; Georgiou, S.; Fotakis, C. *Appl. Surf. Sci.* **2000**, *154*−*155*, 89.
(75) Atanassiou, A.; Andreou, E.; Anglos, D.; Georgiou, S.; Fotakis, C. *Appl. Phys. A* **1999**, *69*, S285.
(76) Lassithotaki, M.; Atanassiou, A.; Anglos, D.; Georgiou, S.; Fotakis, C. *Appl. Phys. A* **1999**, *69*, 363.
(77) Lazare, S.; Granier, V. *J. Appl. Phys.* **1988**, *63*, 2110.
(78) Kukreja, L. M.; Hess, P. *Appl. Surf. Sci.* **1994**, *79*−*80*, 158.
(79) Sell, J. A.; Heffelfinger, D.; Ventzek, P. L. G.; Gilgenbach, R. L. *J. Appl. Phys.* **1991**, *69*, 1330.
(80) Efthimiopoulos, T.; Kritsotakis, E.; Kiagias, H.; Savvakis, C.; Bertachas, Y. *J. Phys. D: Appl. Phys.* **1998**, *31*, 2648.
(81) Zweig, A. D.; Venugopalan, V.; Deutsch, T. F. *J. Appl. Phys.* **1993**, *74*, 4181.
(82) Diaci, J.; Mozina, J. *Appl. Phys. A* **1992**, *55*, 352.
(83) Wang, J.; Niino, H.; Yabe, A. *Jpn. J. Appl. Phys.* **1999**, *38*, 871.
(84) Lengl, G.; Plettl, A.; Ziemann, P.; Spatz, J. P.; Moeller, M. *Appl. Phys. A* **2001**, *72*, 679.
(85) Sylvain, J.-F.; Niino, H.; Ono, S.; Nakaoka, S.; Yabe, A. *Appl. Surf. Sci.* **1999**, *141*, 25.
(86) Ono, S.; Nakaoka, S.; Wang, J.; Niino, H.; Yabe, A. *Appl. Surf. Sci.* **1998**, *127*−*129*, 821.
(87) Low, D. K. Y.; Schmidt, M. J. J.; Li, L. *Appl. Surf. Sci.* **2000**, *168*, 170.
(88) Slocombe, A.; Taufik, A.; Li, L. *Appl. Surf. Sci.* **2000**, *168*, 17.
(89) Davis, C. R.; Snyder, R. W.; Egitto, F. D.; D'Couto, G. C.; Babu, S. V. *J. Appl. Phys.* **1994**, *76*, 3049.
(90) Lippert, T.; Kunz, T.; Hahn, C.; Wokaun, A. *Recent Res. Devel. Macromol. Res.* **1997**, *2*, 121.
(91) Kunz, T.; Stebani, J.; Ihlemannn, J.; Wokaun, A. *Appl. Phys. A* **1998**, *67*, 347.
(92) Suzuki, K.; Matsuda, M.; Ogino, T.; Hayashi, T.; Terabayashi, T.; Amemiya, K. *Proc. SPIE*, **1997**; p 98.
(93) Hayashi, N.; Suzuki, K.; Matsuda, M.; Ogino, T.; Tomita, Y. *Proc. SPIE*, **1997**; p 129.
(94) Suzuki, K.; Matsuda, M.; Hayashi, N. *Appl. Surf. Sci.* **1998**, *127*−*129*, 905.
(95) Panitz, J.-C.; Lippert, T.; Stebani, J.; Nuyken, O.; Wokaun, A. *J. Phys. Chem.* **1993**, *97*, 5246.
(96) Lippert, T.; Stebani, J.; Ihlemann, J.; Nuyken, O.; Wokaun, A. *Angew. Makromol. Chem.* **1993**, *206*, 97.
(97) Stebani, J.; Nuyken, O.; Lippert, T.; Wokaun, A. *Makromol Chem. Rapid Commun.* **1993**, *14*, 365.
(98) Nuyken, O.; Nobis, M.; Scherer, C.; Ihlemann, J.; Beinhorn, F. *Macromol. Mater. Eng.* **2000**, *275*, 1.
(99) Nuyken, O.; Scherer, C.; Nobis, M. N.; Ihlemann, J. *Polym. Mater. Sci. Eng* **1997**, *76*, 206.
(100) Kunz, T.; Hahn, C.; Wokaun, A. *Adv. Mater.* **1998**, *10*, 786.
(101) Hahn, C.; Kunz, T.; Dahn, U.; Nuyken, O.; Wokaun, A. *Appl. Surf. Sci.* **1998**, *127*−*129*, 899.
(102) Nuyken, O.; Dahn, U.; Wokaun, A.; Kunz, T.; Hahn, C.; Hessel, V.; Landsiedel, J. *Acta Polym.* **1998**, *49*, 427.
(103) Nuyken, O.; Dahn, U.; Ehrfeld, W.; Hessel, V.; Hesch, K.; Landsiedel, J.; Diebel, J. *Chem. Mater.* **1997**, *9*, 485.
(104) Andrews, J. E.; Dyer, P. E.; D., F.; Key, P. H. *Appl. Phys. Lett.* 1983, *43*, 717.
(105) Srinivasan, R.; Braren, B. *J. Polym. Sci.* **1984**, *22*, 2601.
(106) Lippert, T.; Ortelli, E.; Panitz, J.-C.; Raimondi, F.; Wambach, J.; Wei, J.; Wokaun, A. *Appl Phys. A* **1999**, *69*, S651.
(107) Raimondi, F.; Abolhassani, S.; Brütsch, R.; Geiger, F.; Lippert, T.; Wambach, J.; Wei, J.; Wokaun, A. *J. Appl. Phys.* **2000**, *88*, 3659.
(108) Lippert, T.; Bennett, L. S.; Nakamura, T.; Niino, H.; Yabe, A. *Appl. Surf. Sci.* **1996**, *96*−*98*, 601.
(109) Lippert, T.; Dickinson, J. T.; Hauer, M.; Kopitkovas, G.; Langford, S. C.; Masuhara, H.; Nuyken, O.; Robert, J.; Salmio, H.; Tada, T.; Tomita, K.; Wokaun, A. *Appl. Surf. Sci.* **2002**, *197*−*198*, 746.
(110) Srinivasan, R.; Braren, B.; Casey, K. G.; Yeh, M. *J. Appl. Phys.* **1990**, *67*, 1604.
(111) Furutani, H.; Fukumura, H.; Masuhara, H. *J. Phys. Chem.* **1996**, *100*, 6871.
(112) Kim, H.; Postlewaite, J. C.; Zyung, T.; Dlott, D. D. *J. Appl. Phys.* **1988**, *64*, 2955.
(113) Bennett, L. S.; Lippert, T.; Furutani, H.; Fukumura, H.; Masuhara, H. *Appl. Phys. A* **1996**, *63*, 327.
(114) Hauer, M.; Funk, D. J.; Lippert, T.; Wokaun, A. *Appl. Phys. A*, in press.
(115) Furutani, H.; Fukumura, H.; Masuhara, H. *Appl. Phys. Lett.* **1994**, *65*, 3413.
(116) Furutani, H.; Fukumura, H.; Masuhara, H.; Lippert, T.; Yabe, A. *J. Phys. Chem. A* **1997**, *101*, 5742.
(117) Hauer, M.; Funk, D. J.; Lippert, T.; Wokaun, A. *Proc. SPIE-Int. Soc. Opt. Eng.* **2002**, *4760*, 259.
(118) Masabuchi, T.; Tada, T.; Nomura, E.; Hatanaka, K.; Fukumura, H.; Masuhara, H. *J. Phys. Chem. A* **2002**, *106*, 2180.
(119) Lippert, T.; David, C.; Hauer, M.; Masabuchi, T.; Masuhara, H.; Nomura, E.; Nuyken, O.; Phipps, C.; Robert, J.; Tada, T.; Tomita, K.; Wokaun, A. *Appl. Surf. Sci.* **2002**, *186*, 14.
(120) Lippert, T.; Wokaun, A.; Langford, S. C.; Dickinson, J. T. *Appl. Phys. A* **1999**, *69*, S655.
(121) Lippert, T.; Langford, S. C.; Wokaun, A.; Georgiou, S.; Dickinson, J. T. *J. Appl. Phys.* **1999**, *86*, 7116.

(122) Nuyken, O.; Stebani, J.; Lippert, T.; Wokaun, A.; Stasko, A. *Macromol. Chem. Phys.* **1995**, *196*, 751.
(123) Langford, S. C.; Dickinson, J. T.; Hauer, M.; Lippert, T.; Wokaun, A., submitted.
(124) Lippert, T.; Gerber, T.; Wokaun, A.; Funk, D. J.; Fukumura, H.; Goto, M. *Appl. Phys. Lett.* **1999**, *75*, 1018.
(125) David, C.; Wei, J.; Lippert, T.; Wokaun, A. *Microlectr. Eng.* **2001**, *57*−*58*, 453.
(126) Lippert, T.; Wei, J.; Wokaun, A.; Hoogen, N.; Nuyken, O. *Appl. Surf. Sci.* **2000**, *168*, 270.
(127) Lippert, T.; Wei, J.; Wokaun, A.; Hoogen, N.; Nuyken, O. *Macromol. Mater. Eng.* **2000**, *283*, 140.
(128) Bachman, F. *Chemtronics* **1989**, *4*, 149.
(129) Lankard, J. R.; Wolbold, G. *Appl. Phys. A* **1992**, *54*, 355.
(130) Beuhler, A.; Tungare, A.; Savic, J. *Circuit World* **1998**, *24*, 36.
(131) Inagaki, M.; Takichi, T.; Hishiyama, Y.; Obslei, A. *Chemistry and Physics of Carbon*; Marcel Dekker: New York, 1999; p 245.
(132) Schnyder, B.; Wambach, J.; Kunz, T.; Hahn, C.; Koetz, R. *J. Electron. Spectrosc.* **1999**, *105*, 113.
(133) Wesner, D. A.; Aden, M.; Gottmann, J.; Husmann, A.; Kreutz, E. W. *Fresenius J. Anal. Chem.* **1999**, *105*, 113.
(134) Zeng, K. C.; Yung, K. C.; Xie, C. S. *Surf. Coat. Technol.* **2002**, *153*, 210.
(135) Yung, K. C.; Zeng, D. W.; Yue, T. M. *Appl. Surf. Sci.* **2001**, *173*, 193.
(136) Zeng, D. W.; Yung, K. C. *Appl. Surf. Sci.* **2001**, *180*, 280.
(137) Ortelli, E. E.; Geiger, F.; Lippert, T.; Wei, J.; Wokaun, A. *Macromolecules* **2000**, *33*, 5090.
(138) Ortelli, E. E.; Geiger, F.; Lippert, T.; Wokaun, A. *Appl. Spectrosc.* **2001**, *55*, 412.
(139) Srinivasan, R.; Braren, B.; Seeger, D. E.; Dreyfus, R. W. *Macromolecules* **1986**, *19*, 916.
(140) Singleton, D. L.; Paraskevopoulos, G.; Irwin, R. S. *J. Appl. Phys.* **1989**, *66*, 3324.
(141) Lazare, S.; Guan, W.; Drilhole, D. *Appl. Surf. Sci.* **1996**, *96*−*98*, 605.
(142) Schumann, M.; Sauerbrey, R.; Smayling, M. C. *Appl. Phys. Lett.* **1991**, *58*, 428.
(143) Feurer, T.; Sauerbrey, R.; Smayling, M. C.; Story, B. J. *Appl. Phys. A* **1993**, *56*, 275.
(144) Philips, H. M.; Wahl, S.; Sauerbrey, R. *Appl. Phys. Lett.* **1995**, *62*, 2572.
(145) Walther, H. G.; Kitzing, T.; Bozoki, Z.; Liakhou, G. L.; Paloni, S. *J. Appl. Phys.* **1999**, *85*, 7540.
(146) Qin, Z. Y.; Du, B. Y.; Zhang, J.; He, T. B.; Qin, L.; Zhang, Y. S. *Appl. Phys. A* **2001**, *72*, 711.
(147) Ball, Z.; Feurer, T.; Callahan, D. L.; Sauerbrey, R. *Appl. Phys. A* **1996**, *62*, 203.
(148) Gu, J.; Tay, E.; Lim, P. K.; Lim, P. *Appl. Phys. A* **2002**, *74*, 487.
(149) Reyna, L. G.; Sobehart, J. R. *J. Appl. Phys.* **1995**, *78*, 3423.
(150) Burns, F. C.; Cain, S. R. *J. Phys. D: Appl. Phys.* **1996**, *29*, 1349.
(151) Efthimiopoulos, T.; Kiagia, C.; Heliotis, G.; Helidonis, E. *Can. J. Phys.* **2000**, *78*, 509.
(152) Costela, A.; Figuera, J. M.; Florido, F.; Garcia-Moreno, I.; Collar, E. P.; Sastre, R. *Appl. Phys. A* **1995**, *60*, 261.
(153) Bityurin, N.; Muraviov, S.; Alexandrov, A.; Malyshev, A. *Appl. Surf. Sci.* **1997**, *109*−*110*, 270.
(154) Schmidt, H.; Luther, K.; Troe, J. *Appl. Surf. Sci.* **1999**, *138*−*139*, 102.
(155) Lade, R. J.; Morley, I. W.; May, P. W.; Rosser, K. N.; Ashfold, M. N. R. *Diamond Relat. Mater.* **1999**, *8*, 1654.
(156) Küper, S.; Stuke, M. *Appl. Phys. A* **1989**, *49*, 211.
(157) Srinivasan, R.; Braren, B.; Casey, K. G.; Yeh, M. *J. Appl. Phys.* **1990**, *68*, 1842.
(158) Blanchet, G. C.; Cotts, P.; Fincher Jr., C. R. *J. Appl. Phys.* **2000**, *88*, 2975.
(159) Lippert, T.; Webb, R. L.; Langford, S. C.; Dickinson, J. T. *J. Appl. Phys.* **1999**, *85*, 1838.
(160) Baker, A. K.; Dyer, P. E. *Appl. Phys. A* **1993**, *57*, 543.
(161) Hopp, B.; Csete, M.; Szabo, G.; Bor, Z. *Appl. Phys. A* **1995**, *61*, 339.
(162) Srinivasan, R. *J. Appl. Phys.* **1993**, *73*, 2743.
(163) Hare, D. E.; Dlott, D. D. *Appl. Phys. Lett.* **1994**, *64*, 715.
(164) Hare, D. E.; Franken, J.; Dlott, D. D. *J. Appl. Phys.* **1995**, *77*, 5950.
(165) Dyer, P. E.; Oldershaw, G. A.; Schudel, D. *J. Phys. D: Appl. Phys.* **1992**, *25*, 323.
(166) Wagner, F.; Hoffmann, P. *Appl. Surf. Sci.* **2000**, *154*−*155*, 627.
(167) Wagner, F.; Hoffmann, P. *Appl. Surf. Sci.* **2000**, *168*, 158.
(168) Wagner, F.; Hoffmann, P. *Appl. Phys. A* **1999**, *69*, S841.
(169) Mansour, N.; Ghaleh, K. J. *Appl. Phys. A* **2002**, *74*, 63.
(170) Klose, S.; Arenholz, E.; Heitz, J.; Bäuerle, D. *Appl. Phys. A* **1999**, *69*, S487.
(171) Srinivasan, R.; Lazare, S. *J. Phys. Chem.* **1986**, *90*, 2124.
(172) Lippert, T.; Zimmermann, F.; Wokaun, A. *Appl. Spectrosc.* **1993**, *47*, 1931.
(173) Chtaib, M.; Roberfroid, E. M.; Novis, Y.; Pireaux, J. J.; Caudano, R.; Lutgen, P.; Feyder, G. *J. Vac. Sci. Technol.* **1989**, *A7*, 3233.
(174) Kokai, F.; Saito, H.; Fujioka, T. *Macromolecules* **1990**, *23*, 674.
(175) Dyer, P. E.; Oldershaw, G. A.; Sidhu, J. *J. Phys. Chem.* **1991**, *95*, 10004.
(176) Lazare, S.; Hoh, P. D.; Baker, J. M.; Srinivasan, R. *J. Am. Chem. Soc.* **1984**, *106*, 4288.
(177) Watanabe, H.; Yamamoto, M. *J. Appl. Polym. Sci.* **1999**, *71*, 2027.
(178) Rossier, J. S.; Bercier, P.; Scwarz, A.; Loridant, S.; Girault, H. H. *Langmuir* **1999**, *15*, 5173.
(179) Huber, N.; Gruber, J.; Arnold, N.; Heitz, J.; Bäuerle, D. *Europhys. Lett.* **2000**, *51*, 674.
(180) Blanchet, G. B.; Fincher Jr., C. R. *Appl. Phys. Lett.* **1994**, *65*, 1311.
(181) Dickinson, J. T.; Shin, J.-J. *Nucl. Instrum. Methods Phys. Res. B* **1994**, *91*, 672.
(182) Blanchet, G. B.; Fincher Jr., C. R. *Appl. Phys. Lett.* **1996**, *68*, 929.
(183) Haba, B.; Morishige, Y.; Kishida, S. *Appl. Phys. A* **1995**, *60*, 27.
(184) Skordoulis, C. D.; Makropoulou, M. I.; Bolovinos, A. L.; Serafetinides, A. A. *Laser Med. Sci.* **1997**, *12*, 313.
(185) Smausz, T.; Kresz, N.; Hopp, B. *Appl. Surf. Sci.* **2001**, *177*, 66.
(186) Hamada, Y.; Kawanishi, S.; Nishii, M.; Sugimoto, S.; Yamamoto, T. *Jpn. J. Appl. Phys.* **1994**, *33*, 4764.
(187) Izumi, Y.; Kawanishi, S.; Hara, S.; Yoshikawa, D.; Yamamoto, T. *Bull. Chem. Soc. Jpn.* **1998**, *71*, 2721.
(188) Niino, H.; Okano, H.; Inui, K.; Yabe, A. *Appl. Surf. Sci.* **1997**, *109*−*110*, 259.
(189) Niino, H.; Yabe, A. *Appl. Phys. Lett.* **1993**, *63*, 3527.
(190) Okoshi, M.; Murahara, M.; Toyoda, K. *J. Mater. Res.* **1992**, *7*, 1912.
(191) Murahara, M.; Toyoda, K. *J. Adhes. Sci. Technol.* **1995**, *9*, 1601.
(192) Heitz, J.; Niino, H.; Yabe, A. *Appl. Phys. Lett.* **1996**, *68*, 2648.
(193) Heitz, J.; Niino, H.; Yabe, A. *Jpn. J. Appl. Phys.* **1996**, *35*, 4110.
(194) Matienzo, L. J.; Zimmernmann, J. A.; Egitto, F. D. *J. Vac. Sci. Technol A* **1994**, *12*, 2662.
(195) Hopp, B.; Smausz, T.; Tombacz, E.; Wittmann, T.; Ignacz, F. *Opt. Commun.* **2000**, *181*, 337.
(196) Hopp, B.; Smausz, T.; Wittmann, T.; Ignacz, F. *Appl. Phys. A* **2000**, *71*, 315.
(197) Dyer, P. E.; Karnakis, D. M. *Appl. Phys. Lett.* **1994**, *64*, 1344.
(198) Feng, Y.; Liu, Z. Q.; Yi, X.-S. *Appl. Surf. Sci.* **2000**, *156*, 177.
(199) Hopp, B.; Bor, Z.; Homolya, E.; Mihalik, E. *Appl. Surf. Sci.* **1997**, *109*−*110*, 232.
(200) Devalckenaere, M.; Jadin, A.; Kolev, K.; Laude, L. D. *Nucl. Instrum. Methods Phys. Res. B* **1999**, *151*, 263.
(201) Sabbert, D.; Landsiedel, J.; Bauer, A.-D.; Ehrfeld, W. *Appl. Surf. Sci.* **1999**, *150*, 185.
(202) Laurens, P.; Sadras, B.; Decobert, F.; Arefei, F.; Amouroux, J. *Appl. Surf. Sci.* **1999**, *138*−*139*, 93.
(203) Schmidt, M. J. J.; Li, L.; Spencer, J. T.; Key, P. H. *Appl. Surf. Sci.* **1999**, *138*−*139*, 418.
(204) Skordoulis, C. D.; Makropoulou, M.; Serafetinides, A. A. *Appl. Surf. Sci.* **1995**, *86*, 239.
(205) Laude, L. D.; Soudant, S.; Beauvois, S.; Renaut, D.; Jadin, A. *Nucl. Instrum. Methods Phys. Res. B* **1997**, *131*, 211.
(206) Tsuboi, Y.; Goto, M.; Itaya, A. *Chem. Lett.* **1998**, 521.
(207) Tsuboi, Y.; Goto, M.; Itaya, A. *J. Appl. Phys.* **2001**, *89*, 7917.
(208) Tsuboi, Y.; Ikejiri, T.; Yamada, K.; Itaya, A. *Appl. Phys. A* **2001**, *73*, 637.
(209) Fuhr, G.; Ronacher, B.; Krahe, R.; Fest, S.; Shirley, S. G.; Rogaschewski, S. *Appl. Phys. A* **1999**, *68*, 379.
(210) Küper, S.; Brannon, J.; Brannon, K. *Appl. Phys. A* **1993**, *57*, 255.
(211) Okoshi, M.; Kuramatsu, M.; Inoue, N. *Jpn. J. Appl. Phys.* **2001**, *40*, L41.
(212) Graubner, V.-M.; Jordan, R.; Nuyken, O.; Lippert, T.; Hauer, M.; Schnyder, B.; Wokaun, A. *Appl. Surf. Sci.* **2002**, *197*−*198*, 786.
(213) Baumann, R.; Bargon, J. *Appl. Surf. Sci.* **1996**, *106*, 287.
(214) Van Dyke, L. S.; Brumlik, C. J.; Martin, C. R.; Yu, Z.; Collins, G. J. *Synth. Metals* **1992**, *52*, 299.
(215) Kay, E. *Methods and Materials in Microelectronic Technology*; Plenum: New York, 1984.
(216) Lippert, T.; Raimondi, F.; Wambach, J.; Wei, J.; Wokaun, A. *Appl Phys. A* **1999**, *63*, S291.
(217) Abdou, M. S. A.; Xie, Z. W.; Leung, A. M.; Holdcroft, S. *Synth. Met.* **1992**, *52*, 159.
(218) Wong, T. K. S.; Gao, S.; Hu, X.; Liu, H.; Chan, Y. C.; Lam, Y. L. *Mater. Sci. Engin. B* **1998**, *55*, 71.
(219) Tsunoda, K.; Ishii, T.; Tezuka, Y.; Yajima, H. *J. Photochem. Photobiol. A: Chem.* **1997**, *106*, 21.
(220) Tsunoda, K.; Kakinuma, K.; Yajima, H.; Ishii, T. *Appl. Phys. Lett.* **1998**, *73*, 3381.
(221) Himmelbauer, M.; Arenholz, E.; Bäuerle, D.; Schilcher, K. *Appl. Phys. A* **1996**, *63*, 337.
(222) Bäuerle, D.; Himmelbauer, M.; Arenholz, E. *J. Photochem. Photobiol. A: Chem.* **1997**, *106*, 27.
(223) Piglmayer, K.; Arenholz, E.; Ortwein, C.; Arnold, N.; Bäuerle, D. *Appl. Phys. Lett.* **1998**, *73*, 847.
(224) Hansen, S. G.; Robitaille, T. E. *J. Appl. Phys.* **1988**, *64*, 2122.
(225) Kokai, F.; Koga, Y.; Kakudate, Y.; Kawaguchi, M.; Fujiwara, S.; Kubota, M.; Fukuda, M. *Appl. Phys. A* **1994**, *59*, 299.

(226) Estler, R. C.; Nogar, N. S. *Appl. Phys. Lett.* **1986**, *49*, 1175.
(227) Krajnovich, D. J. *J. Phys. Chem. A* **1997**, *101*, 2033.
(228) Dickinson, J. T.; Shin, J.-J.; Jiang, W.; Norton, M. G. *J. Appl. Phys.* **1993**, *74*, 4729.
(229) Blanchet, G. B.; Fincher, J. C. R. *Appl. Phys. Lett.* **1996**, *68*, 929.
(230) Hansen, S. G. *J. Appl. Phys.* **1989**, *66*, 1411.
(231) Creasy, W. R.; Brenna, J. T. *Chem. Phys.* **1988**, *126*, 453.
(232) Larciprete, R.; Stuke, M. *Appl. Phys. B* 1987, *42*, 181.
(233) Shibagaki, K.; Takada, N.; Sasaki, K.; K., K. *J. Appl. Phys.* **2002**, *91*, 2449.
(234) Tsunekawa, M.; Nishio, S.; Sato, H. *J. Appl. Phys.* **1994**, *76*, 5598.
(235) Tsunekawa, M.; Nishio, S.; Sato, H. *Jpn. J. Appl. Phys.* **1995**, *34*, 218.
(236) Danielzik, B.; Fabricius, N.; Röwekamp, M.; Linde, D. v. d. *Appl. Phys. Lett* **1986**, *48*, 212.
(237) Feldmann, D.; Kutzner, J.; Laukemper, J.; MacRobert, S.; Welge, K. H. *Appl. Phys. B* **1987**, *44*, 81.
(238) Cefalas, A. C.; Sarantopoulou, E.; Argitis, P.; Gogolides, E. *Appl Phys. A* **1999**, *69*, S929.
(239) Cefalas, A. C.; Vassilopoulos, N.; Sarantopoulou, E.; Kollia, Z.; Skordoulis, C. *Appl. Phys. A* **2000**, *70*, 21.
(240) Hauer, M.; Dickinson, J. T.; Langford, S. C.; Lippert, T.; Wokaun, A. *Appl. Surf. Sci.* **2002**, *197*−*198*, 791.
(241) Brannon, J. H.; Lankard, J. R.; Baise, A. I.; Burns, F.; Kaufman, J. *J. Appl. Phys.* **1985**, *58*, 2036.
(242) Kelly, R. *J. Chem. Phys.* **1988**, *92*, 5047.
(243) Grivas, C.; Niino, H.; Yabe, A. *Appl Phys. A* **1999**, *69*, S159.
(244) Kelly, R.; Rothenberg, J. E. *Nucl. Instrum. Methods Phys. Res. B* **1985**, *7*−*8*, 755.
(245) Kelly, R.; Dreyfus, R. W. *Nucl. Instrum. Methods Phys. Res. B* **1988**, *32*, 341.
(246) Campbell, E. E. B.; Ulmer, G.; Bues, K.; Hertel, I. V. *Appl Phys. A* **1989**, *48*, 543.
(247) Campbell, E. E. B.; Ulmer, G.; Hasselberger, B.; Hertel, I. V. *Appl. Surf. Sci.* **1989**, *43*, 346.
(248) Press, W. H.; Flannery, B. P.; Teukolsky, S. A.; Vetterling, W. T. *Numerical Recipies in Pascal*; Cambridge University: Cambridge, 1989.
(249) Dyer, P. E.; Jenkins, S. D.; Sidhu, J. *Appl. Phys. Lett.* **1986**, *49*, 453.
(250) Dyer, P. E.; Jenkins, S. D.; Sidhu, J. *Appl. Phys. Lett.* **1988**, *52*, 1880.
(251) Hopp, B.; Bor, Z.; Homolya, E.; Mihalik, E. *Proc. SPIE-Int. Soc. Opt. Eng.* **1998**, *3423*, 389.
(252) Wei, J.; Hoogen, N.; Lippert, T.; Hahn, C.; Nuyken, O.; Wokaun, A. *Appl. Phys. A* **1999**, *69*, S849.
(253) Novis, Y.; Pireaux, J. J.; Brezini, A.; Petit, E.; Caudano, R.; Lutgen, P.; Feyder, G.; Lazare, S. *J. Appl. Phys.* **1988**, *64*, 365.
(254) Bahners, T.; Schollmeyer, E. *J. Appl. Phys.* **1989**, *66*, 1884.
(255) Arenholz, E.; Wagner, M.; Heitz, J.; Bäuerle, D. *Appl. Phys. A* **1992**, *55*, 119.
(256) Tonyali, K.; Jensen, L. C.; Dickinson, J. T. *J. Vac. Sci. Technol. A* **1988**, *6*, 941.
(257) Dyer, P. E.; Farley, R. J. *Appl. Phys. Lett.* **1990**, *57*, 765.
(258) Niino, H.; Yabe, A. *J. Photochem. Photobiol. A: Chem.* **1992**, *65*, 303.
(259) Emel'yanov, V. I.; Eriomin, K. I. *Proc. SPIE-Int. Soc. Opt. Eng.* **1998**, *3343*, 1056.
(260) Heitz, J.; Arenholz, E.; Bäuerle, D.; Schilcher, K. *Appl. Surf. Sci.* **1994**, *81*, 108.
(261) Heitz, J.; Arenholz, E.; Bäuerle, D.; Hibst, H.; Hagemeyer, A.; Cox, G. *Appl. Phys. A* **1993**, *56*, 329.
(262) Beleznai, C.; Vajtai, R.; Nanai, L. *Fractals* **1997**, *5*, 275.
(263) Bolle, M.; Lazare, S.; Le Blanc, M.; Wilmes, A. *Appl. Phys. Lett.* **1992**, *60*, 674.
(264) Bolle, M.; Lazare, S. *J. Appl. Phys.* **1993**, *73*, 3516.
(265) Bolle, M.; Lazare, S. *Appl. Surf. Sci.* **1993**, *65*−*66*, 349.
(266) Bolle, M.; Lazare, S. *Appl. Surf. Sci.* **1993**, *69*, 31.
(267) Niino, H.; Kawabata, Y.; Yabe, A. *Jpn. J. Appl. Phys.* **1989**, *28*, L2225.
(268) Lazare, S.; Drilhole, D. *J. Photochem. Photobiol. A: Chem.* **1997**, *106*, 15.
(269) Lazare, S.; Bolle, M.; Cros, A.; Bellard, C. *Nucl. Instrum. Methods Phys. Res. B* **1995**, *105*, 159.
(270) Hopp, B.; Csete, M.; Revesz, K.; Vinko, J.; Bor, Z. *Appl. Surf. Sci.* **1996**, *96*−*98*, 611.
(271) Csete, M.; Marti, O.; Bor, Z. *Appl. Phys. A* **2001**, *73*, 521.
(272) Sendova, M.; Hiraoka, H. *Jpn. J. Appl. Phys.* **1993**, *32*, 6182.
(273) Hiraoka, H.; Lätsch, S.; Sendova, M. *J. Photopolym. Sci. Technol.* **1994**, *7*, 299.
(274) Hiraoka, H.; Sendova, M. *Appl. Phys. Lett.* **1994**, *64*, 563.
(275) Hiraoka, H. *J. Photochem. Photobiol. A: Chem.* **1995**, *92*, 129.
(276) Sendova, M.; Hiraoka, H.; Lee, C.-H. *Jpn. J. Appl. Phys.* **1994**, *33*, 7135.
(277) Lazare, S.; Benet, P.; Guan, W.; Bolle, M.; Mihailov, S. *Excimer Lasers*; Kluwer Academic Publishers: Dordrecht, 1994; p 201.
(278) Chan, C.-M.; Ko, T.-M.; Hiraoka, H. *Surf. Sci. Rep.* **1996**, *24*, 1.
(279) Fourrier, T.; Schrems, G.; Muehlberger, T.; Heitz, J.; Arnoild, N.; Bäuerle, D.; Mosbacher, M.; Boneberg, J.; Leiderer, P. *Appl. Phys. A* **2001**, *72*, 1.
(280) Gerenser, L. J. *Metallization of Polymers*; American Chemical Society: Washington, DC, 1990; p 443.
(281) Ehrlich, D. J.; Tsao, J. Y. *Laser Microfabrication: Thin Film Processes and Lithography*; Academic Press: London, 1989.
(282) Bauer, A.; Ganz, J.; Hesse, K.; Koehler, E. *Appl. Surf. Sci.* **1990**, *46*, 113.
(283) Liebel, G. *Galvanotechnik* **1988**, *79*, 2883.
(284) Hiraoka, H.; Lazare, S. *Appl. Surf. Sci.* **1990**, *46*, 246.
(285) Wesner, D. A.; Weichenhain, R.; Pfleging, W.; Horn, H.; Kreutz, E. W. *Fresenius J. Anal. Chem.* **1997**, *358*, 248.
(286) Horn, H.; Beil, S.; Wesner, D. A.; Weichenhein, R.; Kreutz, E. W. *Nucl. Instrum. Methods Phys. Res. B* **1999**, *151*, 279.
(287) Zhao, G.; Philips, H. M.; Zheng, H.; Tam, S.; Li, W.; Wen, G.; Gong, Z.; Lam, Y. *Proc. SPIE-Int. Soc. Opt. Eng.* **2000**, *3933*, 505.
(288) Petit, S.; Laurens, P.; Amouroux, J.; Arefi-Khonsari, F. *Appl. Surf. Sci.* **2000**, *168*, 300.
(289) Lazare, S.; Benet, P. *J. Appl. Phys.* **1993**, *74*, 4953.
(290) Laurens, P.; Sadras, B.; Decobert, F.; Arefi-Khonsari, F.; Amouroux, J. *Internat. J. Adhes. Adhes.* **1998**, *18*, 19.
(291) Watanabe, H.; Takata, T. *Angew. Makromol. Chem.* **1996**, *235*, 95.
(292) Catry, C.; Jeuris, K.; Jackers, C.; Hofkens, J.; Bastin, L.; Gensch, T.; Grim, P. C. M.; De Schryver, F. C.; Van Damme, M. *Langmuir* **1999**, *15*, 1364.
(293) Niino, H.; Yabe, A. *Appl. Surf. Sci.* **1996**, *96*−*98*, 572.
(294) Niino, H.; Yabe, A. *J. Photochem. Photobiol. A: Chem.* **1997**, *106*, 9.
(295) Srinivasan, R.; Lazare, S. *Polymer* **1985**, *26*, 1297.
(296) Vasilets, V. N.; Yuranova, T. I.; Ponomarev, A. N. *J. Photopolym. Sci. Technol.* **1994**, *7*, 309.
(297) Vasilets, V. N.; Nakamura, K.; Uyama, Y.; Ogata, S.; Ikada, Y. *Polymer* **1998**, *39*, 2875.
(298) Vasilets, V. N.; Hirata, I.; Iwata, H.; Ikada, Y. *J. Polym Sci., Part A: Polym. Chem.* **1998**, *36*, 2215.
(299) Zhang, J.-Y.; Boyd, I. W.; Esrom, H. *Surf. Interface Anal.* **1996**, *24*, 718.
(300) Zhang, J.-Y.; Esrom, H.; Kogelschatz, U.; Emig, G. *Appl. Surf. Sci.* **1993**, *69*, 299.
(301) Srinivasan, R.; Leigh, W. J. *J. Am. Chem. Soc.* **1982**, *104*, 6784.
(302) Srinivasan, R. *Polymer* **1982**, *23*, 1863.
(303) Shirai, M.; Yamamoto, T.; Tsunooka, M. *Polym. Degrad. Stab.* **1999**, *63*, 481.
(304) Shinozuka, T.; Shirai, M.; Tsunooka, M. *J. Photopolym. Sci. Technol.* **2000**, *13*, 751.
(305) Fuchs, F.; Goetzberger, O.; Henck, R.; Fogarassy, E. *Appl. Phys. A* **1995**, *60*, 505.
(306) Srinivasan, R. *Appl. Phys. Lett.* **1991**, *58*, 2895.
(307) Srinivasan, R. *J. Appl. Phys.* **1992**, *72*, 1651.
(308) Srinivasan, R. *Appl. Phys. A* **1992**, *55*, 269.
(309) Srinivasan, R. *J. Appl. Phys.* **1991**, *70*, 7588.
(310) Bozhevolnyi, S. I.; Potemkin, I. V.; Svetovoy, V. B. *J. Appl. Phys.* **1992**, *71*, 2030.
(311) Bozhevolnyi, S. I.; Potemkin, I. V. *J. Phys. D: Appl. Phys.* **1994**, *27*, 19.
(312) Bonlie, J. D.; Patterson, F.; Price, D.; White, B.; Springer, P. *Appl. Phys. B* **2000**, *70*, S155.
(313) Bloembergen, N. *IEEE J. Qaunt. Electron.* **1974**, *QE*−*10*, 375.
(314) Stuart, B. C.; Feit, M. D.; Rubenchik, A. M.; Shore, B. W.; Perry, M. D. *Phys. Rev. Lett.* **1995**, *74*, 2248.
(315) Haight, R.; Hayden, D.; Longo, P.; Neary, T.; Wagner, A. *Proc. SPIE-Int. Soc. Opt. Eng.* **1998**, *3546*, 477.
(316) Shani, Y.; Melnick, I.; Yoffe, S.; Sharon, Y.; Lieberman, K.; Terkel, H. *Proc. SPIE-Int. Soc. Opt. Eng.* **1998**, *3546*, 112.
(317) Srinivasan, R.; Sutcliffe, E.; Braren, B. *Appl. Phys. Lett.* **1987**, *51*, 1285.
(318) Küper, S.; Stuke, M. *Appl. Phys. B* **1987**, *44*, 199.
(319) Küper, S.; Stuke, M. *Appl. Phys. Lett.* **1989**, *54*, 4.
(320) Küper, S.; Stuke, M. *Mater. Res. Soc. Symp Proc.* **1989**, *129*, 375.
(321) Preuss, S.; Späth, M.; Zhang, Y.; Stuke, M. *Appl. Phys. Lett.* **1993**, *62*, 3049.
(322) Preuss, S.; Späth, M.; Stuke, M. *Microelectron. Eng.* **1994**, *25*, 313.
(323) Kautek, W.; Mitterer, S.; Krüger, J.; Husinsky, W.; Grabner, W. *Appl. Phys. A* **1994**, *58*, 513.
(324) Kumagai, H.; Midorikawa, K.; Toyoda, K.; Nakamura, S.; Okamoto, T.; Obara, M. *Appl. Phys. Lett.* **1994**, *65*, 1850.
(325) Nakamura, S.; Midorikawa, K.; Kumagai, H.; Obara, M.; Toyoda, K. *Jpn. J. Appl. Phys.* **1996**, *35*, 101.
(326) Zhang, Y.; Lowe, R. M.; Harvey, E.; Hannaford, P.; Endo, A. *Appl. Surf. Sci.* **2002**, *186*, 345.
(327) Serafetinides, A. A.; Skordoulis, C. D.; Makropoulou, M. I.; Kar, A. K. *Appl. Surf. Sci.* **1998**, *135*, 276.
(328) Serafetinides, A. A.; Skordoulis, C. D.; Makropoulou, M. I.; Kar, A. K. *Appl. Surf. Sci.* **2001**, *180*, 42.
(329) Baudach, S.; Bonse, J.; Kautek, W. *Appl. Phys. A* **1999**, *69*, S395.

(330) Baudach, S.; Bonse, J.; Krüger, J.; Kautek, W. *Appl. Surf. Sci.* **2000**, *154−155*, 555.
(331) Bonse, J.; Baudach, S.; Krüger, J.; Kautek, W. *Proc. SPIE-Int. Soc. Opt. Eng.* **2000**, *4065*, 161.
(332) Baudach, S.; Krüger, J.; Kautek, W. *Rev. Laser Engin.* **2001**, *29*, 705.
(333) Heitz, J.; Arenholz, E.; Bäuerle, D.; Sauerbrey, R.; Phillips, H. M. *Appl. Phys. A* **1994**, *59*, 289.
(334) Niino, H.; Ihlemann, J.; Ono, S.; Yabe, A. *J. Photopolym Sci. Technol.* **2000**, *13*, 167.
(335) Niino, H.; Yabe, A. *J. Photopolym Sci. Technol.* **2001**, *14*, 197.
(336) Yamasaki, K.; Juodkazis, S.; Lippert, T.; Watanabe, M.; Matsuo, S.; Misawa, H. *Appl. Phys. A* 2003, *76*, 325.
(337) Hopp, B.; Toth, Z.; Gal, K.; Mechler, A.; Bor, Z.; Moustaizis, S. D.; Georgiou, S.; Fotakis, C. *Appl. Phys. A* **1999**, *69*, S191.
(338) Toth, Z.; Hopp, B.; Mechler, A.; Bor, Z.; Moustaizis, S. D.; Athanassiou, A.; Georgiou, S.; Kalpouzos, C.; Fotakis, C. *Laser Phys.* **2000**, *10*, 241.
(339) Hosokawa, Y.; Yashiro, M.; Asahi, T.; Masuhara, H. *Proc. SPIE-Int. Soc. Opt. Eng.* **2001**, *4274*, 78.
(340) Hosokawa, Y.; Yashiro, M.; Asahi, T.; Masuhara, H.; Kadota, T.; Shirota, Y. *Jpn. J. Appl. Phys.* **2001**, *40*, L1116.
(341) Hahn, C.; Lippert, T.; Wokaun, A. *J. Phys. Chem. B* **1999**, *103*, 1287.
(342) Wen, X.; Tolbert, W.; Dlott, D. D. *Chem. Phys. Lett.* **1992**, *192*, 315.
(343) Kim, H.; Postlewaite, J. C.; Zhung, T.; Dlott, D. D. *Appl. Phys. Lett.* **1989**, *54*, 2274.
(344) Zhung, T.; Kim, H.; Postlewaite, J. C.; Dlott, D. D. *J. Appl. Phys.* **1989**, *65*, 4548.
(345) Wen, X.; Hare, D. E.; Dlott, D. D. *Appl. Phys. Lett.* **1994**, *64*, 184.
(346) Sandy Lee, I.-Y.; Wen, X.; Tolbert, W. A.; Dlott, D. D.; Doxtader, M.; Arnold, D. R. *J. Appl. Phys.* **1992**, *72*, 2440.
(347) Hare, D. E.; Franken, J.; Dlott, D. D.; Chronister, E. L.; Flores, J. J. *Appl. Phys. Lett.* **1994**, *65*, 3051.
(348) Hare, D. E.; Rhea, S. T.; Dlott, D. D.; D'Amato, R. J.; Lewis, T. E. *J. Imag. Sci. Technol.* **1998**, *42*, 187.
(349) Moore, D. S.; Gahagan, K. T.; Reho, J. H.; Funk, D. J.; Buelow, S. J.; Rabie, R. L.; Lippert, T. *Appl. Phys. Lett.* **2001**, *78*, 40.
(350) Simon, P.; Bekesi, J.; Doelle, C.; Klein-Wiele, J.-H.; Marowsky, G.; Szatmari, S.; Wellegehausen, B. *Appl. Phys. B* **2002**, *74*, S189.
(351) Henderson, D.; White, J. C.; Craighead, H. G.; Adesida, I. *Appl. Phys. Lett.* **1985**, *45*, 900.
(352) Dyer, P. E.; Sidhu, J. *J. Opt. Soc. Am. B* **1986**, *3*, 792.
(353) Wada, S.; Toshiro, H.; Toyoda, K.; Niino, H.; Yabe, A. *Appl. Phys. Lett.* **1993**, *62*, 211.
(354) Herman, P. R.; Chen, B.; Moore, J. D. *Mater. Res. Soc. Proc.* **1993**, *285*, 163.
(355) Herman, P. R.; Chen, B.; Moore, J. D. *AIP. Conf. Proc.* **1993**, *288*, 297.
(356) Herman, P. R.; Chen, B.; Moore, J. D.; Canaga-Retnam, M. *Mater. Res. Soc. Proc.* **1992**, *236*, 53.
(357) Costela, A.; Garcia-Moreno, I.; Florido, F.; Figuera, J. M.; Sastre, R.; Hooker, S. M.; Cashmore, J. S.; Webb, C. E. *J. Appl. Phys.* **1995**, *77*, 2343.
(358) Padeletti, G.; Lapczyna, M.; Stuke, M. *Mater. Res. Soc. Proc.* **1999**, *544*, 3.
(359) Lapczyna, M.; Stuke, M. *Mater. Res. Soc. Proc.* **1998**, *526*, 143.
(360) Lapczyna, M.; Stuke, M. *Appl. Phys. A* **1998**, *66*, 473.
(361) Museur, L.; Zheng, W. Q.; Kanaev, A. V.; Castex, M. C. *IEEE J. Sel. Top. Quantum Electron.* **1995**, *1*, 900.
(362) Riedel, D.; Castex, M. C. *Proc. SPIE*, **1998**, p 234.
(363) Riedel, D.; Castex, M. C. *Appl. Phys. A* **1999**, *69*, 375.
(364) Castex, M. C.; Bityurin, N.; Olivero, C.; Muriaviov, S.; Bronnikova, N.; Riedel, D. *Appl. Surf. Sci.* **2000**, *168*, 175.
(365) Katoh, T.; Zhang, Y. *J. Synchrotron Rad.* **1998**, *5*, 1153.
(366) Katoh, T.; Yamaguchi, D.; Satoh, Y.; Ikeda, S.; Aoki, Y.; Washio, M.; Tabata, Y. *Appl. Surf. Sci.* **2002**, *186*, 24.
(367) Zhang, Y.; Hori, T. *Synchrotron Radiat. News* **2000**, *13*, 32.
(368) Zhang, Y.; Katoh, T.; Washio, M.; Yamada, H.; Hamada, S. *Appl. Phys. Lett.* **1995**, *67*, 872.
(369) Katoh, T.; Nishi, N.; Fukagawa, M.; Ueno, H.; Sugiyama, S. *Sens. Actuators A* **2001**, *89*, 10.
(370) Katoh, T.; Zhang, Y. *Appl. Surf. Sci.* **1999**, *138−139*, 165.
(371) Zhang, Y.; Katoh, T.; Endo, E. *J. Electron Spectrosc. Relat. Phenom.* **2001**, *119*, 247.
(372) Cozzens, R. F.; Fox, R. B. *Polym. Eng. Sci.* **1978**, *18*, 900.
(373) Koren, G. *Appl. Phys. Lett.* **1984**, *45*, 10.
(374) Brannon, J. H.; Lankard, J. R. *Appl. Phys. Lett.* **1986**, *48*, 1226.
(375) Braun, R.; Nowak, R.; Hess, P.; Oetzmann, H.; Schmidt, C. *Appl. Surf. Sci.* **1989**, *43*, 352.
(376) Sonnenschein, M. F.; Roland, C. M. *Appl. Phys. Lett.* **1990**, *57*, 425.
(377) Dyer, P. E.; Oldershaw, G. A.; Sidhu, J. *Appl. Phys. B* **1989**, *48*, 489.
(378) Sumiyoshi, T.; Ninomiya, Y.; Ogasawara, H.; Obara, M.; Tanaka, H. *Appl. Phys. A* **1994**, *58*, 475.
(379) Dyer, P. E.; Karnakis, D. M.; Oldershaw, G. A.; Roberts, G. C. *J. Appl. Phys. D: Appl. Phys.* **1996**, *26*, 2554.
(380) Dyer, P. E.; Waldeck, I.; Roberts, G. C. *J. Appl. Phys. D: Appl. Phys.* **1997**, *30*, L19.
(381) Coupland, K.; Herman, P. R.; Gu, B. *Appl. Surf. Sci.* **1998**, *127−129*, 731.
(382) Wong, K. H.; Tou, T. Y.; Low, K. S. *J. Appl. Phys.* **1998**, *83*, 2286.
(383) Tolsopyatov, E. M.; Ivanov, L. F.; Grakovich, P. N.; Krasovsky, A. M. *Proc. SPIE-Int. Soc. Opt. Eng.* **1998**, *3343*, 1010.
(384) Ionin, A.; Klimachev, Y.; Kobsa, H.; Sinistyn, D. *Proc. SPIE-Int. Soc. Opt. Eng.* **1998**, *3343*, 1032.
(385) Freund, H. P.; Neill, G. R. *Proc. IEEE* **1999**, *87*, 782.
(386) Kelly, M. J. *Mater. Res. Soc. Symp. Proc.* **2001**, *617*, J5.7.
(387) Bubb, D. M.; Toftmann, B.; Haglund Jr., R. F.; Horowitz, J. S.; Papantonakis, M. R.; McGill, R. A.; Wu, P. W.; Chrisey, D. B. *Appl. Phys. A* **2002**, *74*, 123.
(388) Bubb, D. M.; Papantonakis, M. R.; Toftmann, B.; Horowitz, J. S.; McGill, R. A.; Chrisey, D. B.; Haglund Jr., R. F. **2002**, *91*, 9809.
(389) Silverstein, M. S.; Visoly, I.; Kesler, O.; Janai, M.; Cassuto, Y. *J. Vac. Sci. Tchnol. B* **1998**, *16*, 2957.
(390) Egami, C.; Kawata, Y.; Aoshima, Y.; Takeyama, H.; Iwata, F.; Sugihara, O.; Tsuchimori, M.; Watanabe, O.; Fujimura, H.; Okamoto, N. *Opt. Commun.* **1998**, *157*, 150.
(391) Hu, A. *CircuiTree* **1998**, *11*, 86.
(392) Owen, M.; Roelants, E.; Van Pyumbroeck, J. *Circuit World* **1997**, *24*, 45.
(393) Maryniuk, J. *AMP J. Technol.* **1995**, *4*, 77.
(394) Yung, W. K. C.; Liu, J. S.; Man, H. C. *Circuit World* **1999**, *25*, 13.
(395) Illy, E. K.; Brown, D. J. W.; Withford, M. J.; Piper, J. A. *IEEE J. Sel. Top. Quantum Electron.* **1999**, *5*, 1543.
(396) Glover, A. C. J.; Illy, E. K.; Piper, J. A. *IEEE J. Sel. Top. Quantum Electron.* **1995**, *1*, 830.
(397) Yung, K. C.; Zeng, D. W.; Yue, T. M. *Surf. Coat. Technol.* **2002**, *160*, 1.

CR010460Q